PROJECTE O TESINA D'ESPECIALITAT

Títol

INTEGRATING AESTHETICS AND STATICS:

STUDY OF A GEODESIC DOME

Autor/a

Vinyes Raso, Raül

Tutor/a

Codina Rovira, Ramon

Departament

RMEE

Intensificació

Estructures

Data

Setembre de 2009

Integrating aesthetics and statics

study of a geodesic dome

Raül Vinyes Raso

Final Year Project

September 2009

My mother, **Maria Raso Artiga**, passed away April 19th 2009. Born in Ólvega (Soria), she showed me how love, joy, effort and creativity can intermingle.

Raül Vinyes Raso
Frankfurt am Main, August 31st 2009

<div style="columns:2">

CANT ESPIRITUAL

Si el món ja és tan formós, Senyor, si es mira
amb la pau vostra a dintre de l'ull nostre,
què més ens podeu dar en una altra vida?

Perxò estic tan gelós dels ulls, i el rostre,
i el cos que m'he donat, Senyor, i el cor
que s'hi mou sempre... i temo tant la mort!

¿Amb quins altres sentits me'l fareu veure
aquest cel blau damunt de les muntanyes,
i el mar immens, i el sol que pertot brilla?
Deu-me en aquests sentits l'eterna pau
i no voldré més cel que aquest cel blau.
Aquell que a cap moment li digué «—Atura't»
sinó al mateix que li dugué la mort,
jo no l'entenc, Senyor; jo, que voldria
aturar a tants moments de cada dia
per fé'ls eterns a dintre del meu cor!...
O és que aquest «fer etern» és ja la mort?
Mes llavores, la vida, què seria?
¿Fóra només l'ombra del temps que passa,
i la il·lusió del lluny i de l'a prop,
i el compte de lo molt, i el poc, i el massa,
enganyador, perquè ja tot ho és tot?

Tant se val! Aquest món, sia com sia,
tan divers, tan extens, tan temporal;
aquesta terra, amb tot lo que s'hi cria,
és ma pàtria, Senyor: i ¿no podria
esser també una pàtria celestial?
Home só i és humana ma mesura
per tot quant puga creure i esperar:
si ma fe i ma esperança aquí s'atura,
me'n fareu una culpa més enllà?
Més enllà veig el cel i les estrelles,
i encara allí voldria esser-hi hom:
si heu fet les coses a mos ulls tan belles,
si heu fet mos ulls i mos sentits per elles,
per què aclucà'ls cercant un altre com?
Si per mi com aquest no n'hi haurà cap!
Ja ho sé que sou, Senyor; pro on sou, qui ho sap?
Tot lo que veig se vos assembla en mi...
Deixeu-me creure, doncs, que sou aquí.
I quan vinga aquella hora de temença
en què s'acluquin aquests ulls humans,
obriu-me'n, Senyor, uns altres de més grans
per contemplar la vostra faç immensa.
Sia'm la mort una major naixença!

Joan Maragall. "Cant espiritual".
Glòria Casals (1998), *Poesia*, Edicions La Magrana, pages 814-815, Barcelona

SPIRIT SONG

Since the world is already so lovely, Lord
—seen with your peace in our eyes—
what more could you give us in another life?

Therefore I am jealous of my eyes, Lord,
and of my face and of the body you have given me
and of my ever-beating heart… and fear so much to die!

With what further senses would you make me see
the blue that overhangs the mountains,
and the vast sea, and the all-enlightening sun?
Give me in my herebound senses everlasting peace
and I'll ask for no further heaven than this one of blue.
The man who bids no moment "stop",
except the one that seals his death,
I cannot understand, Lord; I, who would
hold back so many moments of each day,
to make them everlasting in my heart…!
Or is that "everlastingness" itself a form of death?
But then, what of life — what would it be?
No more than time's shadow passing,
the illusion of the far and near,
the tally of the great, the small, the overmuch,
deceptive, since all that is, is all there is?

So much for that! This world, just as it is,
so divers, so extense, so temporal;
this earth, with all that grows within it,
is my homeland, Lord; and might it not
as well be a heavenly homeland?
I am a man, and human is my measure
for all I can believe and hope:
if my faith and hope are anchored here
will you hold it against me there beyond?
There beyond I see the sky, the stars,
and even there I would be a man.
If you have made all things so lovely to my eyes,
if you have made my eyes and senses for them,
why close them, then, in search of other worlds?
Seeing that for me, there'll be no other such as this!
Lord, I know now that you exist, but who knows where?
All that I behold resembles you in me…
Let me, then, believe that you are here.
And when the dreaded moment comes
in which these human eyes are closed,
then open up still greater eyes in me,
that I may gaze upon your endless face.
Let death for me be a yet greater birth!

Joan Maragall. "Spirit Song" ("Cant espiritual").
Tranlsated by Joseph Daries with J.M.Coromines' assistance. Maragalll Archive.

</div>

0 PRELIMINARY

0.1 Abstract

ENGLISH VERSION

Title: Integrating aesthetics and statics: study of a geodesic dome

Author: Raül Vinyes Raso

Tutors: Maurizio Brocato, Ramon Codina Rovira and Dipl.-Ing. Horst Peseke

Abstract:

We usually go to great lengths to separate the roles of engineers and architects so as to *avoid* communication problems in common tasks. However, the role of both architects and engineers can be included in the same task: being *creative designers* (Ove Arup). Architects cannot express their creativity while ignoring the physical constraints (statics) and engineers cannot design solutions in the absence of an understanding of their aesthetical dimension. Thus we propose to integrate aesthetics and statics.

Nevertheless, it would not be coherent to materialize such a general idea without drawing on the work of our predecessors, which led us to the previous approach. It has always existed a fascination of human beings for domes, maybe because they are elegant in their appearance and in their structural behavior. This interesting subject integrates both a historical and modern dimension that can be used to establish a link with the latest tendencies in design.

Thus, we will focus on the study of a very specific geodesic dome (the experimental Zeiss dome in Jena, 1922), the first one made of a steel mesh that allows for the construction of an incredibly thin concrete shell.

First of all, we will do a bibliographical and historical study of the structure, which includes a visit to the Carl Zeiss Archive in Jena to retrieve all of the conserved drawings: the dome was demolished some years after its construction. Thanks to this precious information, we will analyze the structure from the geometrical point of view, going from the steel bars composing the mesh to the connecting elements in the nodes.

Furthermore, we will compare its theoretical behavior using the shell theory applied to its membrane version with the calculations made in 1922 and with the solution of the finite-element calculation. Such an approach helps us to understand the interaction between the steel mesh and the concrete shell. It is precisely through this careful and in-depth study that we will be able to make connections with modern design tools.

Therefore, *scripting* a parametric model of the geometry compatible with both a 3D design program and a 3D statics program will be a powerful tool to achieve these objectives. We can then set up a dialogue between both approaches, helping us to study the structure in a more accurate way and giving us the possibility of thinking of further developments related to geometric imperfections or integrated design. Only creativity can limit us.

Short version:

Human beings have always exhibited a fascination for domes. This is also the case of the experimental Zeiss geodesic dome in Jena (1922), the first made of a steel mesh that allows for the construction of an incredibly thin concrete shell. The careful and in-depth study of its history, the structure geometry, the associated shell theory and the finite-element calculation will allow to make connections with modern design tools. A parametric model of the geometry compatible with both a 3D design program and a 3D statics program has been *scripted*. It renders possible a dialogue between both approaches, enabling a more accurate study of the structure and paving the way for further progress related to geometric imperfections or integrated design. Only creativity can limit us.

Keywords: geodesic dome, Carl Zeiss, shell theory, scripting, finite-element calculation, aesthetics, statics, integrated design, openings

Catalan version

Títol: Intregrant estètica i estàtica: estudi d'una cúpula geodèsica

Autor: Raül Vinyes Raso

Tutors: Maurizio Brocato, Ramon Codina Rovira i Dipl.-Ing. Horst Peseke

Resum:

Sovint es dediquen grans esforços en separar les funcions d'enginyers i arquitectes per evitar problemes de comunicació en les tasques compartides. Tanmateix, el paper de tant arquitectes com enginyers es pot incloure en una mateixa activitat: la de ser dissenyadors creatius (Ove Arup). Els arquitectes no poden expressar la seva creativitat ignorant les limitacions físiques (estàtica) i els enginyers no poden dissenyar solucions sense una comprensió de la dimensió estètica. Proposem, doncs, integrar estètica i estàtica.

No obstant, no seria coherent materialitzar una idea de caire tan general sense revisar l'obra dels nostres predecessors, que ens portarà al punt de vista anunciat. Sempre ha existit una fascinació de l'ésser humà per les cúpules, potser perquè són elegants en la seva aparença i en el seu comportament estructural. Aquest interessant tema integra tant una visió històrica com una visió més moderna que pot ser utilitzada per establir un nexe amb les darreres tendències en disseny.

Per tant, ens centrarem en l'estudi d'una cúpula geodèsica molt concreta (la cúpula experimental de Zeiss a Jena, de 1922), la primera feta d'una malla d'acer que permet construir una closca de formigó extremadament fina.

En primer lloc, farem una recerca bibliogràfica i històrica sobre l'estructura que inclou una visita a l'Arxiu Carl Zeiss a Jena per recuperar tots els documents que es conserven: la cúpula va ser enderrocada pocs anys després de la seva construcció. Gràcies a aquesta preuada informació podrem analitzar l'estructura des del punt de vista geomètric, des de les barres d'acer que componen la malla fins els elements de connexió en els nodes.

A més, compararem el seu comportament teòric utilitzant la teoria de closques, aplicada a la seva versió per a membranes, amb els càlculs fets el 1922 i amb la solució obtinguda gràcies a un model d'elements finits. D'aquesta manera podrem entendre la interacció entre la malla d'acer i la closca de formigó. És precisament aquest estudi profund i precís el que ens permetrà establir connexions amb les eines modernes de disseny.

Per tant, el fet de programar un *script* per a establir un model paramètric de l'estructura compatible tant amb un programa de disseny 3D com amb un programa de calcul estructural 3D representa una eina poderosa per assolir aquests objectius. Podrem, doncs, crear un diàleg entre els dos models, la qual cosa ens ajudarà a aprofundir en l'estudi i ens obrirà les portes de noves perspectives relacionades amb les imperfeccions geomètriques i el disseny integrat. Només ens podrà limitar la creativitat.

Mots clau: cúpula geodèsica, Carl Zeiss, teoria de closques, scripting, càlcul per elements finits, estètica, estàtica, disseny integrat, obertures

SHORT FRENCH VERSION

La fascination de l'homme pour les dômes a toujours existé. C'est aussi le cas pour la coupole géodésique expérimentale de Zeiss à Jena (1922), la première qui a été faite avec un maillage en acier qui permet la construction d'une coque en béton extrêmement fine. L'étude détaillée de son histoire, la géométrie de la structure, la théorie des coques associée et le calcul par éléments finis permettra d'établir un lien avec des nouveaux outils de design. Un modèle paramétrique de la géométrie compatible au même temps avec un logiciel de design 3D et un logiciel de calcul de structures 3D a été *scripté*. Il rend possible un dialogue entre les deux approches, en aidant dans l'étude plus approfondie de la coupole et en ouvrant les portes à des éventuels développements dans le domaine des imperfections géométriques ou du design intégré. Il n'y a que la créativité qui peut nous limiter.

0.2 Index of figures

0.3 Index of tables

0.4 About the office

This work was developed during an internship in *Bollinger+Grohmann,* a German engineering and consulting firm originally located in Frankfurt am Main. After over 20 years of experience in planning and building, a second office was opened in Vienna in 2001, followed by a third in Paris in 2007: needless to say, the company has demonstrated its global presence from the start.

Although the team is composed primarily of engineers, what truly sets this company apart is the integration of a team of architects in its very structure. Thus, it is possible to establish and maintain **dialogue between engineers and architects**, breaking down the *historical* barriers that existed previously. This cooperation begins with the design and permits an aesthetic, economic, and audacious solution; it is thanks to this cooperation early on that both parts are able to produce a common result, based on creativity and rationality.

Figure 0.1: *Pavilion designed for the presentation of the BMW group at the International Automobile show IAA 1999. Its double curved shell made of crystal clear acrylic glass was manufactured thanks to a computer-controlled process.*

While the office provides a wide range of services, its main focus is on structural engineering: from residential buildings to offices and commercial buildings and from exhibitions and event locations to classical structural engineering for bridges, roofs, and towers.

A high-quality standard is assured from the planning process to the completion of the project. Evidence of this fact include projects such as the *BMW 'Bubble' IAA 1999,* which received several awards, the *Vienna DC Towers 2005* (Dominique Perrault Architecte), and a number of other works including a narrow collaboration with Zaha Hadid Architects (figures **0.1** and **0.2**).

Figure 0.2: Render views of the Vienna DC Sky-Towers, with a height of 220 m and 160 m, designed by the French architect Dominique Perrault. The aim is to obtain a slender profile as opposed to the curved-shaped façade.

All this activity would not be possible without a clever and coordinated use of specific software which includes every stage of the conception. The key is not to use many different programs, but rather knowing how to establish common models which can allow the team to work together. Speaking a common language enables optimization of each task, simultaneously taking into account all the stages.

We have sought to accomplish in this work an initial step of this process by giving some integrated design tools. The final objective would be to build a model with a global approach of the whole project and establish a **bidirectional dialog between aesthetics and statics.**

1 INTRODUCTION

"An engineer must be devoted to architecture. He must have enthusiasm. He must not just be a calculator or analyzer, he must be a creative designer."

Ove Arup, Rappaport (2007)

We will begin by presenting, on the one hand, the objectives we wish to achieve and, on the other, the historical background that makes such an approach possible. Both parts are presented in the same chapter because they are inextricably intertwined.

1.1 Goals

The underlying goal of this project is perfectly described by Ove Arup's quotation, reproduced at the beginning of this chapter. We usually go to great lengths to separate the roles of engineers and architects so as to *avoid* communication problems in common tasks. However, the role of both architects and engineers can be included in the same task: being *creative designers*. Architects cannot express their creativity while ignoring the physical constraints (statics) and engineers cannot design solutions in the absence of an understanding of their aesthetical dimension. Thus we propose to **integrate aesthetics and statics.**

Nevertheless, it would not be coherent to materialize such a general idea without drawing on the work of our predecessors, which led us to the previous approach. A fascinating subject that can integrate both a historical and modern dimension is the study of a dome.

Our first goal will be to focus on the **study of a very specific dome** (the first Zeiss dome in Jena, 1922), the first one made of a steel mesh that allows for the construction of an incredibly thin concrete shell. It is precisely through a careful and in-depth study of its **history**, the structure **geometry**, the associated **shell theory** and the **finite-element calculation** that we will be able to make connections with **modern design tools**.

At this point, our underlying goal will appear: we will script a parametric model of the geometry compatible with both a 3D design program and a 3D finite-element analysis program. We can then set up a dialogue between both approaches, helping us to study the structure in a more accurate way and giving us the possibility to think in

further eventual developments related to geometric imperfections or integrated design. Only **creativity** can limit us.

1.2 Historical background: from massive domes to shells

It would be difficult to understand the revolution triggered by Carl Zeiss' dome without first discussing the **evolution** of this kind of structure over the last 2000 years. More specifically, Heine and Schlaich (1996) made a significant contribution by compiling and describing the best examples of domes over the course of human history; we have tried to condense the main aspects into two paragraphs.

Although the Stone Age contains examples of *pre-domes* (in the surroundings of Nice), as well as in Egypt, Mesopotamia (Sanherib Palace in Kujundschik, figure **1.2**) and Greece (Mykene (figure **1.1**), Orchomenos), the first *real* domes appeared with Roman civilization. Springs, palaces, temples, domes began to flourish, and the first masterpiece appeared in 125 a.C. with the achievement of **Rome's Pantheon** (figure **1.3**). With a spread of 44 m, it synthesized the accumulated knowledge in the new materials and techniques of that period.
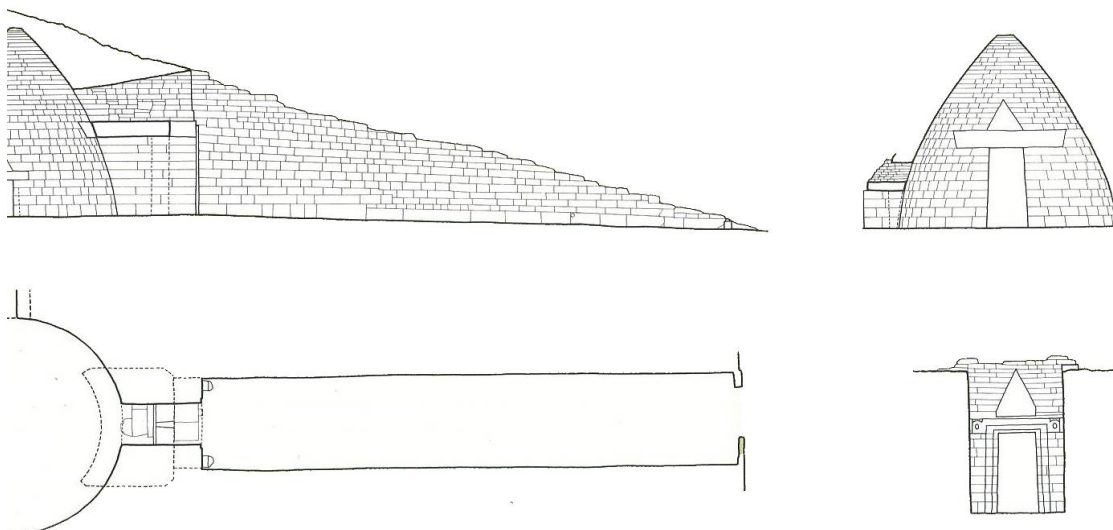
Figure 1.1: Agamemnon tomb in a fortress in Mykene (Greece). Built in 1325 b.C., it contains a console-dome with a spread of 14,5 m and a height of 13,2 m. It represented the night sky, with its gold-plated rosette.

Figure 1.2: In the Sanherib palace (Kujundschik, Mesopotamia, Assyrian) we can find this relief from around the 700 b.C. It shows semi-circular and elliptical domes.
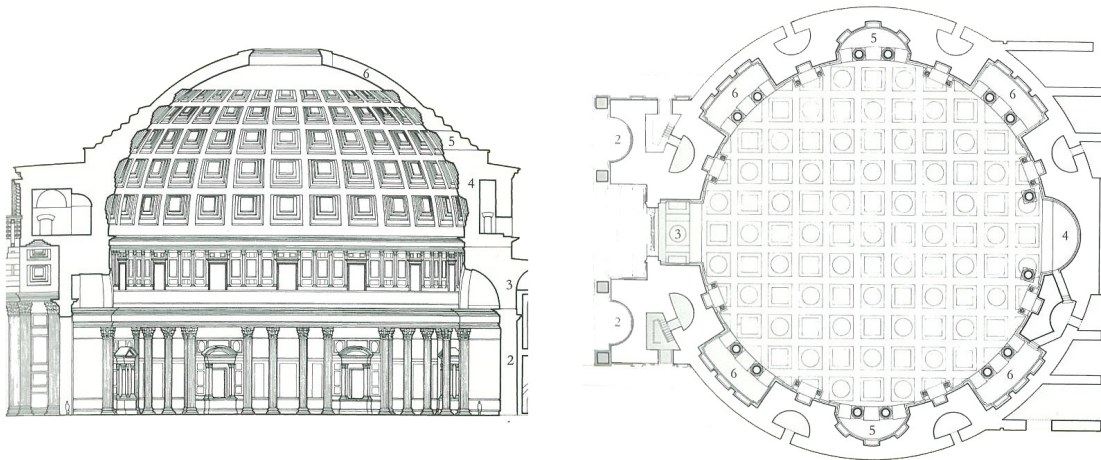
Figure 1.3: Section and floor plan of Rome's pantheon, which was built during the reign of the emperor Hadrian from Apollodorus (Damascus) between the years 118 a.C. and 125 a.C. (the named gold century). It is a very representative Roman dome that would become one of the more famous works from the ancient world.

*We can imagine that the building is interiorly shaped, in its upper part, by a sphere of 43,3 m of diameter; if we extend this sphere to the lower part, its south pole coincides with the ground floor. Furthermore, the section has been **weight-optimized** in the sense that, in its upper part, it is less thick and made of appropriate materials in order to lighten the structure.*

After this important inflexion point in history, other great structures containing impressive domes appeared: the **Hagia Sophia in Constantinople** (537 a.C., spread of 32 m, figure **1.4**), the domes from Byzantine, Islamic, Ottoman and Buddhism architecture and those from the Middle Ages, Romanic and Gothic architecture. However, not until 1420 a.C. did the world discover a new engineering prodigy with **Filippo Brunelleschi's dome in Florence** (spread of 42 m, figure **1.5**). During the Renaissance many domes would be built, followed by **Saint Peter's dome in Rome** (1590 a.C., spread of 40 m, figure **1.6**). It is amazing to see the correlation between the evolution of the dome and human progress; what would happen in the last century is not an exception either.

Figure 1.4: Section (east-west axis on top, north-south axis on bottom) and floor plan (over the gallery on the left, at the level of the window's cornice on the right) of the Hagia Sophia in Byzantium, which was built from 532 a.C. to 537 a.C. when Justinian was emperor.

The connection between lateral and central naves is innovative and the central and lateral domes allow an opened space of 75 m per 30 m with a height of 55 m.

Structurally, the idea is to keep the **thrust line** in the core of the wall section (kern). Thus, the correct transmission of the forces is assured.
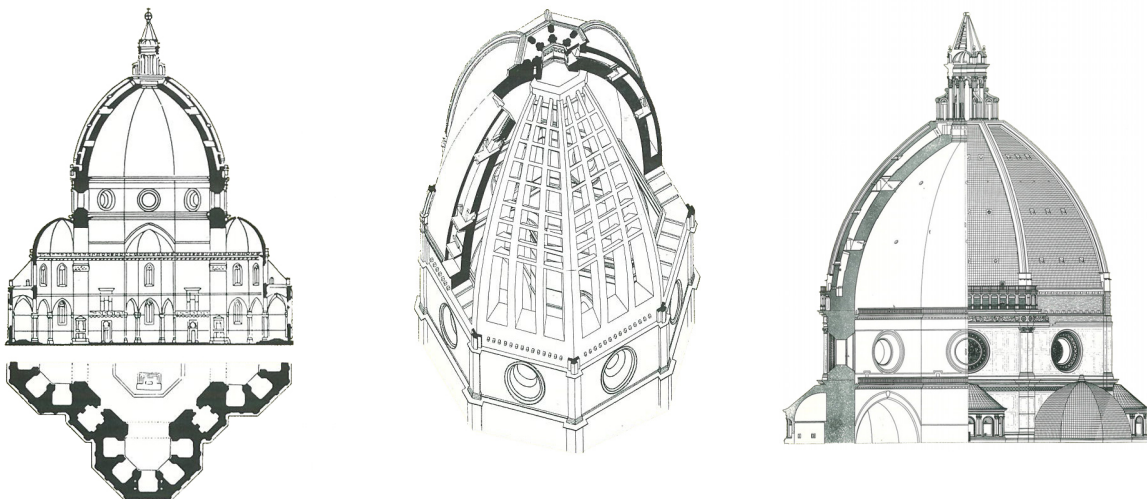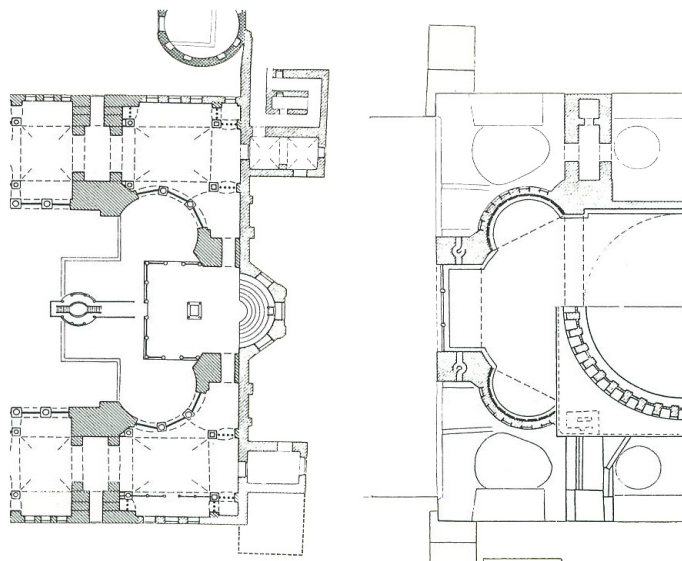
Figure 1.5: Section and floor plane of Santa Maria del Fiore in Florence, isometric perspective of the cathedral dome and view and section of the dome and the reel (from left to right). It has a diameter of 42m, and its higher point is situated 103 m above the floor.

In fact, the exterior dome had the sole function of protecting the interior dome from rain and improving the design. However, Brunelleschi added some massive wood-rings connected with steel brackets in order to minimize the deformations induced by the dome-push. It is also important to highlight the **ribbed structural principle**.
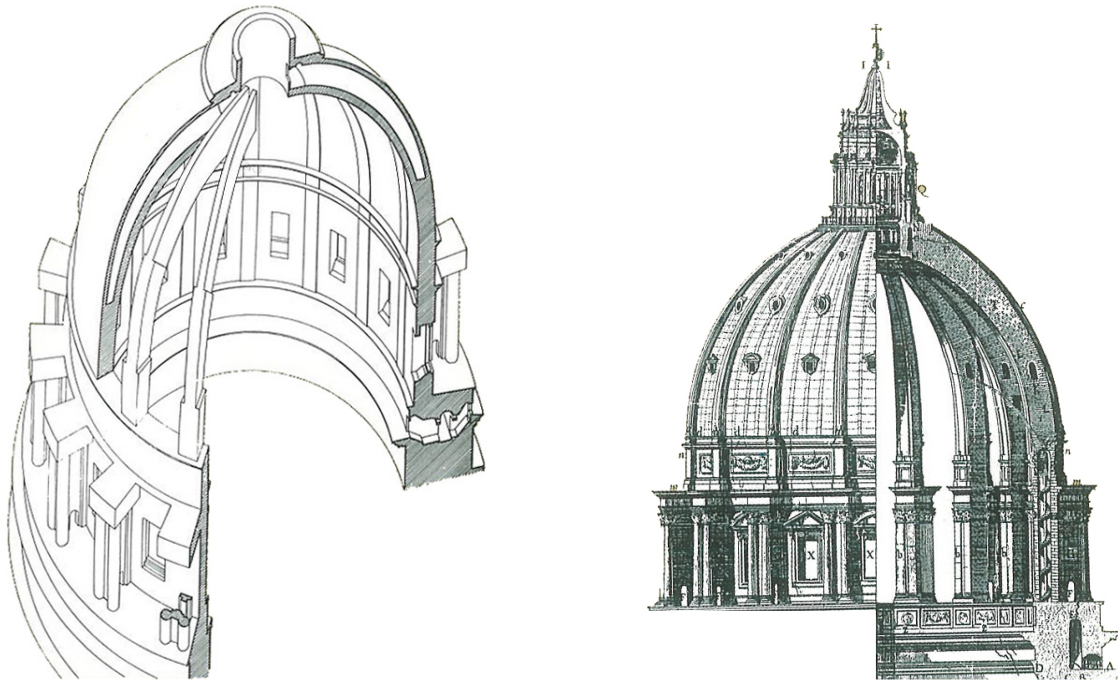
Figure 1.6: *Schematic view and section of Saint Peter's dome in Rome. The original design of Michelangelo included a double dome and 16 counterforts but it suffered some modifications after his death. Giacomo della Porta and Domenico Fontana reduced the thickness of the outside shell and made the profile of the dome more slender.*

The list of great domes goes on, but that is not the purpose of the project at hand. Nevertheless, it is necessary to make mention of an event that took place in 1922 with the construction, among others, of the first Zeiss dome in Jena (Germany), with a diameter of 16m. In the **Carl Zeiss** office Dr. Bauersfeld and his team developed, in collaboration with Dyckerhoff & Widmann AG engineers, a new way of conceiving domes (figure **1.7**) that would remain an integral part of 20th Century engineers' spirit: they managed to build a dome with a spread of 40m with a concrete thickness of only 6 cm. This was undoubtedly revolutionary.

Figure 1.7: The innovative idea of a new conception system: the steel mesh of the 25 m diameter planetarium in Jena. This kind of structure can support great charges suffering a minimal deformation, as we will see in the following chapter.

Figure 1.8: *Interior view of the Breslauer Jahrhunderthalle, built in 1913. This 65 m spread steel-concrete dome with a ribbed structure represents a transition between the massive domes and the new shell domes that would appear in the following years. It was designed by the Dyckerhoff & Widmann AG office.*

If we analyze the relationship between the weight and the spread of the **old massive domes** and the *new* Zeiss domes, we find a relation of 30:1; thus, a 120 m spread Zeiss dome would weigh the same as the 65 m spread Breslauer Jahrhunderthalle (figure **1.8**). How was this possible? We will discuss all the details of this dome in the following chapter, but the *secret* lies both in the **membrane behavior** (spatial structure without bending stiffness) of the structure and in the construction of a steel mesh that reinforces the concrete shell. The study of the mechanic behavior and material properties can lead, thus, to a cost-effective structure.
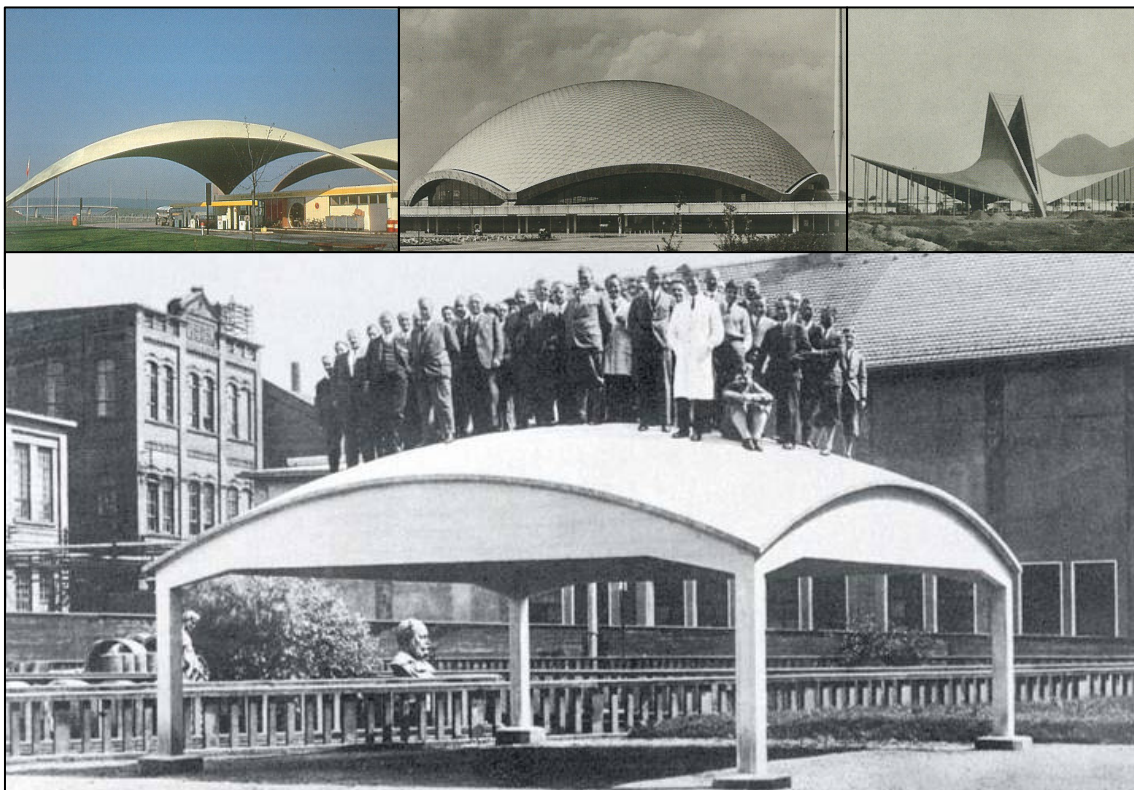
Figure 1.9: *Roof for a fuel station in Switzerland (H.Isler), shell of about 100m diameter in the Jahrhunderthalle in Frankfurt (Dyckerhoo & Widmann) and San José Obrero church in Monterrey (Félix Candela) (above, from left to right).*
Below, a load test (50 people standing on the roof) in a double curved square shell (7,3 m x 7,3 m) with a thickness of only 1,5 cm and reinforced with a steel net of 3 mm (Dischinger-Finsterwalder,1932).

It was a period of great changes, and engineers such as Ulrich Finsterwalder, Franz Dischinger, Walther Bauersfeld, Heinz Isler, Félix Candela, and Eduardo Torroja would continue to study these new structures with origins in Zeiss' dome: **shells** (figure **1.9**). A quotation from Heinz Isler can describe the importance of such an approach: "When a shell turns into a plate, it loses 97% of its load bearing capacity". On the other hand, R. Buckminster Fuller would also apply certain of those ideas to his work with geodesic domes.

Finally, one could assert that this concept has been superseded, but the fact of building a triangular mesh of a dome is related to some **current research projects**. When conceiving freeform surfaces (figure **1.11**), we must be able to build them, and a classical steel-glass structure usually requires plane surfaces on which to dispose the glass planes. Properly meshing freeform surfaces as those shown below (figure **1.10**) then becomes a major problem still being studied, for example, in the case of quadrilateral meshes with planar faces (also known as planar quad meshes, PQ) (Pottmann et al., 2007).
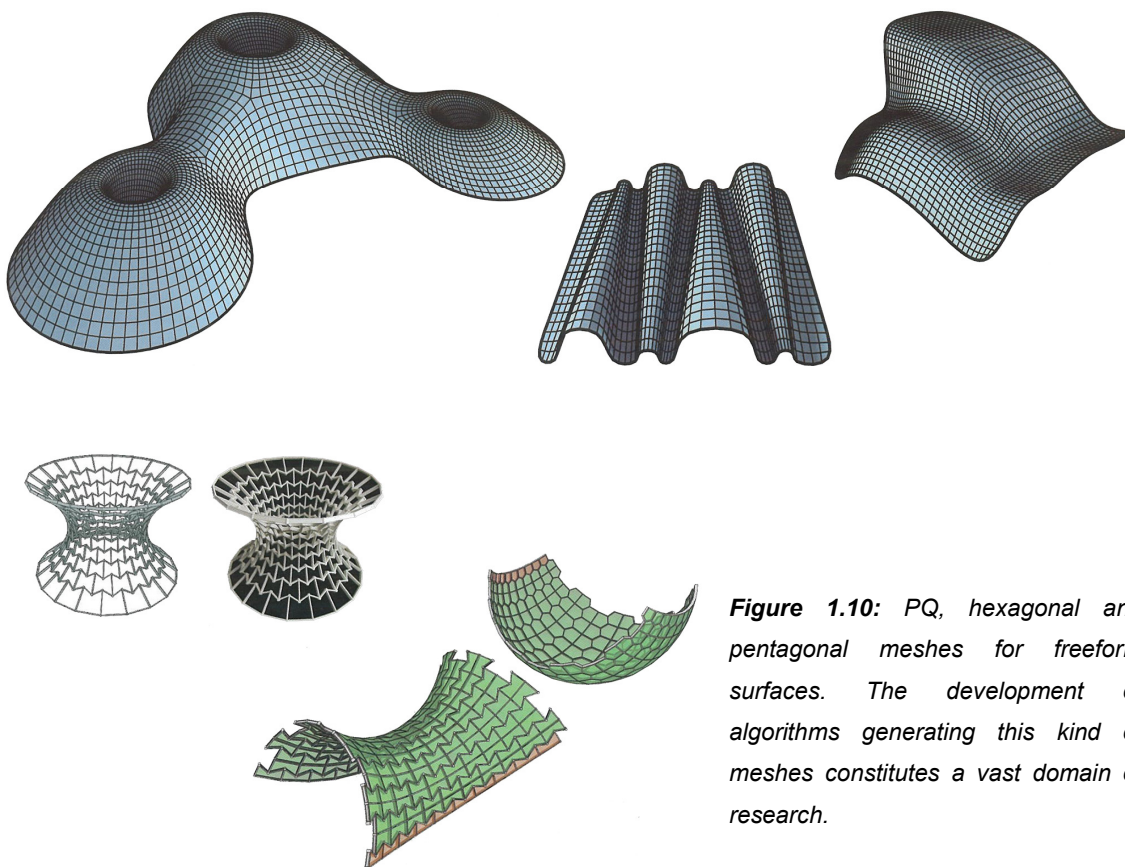
Figure 1.10: PQ, hexagonal and pentagonal meshes for freeform surfaces. The development of algorithms generating this kind of meshes constitutes a vast domain of research.
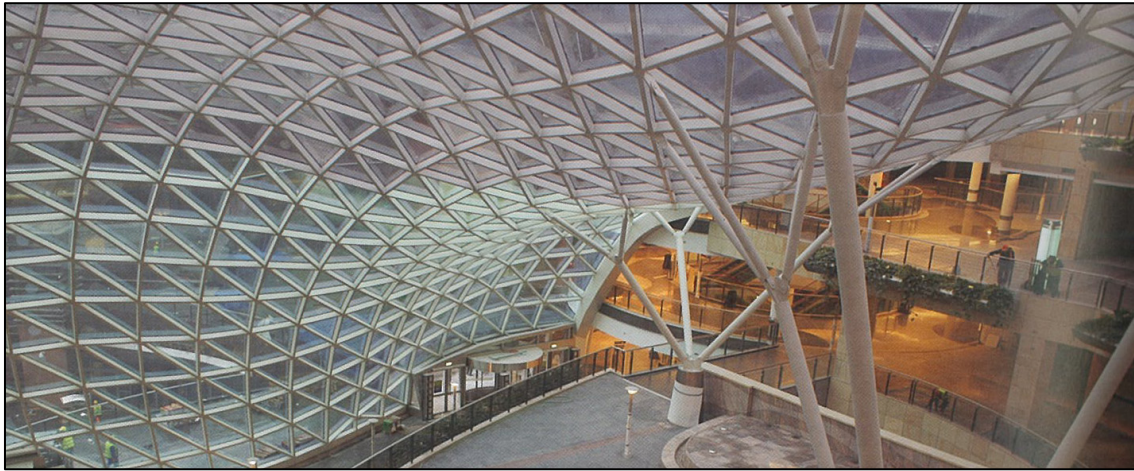
Figure 1.11: *The fluid body of the outer skin of the Zlote Tarasy in Warsaw, by Jerde Partnership. This structure clearly shows the challenge of discretizing a freeform surface using planes.*

It is thanks to the historical approach and study of the first Zeiss dome in Jena that we are able to fully understand the evolution of dome structures. Thus, we will be in the ideal position to apply current methods to the design and calculation of a dome.

2 Study of the first Zeiss dome

"God is in the details."

Mies van der Rohe

In order to accurately describe the geometry and materials of the first Zeiss dome in Jena, it is important to introduce the work of Dr. Bauersfeld and his team in Germany during the 1920. This was a pivotal moment during which a group of German engineers worked in the same direction to develop the theory of thin shells, which originated with the revolutionary idea of the so called ***Kuppelbausystem "Zeiss-Dywidag"*** (dome construction system "Zeiss-Dywidag", Dischinger (1925)). It was the result of new ideas applied to new materials and new times.

At this point, it is important to underline the fact that all of the great domes mentioned in the first chapter merit special attention as they were built in the absence of an accurate method of calculation and using materials without tensile strength. However, Dr. Bauersfeld, of the Carl Zeiss office (Jena), proposed the construction of a dome, which had to reproduce the sky, using a light steel mesh (figure **2.1**). The **tensile strength, as well as the shape itself,** played an essential role.
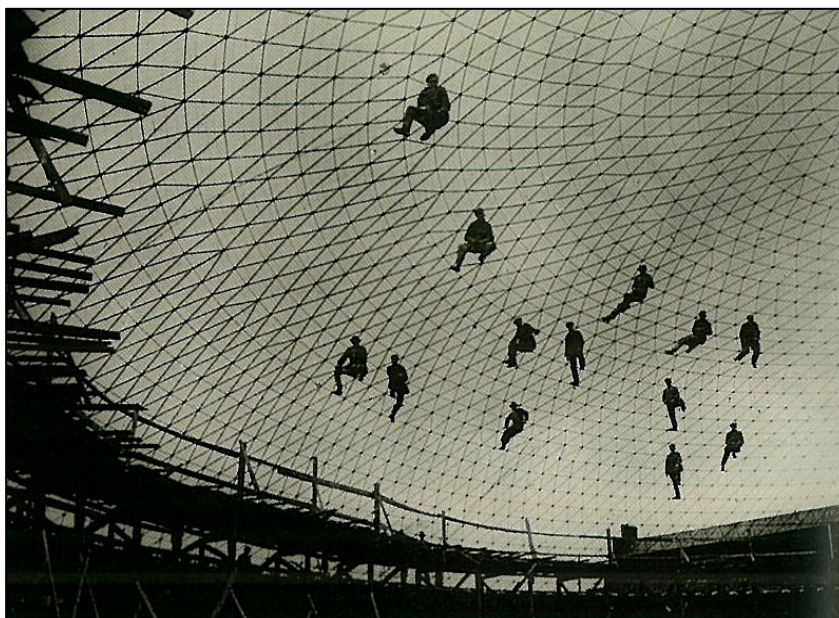
Figure 2.1: Extreme light and resistant steel mesh of a building in Jena made by Schott & Gen. office. The same system was used multiple times to conceive many different structures.

The mesh was built from thin **bars** and audacious **nodes**, which will be studied in detail later on. This mesh was then covered by a thin layer of **shot-fast hardening**

concrete. It is precisely thanks to the shot concrete and the fast hardening concrete (inventions of that time) that such a system could function.

It is not by chance that this new method was patented on October 31[st,] 1925 in the *Deutschen Reichspatentamt* (Zeiss (1925), figure **2.2**). The general idea is described with great emphasis on the node detail. Mies van der Rohe was certainly right : *"God is in the details"*.
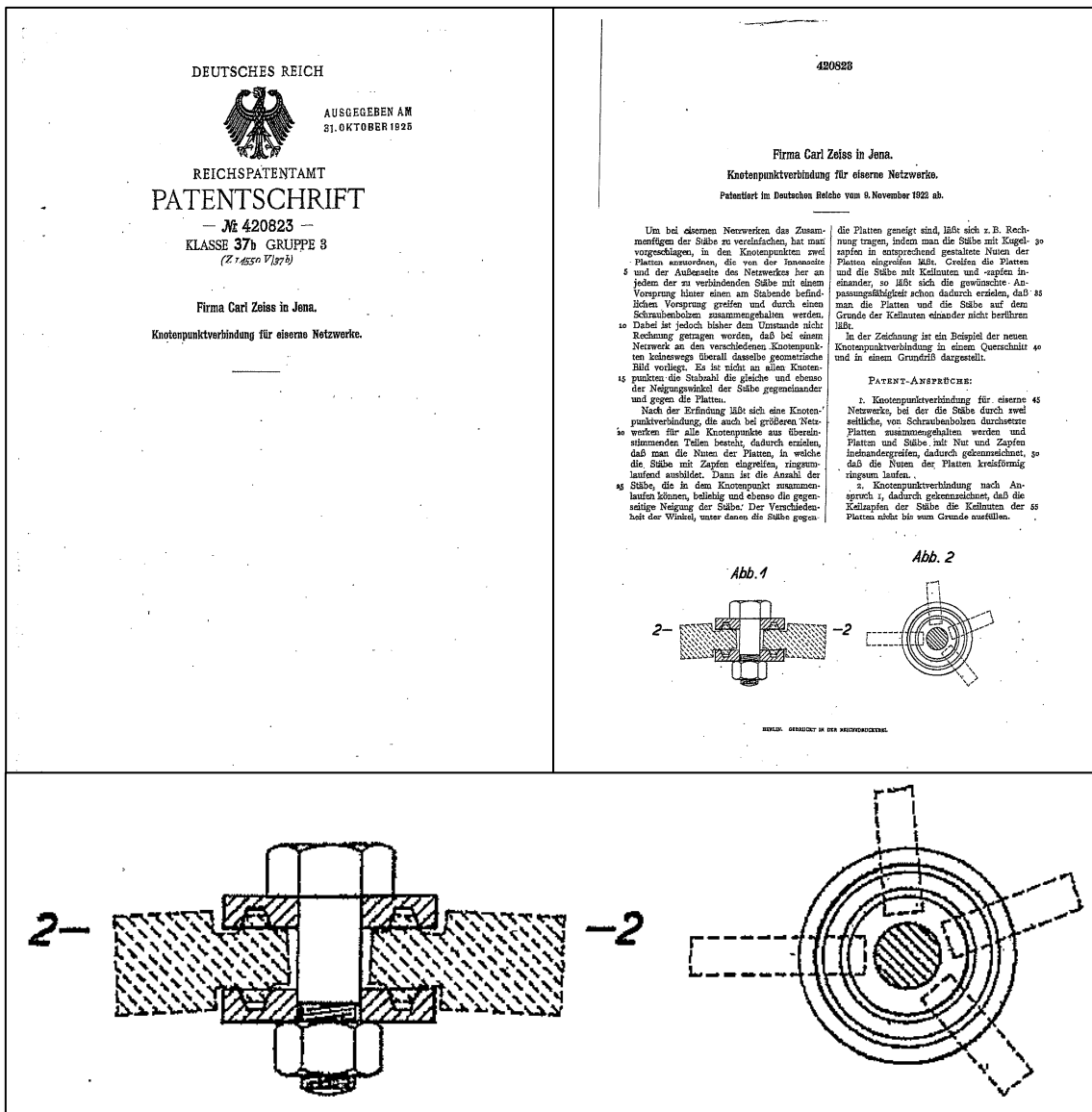
Figure 2.2: Copy of the patent by Carl Zeiss in the Deutschen Reichspatentamt. The text explains how the bars are connected and the illustration shows the detail of the connection element.

2.1 Description of the structure

Many different structures were built using the Zeiss-Dywidag system, but we will study the first because it is the more representative and many further developments rest upon it. In fact, the system evolved between 1920 and 1930, going from a reinforcement system to a shell system: the shape of the structure plays a central role in the stability of the structure. It all began with the first design of an experimental planetarium for a projector that was built on the roof of a factory in the same city (1922). The **historical background** (Kurze, 2006) is essential to understand the chosen structure.

In fact, Zeiss' engineer Walter Bauersfeld needed an accurate spherical dome to test a Planetarium projector that he had designed with Franz Meyer. As the dome had to be built on the roof of an existing building, it needed to be extremely light. They first thought of a structure similar to a circus tent, but the textile material was too expensive during that time of high inflation. Per contra, a steel solution was much more attractive in terms of the price as it was a common product in Germany. Thus, they developed a half spherical dome mesh made of steel-bars which had to be covered with projected concrete. The process was made possible by a wood formwork of approximately 3 m x 3 m that could be displaced and used multiple times in order to cover the entire surface. Unfortunately, the structure was demolished some years after to extend the building.

Thanks to a **visit to the Carl Zeiss Archive in Jena,** we have managed to obtain all the details of the studied structure. It was truly fascinating to have access to original Bauersfeld's documents and pictures taken during the construction of the dome (figure **2.3**).

Figure 2.3: *On the left, negative and positive picture of the construction of the first Zeiss dome in the picture archive. On the right, the documents containing the planes and details of the studied structure.*

2.1.1 OVERVIEW OF THE STRUCTURE

The **geometry** of the studied structure is, therefore, a hemisphere shaped dome (a vertical line passing through the center of the sphere and the zenith of the dome forms an angle of 102,18° with a line passing through the center of the sphere and the support line of the dome) with a diameter of 16m. The steel mesh is constituted of bars (about 60 cm long, rectangular section of 8 x 20 mm), following a pattern related to the principle of geodesic spheres (4600 bars in a triangular mesh obtained from the projection into a sphere of the division in 16 parts of the icosahedron sides). There are 72 different bar lengths due to the geometrical construction method of the dome and, however, they were built with a precision of 1/20 mm; the resulting weight of the steel structure is 9 kg/m^2. The concrete shell is only 3 cm thick. All of the details of the construction details appear in the publication Kurze (2006), in the Zeiss patent (1925) and in some of the documents from the Carl Zeiss Archive.

Concerning the **materials**, we will assume that the bars are made of steel with a yield strength of 370-450 MN/m^2 and a modulus of elasticity E = 210 000 MN/m^2. The concrete used at that time had a compressive strength of 20 MN/m^2, a tensile strength of 2,5 MN/m^2 and a modulus of elasticity E = 21100 MN/m^2. These assumptions are made taking into account the materials that were used at that time, according to Bargmann (1993) and Mörsch (1923). We have a total sum of 0,45 m^3 of steel and 14,5 m^3 of concrete and the weight of the structure is 39,7 tones (3,5 tones of steel and 36,2 tones of concrete). We found some **drawings** in the Carl Zeiss Archive in Jena that are useful to understand how the structure was conceived (figures **2.4** and **2.5** and **2.6**).
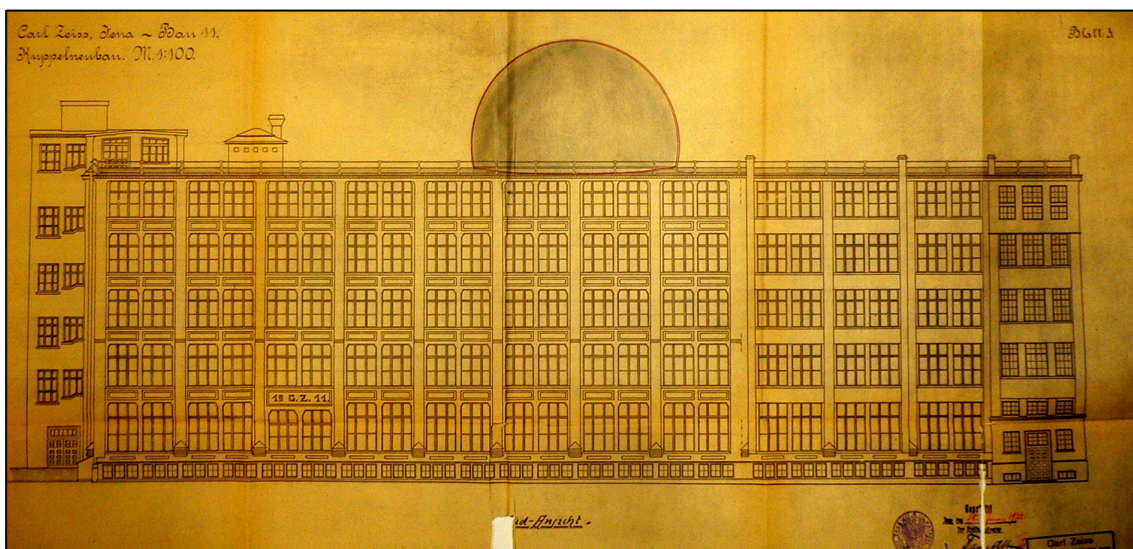
***Figure 2.4:** Elevation of the factory in which the first Zeiss dome was built.*
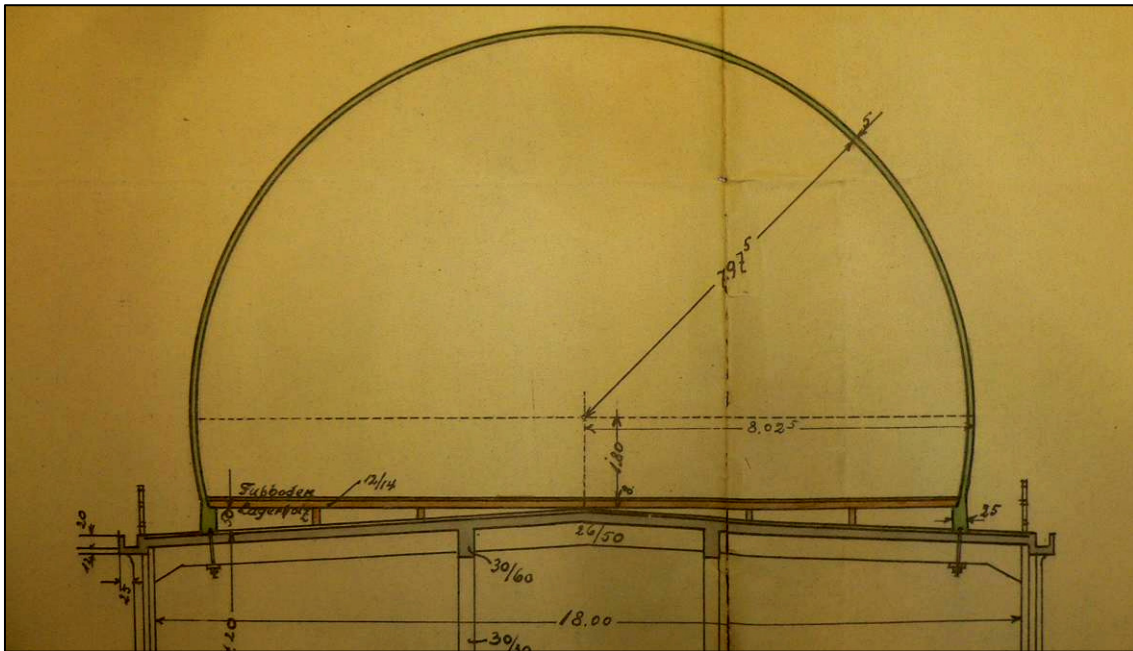
Figure 2.5: *Section of the Zeiss dome and details of the support plates. We can see how the new structure was adapted to the existing factory building.*

Figure 2.6: *Image during the construction process of the dome that is going to be studied in this chapter. We can clearly appreciate the icosahedrons inspired pattern of the mesh.*

2.1.2 CONNECTING ELEMENTS

One of the most brilliants aspects of the Zeiss system could, unfortunately, go unnoticed: the way in which the three elements are **connected**. In fact, in such a structure, the number of bars that meet in a node are not always the same, nor are the angles between them. It consisted, in its first version, of three different elements that were assembled to build a dome shaped steel mesh: **pierced bars**, **discs** (so as to assemble the bars) and **bolts and nuts**. The discs allowed, then, to connect such a variable system with an audacious and *simple* solution.

Before doing a theoretical approach and building our geometrical and structural model it is important to see how this connection works and which movements are allowed, and this detail is fundamental. Using the information from the *Reichspatentamt* we have built a 3D model representing the way in which the bars are connected. It is a good way to understand the system and allows us to see the allowed movements and angles for the incoming bars (see figures **2.7**, **2.8** and **2.9**).
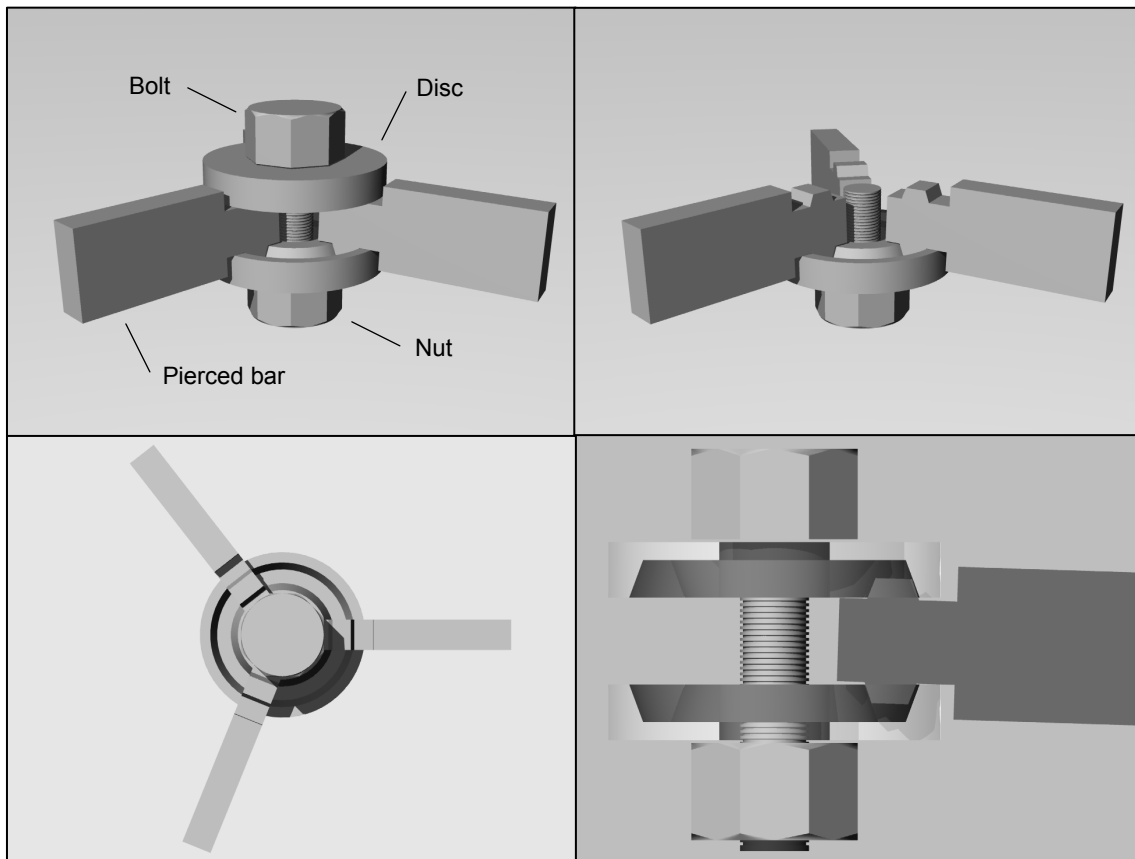
Figure 2.7: *Two perspective views from the connection system for the bars (upper images) and a plan view and a side view of the same system (lower images). In the right lower image we can see how this simple system hides a high complexity concerning the allowed angles for the incoming bars.*
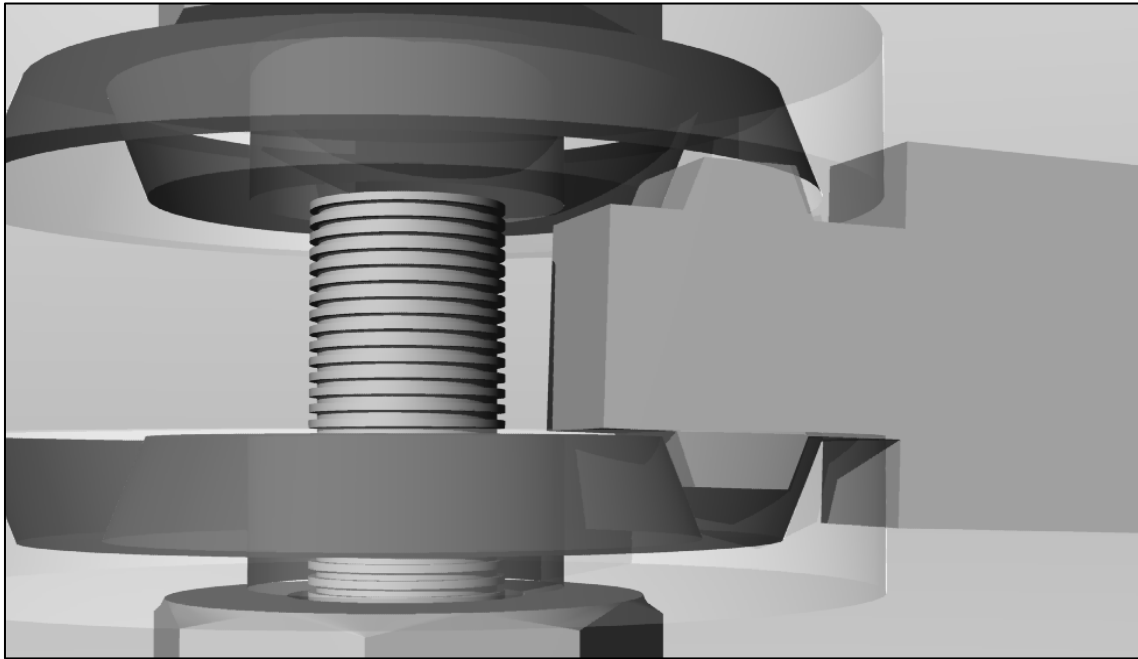
Figure 2.8: *Detail in perspective of the connection system.*

The contact between the incoming bar and the disc is the more delicate part of the mechanism, as it defines the allowed movements. It is precisely those contact points that must be analyzed in order to determine where the system could fail.
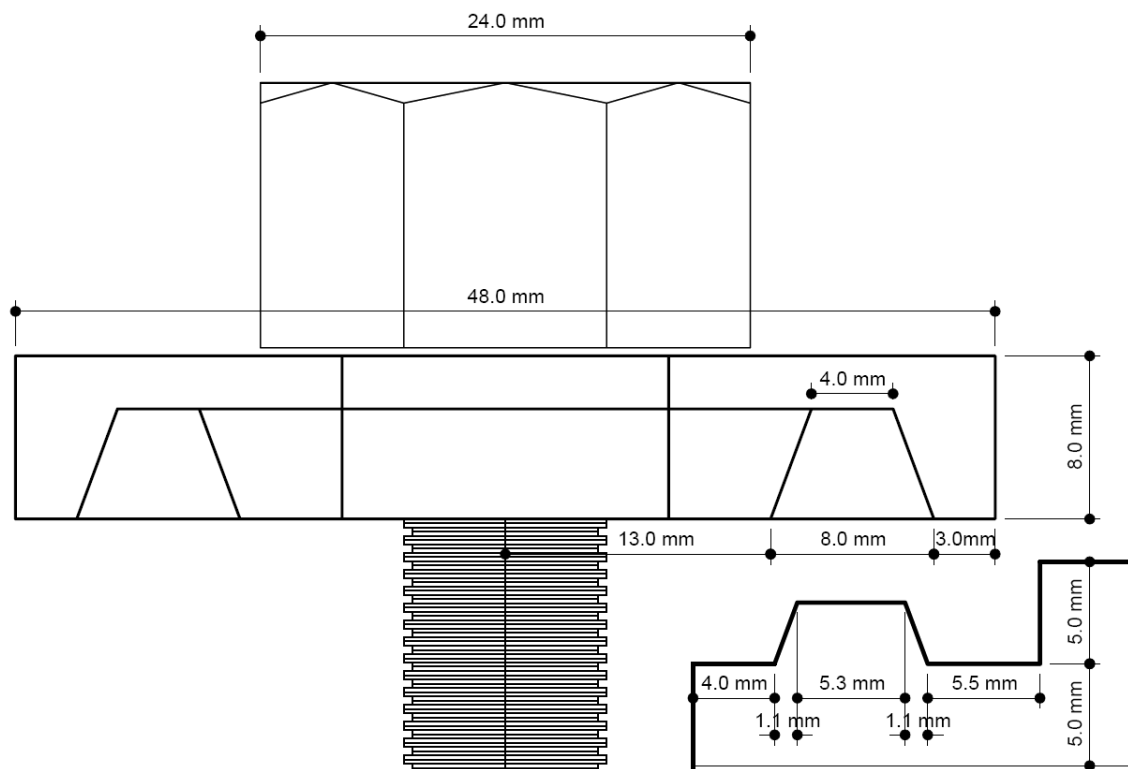
Figure 2.9: *Dimensional details of the steel nodes. Proportional to the patent illustration.*

We have done an angle analysis to understand how the bars are integrated in this system, how *free* are they and how the mechanism could potentially fail (see figures **2.10**). Further analysis by means of a finite-element (FE) calculation could be done, but it is not the purpose of the present study. The sections of the bars are shown divided and shaded in order to highlight the different parts of the design.
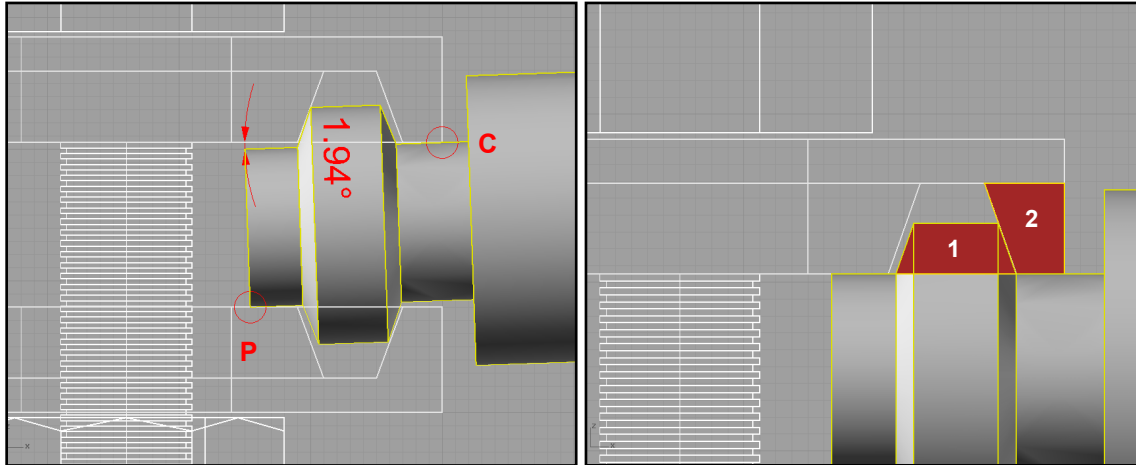
Figure 2.10: *Maximal rotation angle of the incoming bars, center of the rotation (C) and contact point (P) (left image). In the right image we can appreciate the most sensible areas (1 and 2) in terms of stresses: the surfaces separating each of those areas to the object to which they belong are critical.*

These elements are very important for the design phase of the structure. We have to pay close attention not only to the mechanical aspects (in this case, the stresses in the sensible areas) but also to the construction of the structure (for example, the maximal permitted rotation angle has to be bigger than the angle required to obtain the spherical shape). The assembly and realization of the steel mesh is very complex and requires great attention to detail.

2.1.3 GEOMETRICAL BACKGROUND

An introduction to **geodesic spheres** helps to perfectly define the model that we wish to build. Although a sphere is a very simple geometric element to describe - we can determine it just with a point (center) and a distance (radius) -, it is not easy to model as it has to de discretized. In 1954 R.Buckminster Fuller (figure **2.11**) first displayed a geodesic dome at the Milan Triennale; it made a lasting impression despite the fact that engineer Bauersfeld and his team first introduced this idea in 1922.
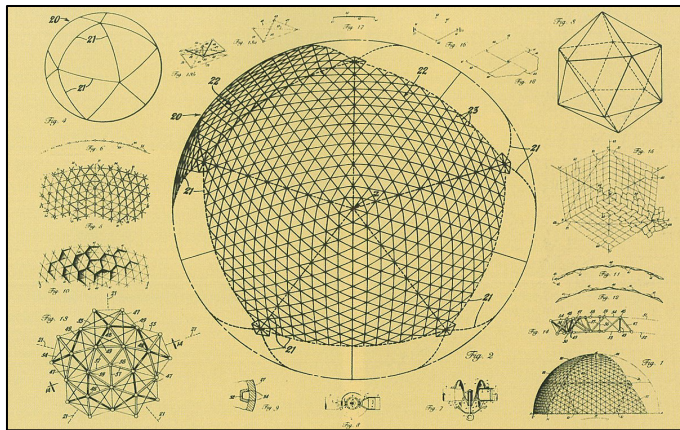
Figure 2.11: On the left, we can see Buckminster Fuller's patent for geodesic domes. His most important realization was in 1967, with the construction of a dome for the American pavilion in the universal exhibition in Montreal.

In fact, a geodesic sphere is a polyhedron that attempts to reproduce the shape of a sphere. Therefore, all vertices lie on a common sphere and certain sequences of vertices are arranged on great circles of the sphere (geodesics). All faces are triangles but not always congruent.

Those spheres are generated thanks to **Platonic solids.** There are only 5 solids of this kind: tetrahedron, cube, octahedron, dodecahedron and icosahedron; we can say that a convex polyhedron is Platonic solid if all faces are congruent regular polygons and if, at each vertex, the same number of faces meet. These solids can all be inscribed in a sphere in such a way that the vertices are contained in that sphere and are equally distributed.

Although we could also start with the other Platonic solids, we usually use the icosahedron as it closely approximates the sphere. There are **two alternatives** (Pottmann et al., 2007) that produce slightly different geodesic spheres; in both cases we obtain faces which are incongruent.

One option is to subdivide each face of the solid into a regular pattern of triangles (we create *n-1* new vertices by dividing edges into the desired *n* number of equal segments, as we see in figure **2.12**) and then project (figure **2.13**) the new vertices into the circumsphere of the Platonic solid. The resulting solid is the desired geodesic sphere level *n* (figure **2.14**) (the term "frequency" is sometimes used instead of "level").
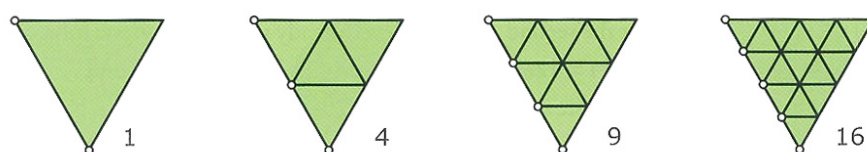
Figure 2.12: Division of one face into the desired number of equal segments (alternative 1).
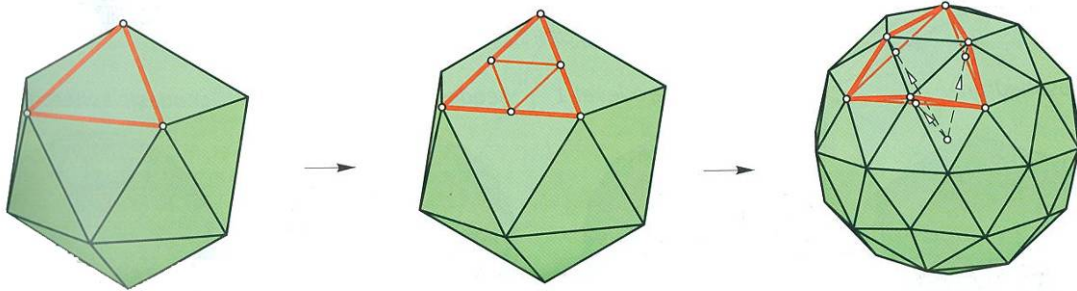
Figure 2.13: *Illustration showing the whole process used to obtain, in this case, a geodesic sphere level 2 using the first method of construction.*
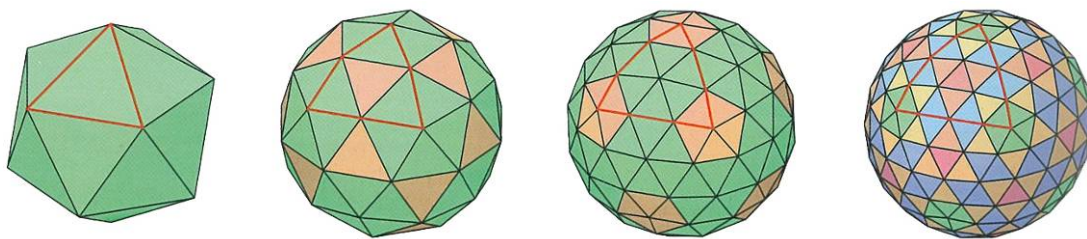
Figure 2.14: *Illustration showing the original icosahedron and the geodesic spheres of levels 1,2 and 3. The first method of construction has been used and the congruent faces are painted in the same color.*

Alternatively, we can repeat the following iterative process *n* times: we take our solid (which is the icosahedron only in the initial step), divide its edges into two segments and project the new vertices into the circumsphere of the Platonic solid. The next *n-1* steps begin with the solid resulting from the previous step. The solid we obtain is the desired geodesic sphere level *n* (figure **2.15**), different from the geodesic sphere level *n* obtained using the first method. A detailed explanation is given in figure **2.16**.
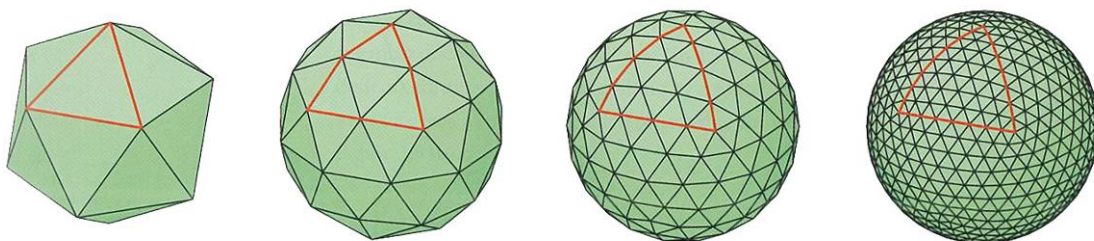
Figure 2.15: *Illustration showing the original icosahedron and the geodesic spheres of levels 1,2 and 3. The second method of construction has been used.*
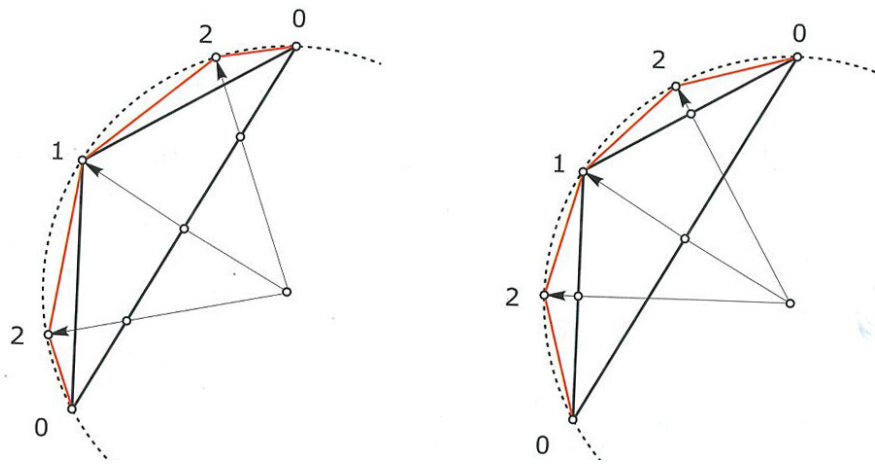
Figure 2.16: *If we take a circular section, we can easily understand why the order of subdivision matters: on the left (alternative 1) we project the vertices contained in the original icosahedron while on the right (alternative 2) we project the vertices contained in the solid obtained in the step before.*

In order to build a model of the planetarium in Jena we will use the first construction method, as it perfectly fits the geometry of the studied structure. Thus, our object of study is half (and a little more) of a geodesic sphere level 16 (alternative 1), called also hemispherical dome level 16 (alternative 1). To obtain the final geometry from the complete sphere, we will have to trim it: talking in terms of the original icosahedron structure, we will remove five original triangles having a common vertex and we will cut the ten original triangles having a common side or vertex with the previous five triangles obtaining five 11-subdivided triangles and five trapezoids.

The **level of the geodesic dome** can play a very important role in the conception and construction of the dome. Different levels lead to different bar lengths and distribution, making the assembly easier or harder and making the final structure more or less accurate. Thus, it is not a trivial question to choose the level for a given geodesic dome structure, as we have to take into account many different aspects. In the following chapters we are going to present some approaches related to this subject which can allow us to better understand the influence of the degree of subdivision of the initial icosahedron.

2.1.3.1 Study of bars' length

First of all, we would like to summarize some of the main geometrical properties of the steel mesh. As we are discussing quite a large amount of geometrical objects, we have decided to analyze its properties so as to provide a good overview. The bar length is one of the most important parameters, as it will be fundamental to successfully assemble the structure. Furthermore, it is important to highlight the fact that the way to proceed in such a study is to first analyze the properties of one of the **original triangles** (an *original* face of the icosahedron) and extrapolate the results

knowing that the complete structure is composed of parts of them. In the following table **2.1** and table **2.2** we can see a summary of those properties, going from the general case of a geodesic sphere level *n* to our particular case (Zeiss dome). We have used the statistics software *SPSS PASW Statistics 17.0* to analyze the bars length.

…in the **original triangle level n**	$S_t (n) = 3 * n (n+1) / 2$
…in the **sphere level n**	$S_s(n) = 30 * n * (n-1)$
…in the **Zeiss dome**	$10 * S_t (16) + 5 * S_t(11) - 5 * (S_t(5) - 5) - 10 * 16 - 10 * 11 =$ **4600**
…of **different length**	$L (n) = (n) * (n+2) / 4$ for even *n*, $L (n) = (n+1)^2 / 4$ for odd *n* $L(16) =$ **72**
….in the **original triangle level n**	$F_t (n) = n^2$
… in the **sphere level n**	$F_s(n) = 20 * n^2$
… in the **Zeiss dome**	$10 * F_t (16) + 5 * F_t (11) - 5 * F_t (5) =$ **3040**

Table 2.1: *General properties of geodesic spheres level n and the Zeiss dome.*

Mean of the bars length *l* (mm)	604,92
Median of *l* (mm)	615,27
Mode of *l* (smallest) **(mm)**	564,65
Standard deviation (mm)	41,46
Range (mm)	198,20
Minimum value of *l* (mm)	462,64
Maximum value of *l* (mm)	660,84
Different values of *l*	72

Table 2:2 *Properties of the bars length in the Zeiss dome.*
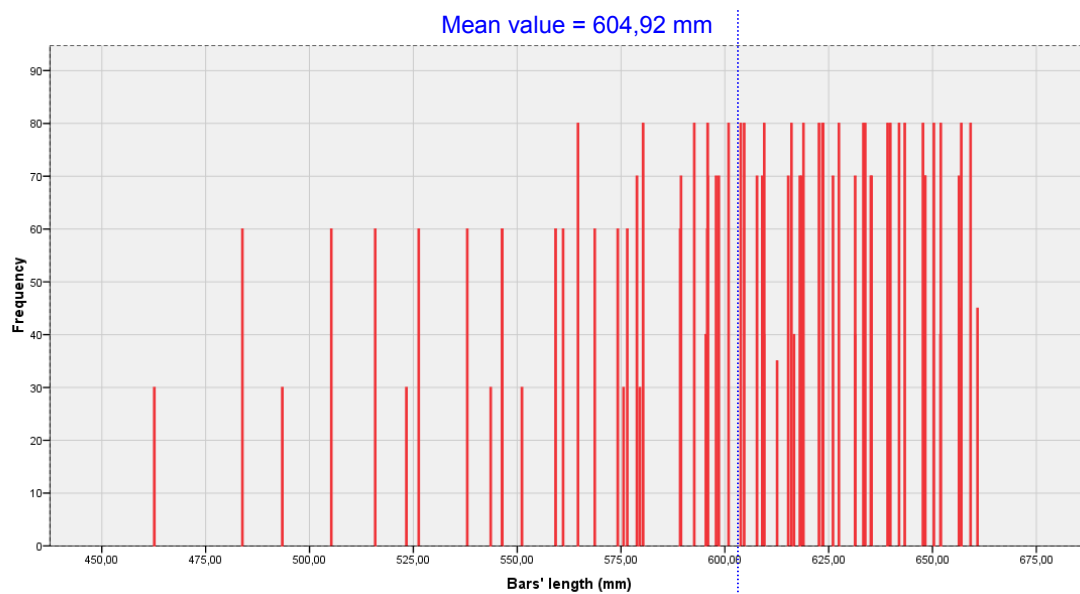
Figure 2.17: *Histogram showing the distribution and frequency of the bars length in the Zeiss dome.*

As we are not studying the complete sphere or exactly half of it, it is more difficult to extract some conclusions from these tables and the preceding figure **2.17** and table **2.3**.

VALUE (MM)	FREQUENCY	PERCENT	CUMULATIVE PERCENT	VALUE (MM)	FREQUENCY	PERCENT	CUMULATIVE PERCENT
462,64	30	0,7	,7	609,49	80	1,7	49,1
483,85	60	1,3	2,0	612,58	35	0,8	49,9
493,46	30	0,7	2,6	615,27	70	1,5	51,4
505,25	60	1,3	3,9	616,04	80	1,7	53,2
515,83	60	1,3	5,2	616,66	40	0,9	54,0
523,34	30	0,7	5,9	618,07	70	1,5	55,5
526,30	60	1,3	7,2	618,46	70	1,5	57,1
537,99	60	1,3	8,5	618,94	80	1,7	58,8
543,63	30	0,7	9,1	622,66	80	1,7	60,5
546,36	60	1,3	10,4	623,48	80	1,7	62,3
546,39	60	1,3	11,7	623,67	80	1,7	64,0
551,15	30	0,7	12,4	626,03	70	1,5	65,5
559,25	60	1,3	13,7	627,47	80	1,7	67,3
561,07	60	1,3	15,0	631,37	40	0,9	68,2
564,65	80	1,7	16,7	631,38	70	1,5	69,7
568,69	60	1,3	18,0	633,35	80	1,7	71,4
574,22	60	1,3	19,3	633,79	80	1,7	73,2
575,61	30	0,7	20,0	635,15	70	1,5	74,7
576,52	60	1,3	21,3	635,33	70	1,5	76,2
578,84	70	1,5	22,8	639,19	80	1,7	77,9
579,54	30	0,7	23,5	639,38	35	0,8	78,7
580,33	80	1,7	25,2	639,84	80	1,7	80,4
589,25	60	1,3	26,5	641,95	80	1,7	82,2
589,45	70	1,5	28,0	643,31	80	1,7	83,9
592,63	80	1,7	29,8	647,70	80	1,7	85,7
595,43	40	0,9	30,7	648,19	70	1,5	87,2
595,78	60	1,3	32,0	648,25	70	1,5	88,7
595,87	80	1,7	33,7	650,32	80	1,7	90,4
595,90	70	1,5	35,2	651,90	40	0,9	91,3
597,90	70	1,5	36,7	652,00	80	1,7	93,0
598,56	70	1,5	38,3	656,36	70	1,5	94,6
600,89	80	1,7	40,0	656,37	45	1,0	95,5
603,84	80	1,7	41,7	656,93	80	1,7	97,3
604,67	80	1,7	43,5	659,16	80	1,7	99,0
607,74	70	1,5	45,0	660,84	45	1,0	100,0
609,01	70	1,5	46,5	Total	4600	100,0	
609,42	40	0,9	47,4				

Table 2.3: *Frequency and percent of the length values for the bars composing the Zeiss dome.*

However, it is interesting to know not only the distribution and frequency of the bars length, but also **where are the bars located** in the structure. It is precisely thanks to this information that we will be able to assemble the bars that form the steel mesh.

Using the script described in *2.3.1 Scripting the geodesic sphere* we have managed to produce the following figure **2.18**, in which the color of each bar depends on its length. Being *c* a coefficient between 0 and 1 (0 for the shortest bar, 1 for the longest), the gradient color is assigned as: RGB (255*coef, 0 , 255 - 255*coef). Thus, the shortest bar is drawn in blue and the longest in red.

l_{min} = 463 mm

l_{max} = 661 mm
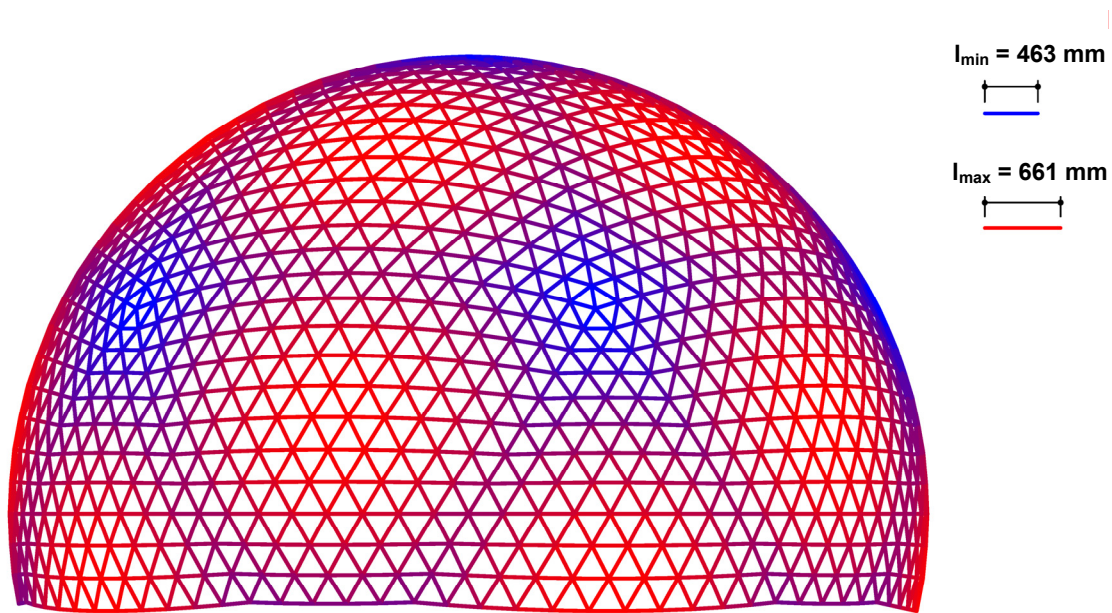
Figure 2.18: Spatial distribution of bars. Shorter bars are shown in blue, longer bars in red.

Even if in this case the steel mesh is going to be covered with shoot-concrete, it can also be interesting to look at the faces area of the Zeiss dome. It is, obviously, going to follow the same pattern, as the area is related to the bars length. Once again, we have used the scripted structure to obtain the desired information and translate it into a graphic result, shown in figure **2.19**.

We can clearly see how the areas which are near to the vertices of the original icosahedron contain the shortest bars and the faces with smallest area: the further we are from the original vertices, the biggest is the **distance-distortion effect** when projecting the vertices onto the ideal sphere. The way we have conceived our mesh obviously determines its properties.
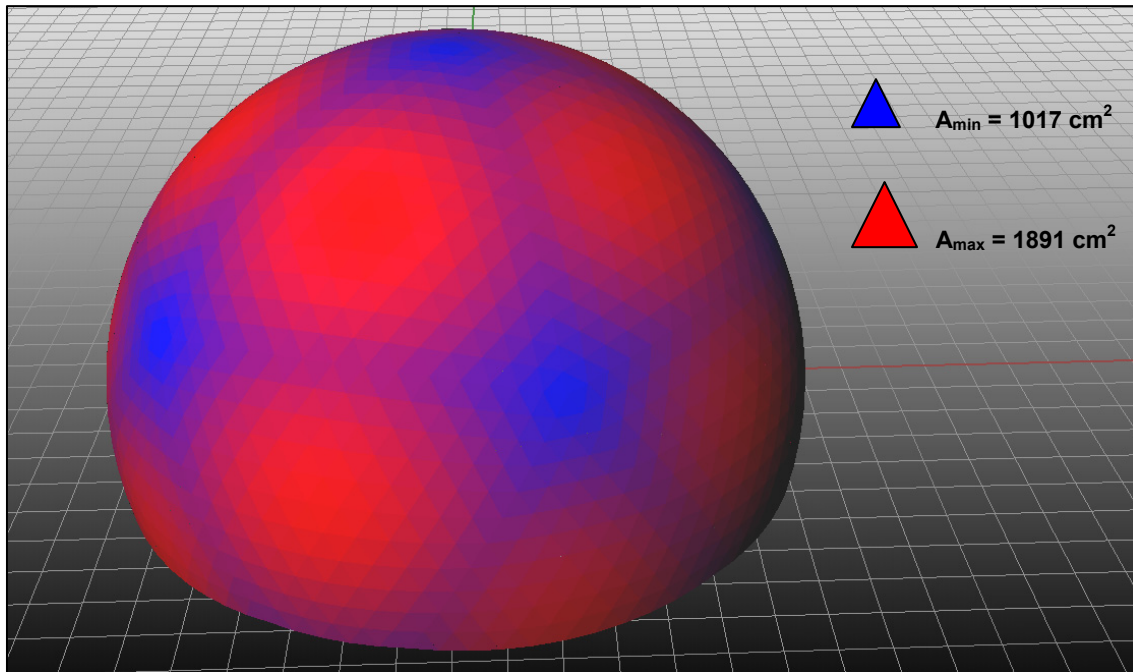
Figure 2.19: Spatial distribution of faces. Faces with smaller area are shown in blue, bigger faces in red.

Finally, we have designed an adapted model in which we can also see the bar length and its position (figures **2.20** and **2.21**). This kind of support is very useful and even essential to make possible the **assembly** of the bars.
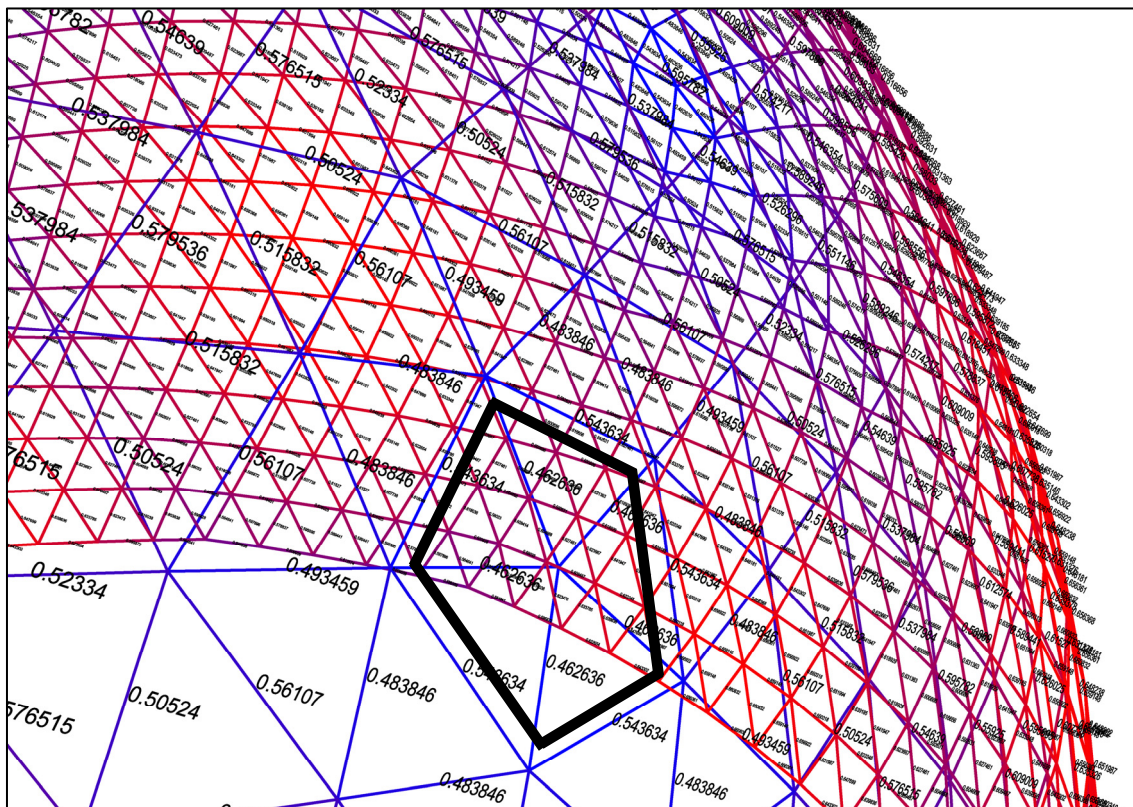
Figure 2.20: Detail of the assembly model in which each bar has a label with its length.
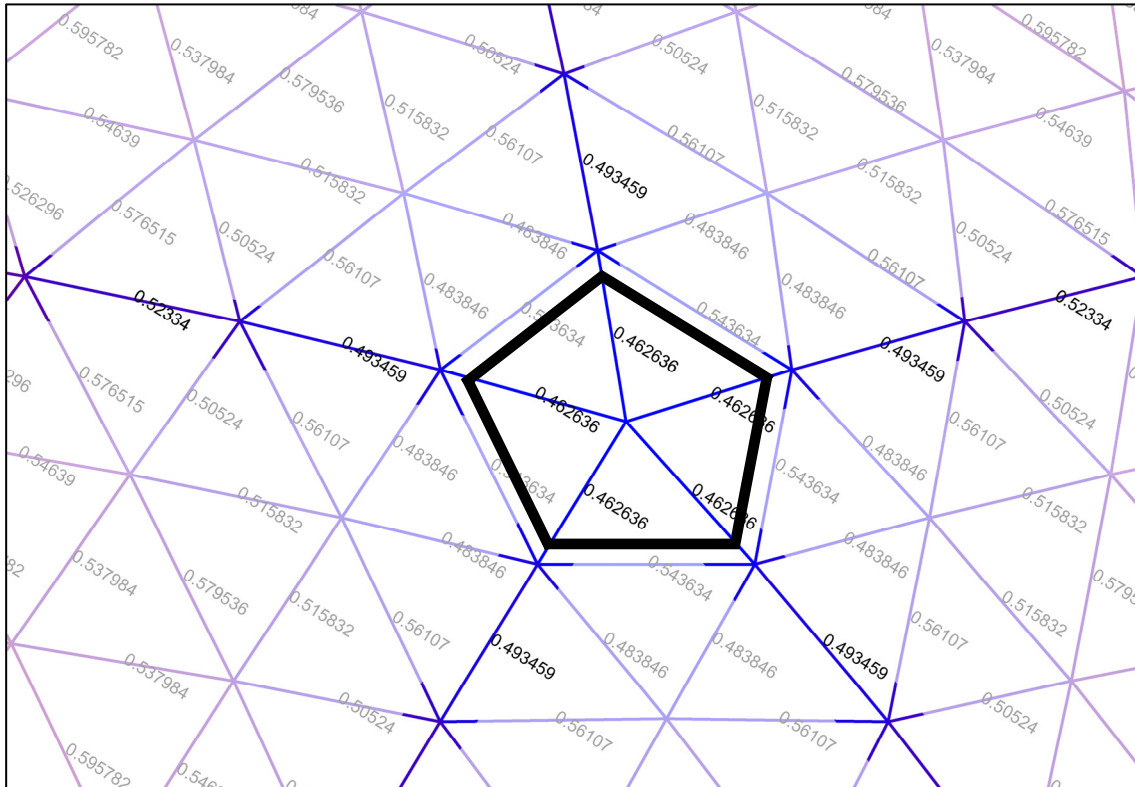
Figure 2.21: *Detail of the assembly model showing the symmetry around the original icosahedron vertex.*

2.1.3.2 Study of angles between bars

Another important aspect to analyze to understand how the mesh can be assembled is the angles between bars. We have already seen that, according to the design of the nodes, the **maximum allowed angle** is circa 4° (2° for each incoming bar in a node). There must also be, however, a minimal angle value to avoid instability phenomena. Let us see how the level of a geodesic sphere determines the angle between its faces (table **2.4**).

Geodesic sphere level	Maximal angle between faces
1 (icosahedron)	40,810 °
5	5,813 °
6	4,588 °
7	3,771 ° **< 4 °**
10	2,432 ° **< 4 °**
16 (Zeiss dome)	1,407 ° **< 4 °**
25	0,939 °**< 4 °**
50	0,410 ° **< 4 °**

Table 2.4: *Maximal angle between the faces of a geodesic sphere level n.*

Thus, it is only for a level equal to or bigger than 7 that the connection system for nodes would work. It also important to highlight the fact that the maximal angle between faces occurs near the barycenter of each *original* triangle: in this area the bars have a maximal length and, as their vertices lie on the ideal sphere, the angle between them is maximal. The complete list of values is in the *Annex 5.2*.

2.1.3.3 Study of accuracy

Finally, apart from conceiving a structure that must be built, we may also require a certain degree of accuracy, depending on the use of the structure. We can imagine that in the conception of Zeiss dome a quite high degree of **accuracy** was required, as it had to be used to test a research projector.

The parameter used to rate the accuracy is the total surface of the **geodesic sphere** faces compared to the **surface** of the **ideal sphere** (we consider a constant radius of 8 m). We have computed these values, thanks once again to the script, obtaining the following table **2.5** :

Ideal sphere area	Geodesic sphere **level**	Geodesic sphere **area**	**Accuracy**
$A (R) = 4 * \pi * R^2$ **A (R=8) = 804,248 m^2**	1 (icosahedron)	A (R=8) = 612,771 m^2	76,192 %
	5	A (R=8) = 794,460 m^2	98,783 %
	10	A (R=8) = 801,778 m^2	99,693 %
	16 (Zeiss dome)	A (R=8) = 803,281 m^2	99,880 %
	25	A (R=8) = 803,852 m^2	99,951 %
	50	A (R=8) = 804,149 m^2	99,988 %

Table 2.5: *Accuracy study of geodesic spheres according to their area.*

Thus, we can see how, as we expected, the degree of accuracy of the Zeiss dome is very high (this degree does not change if we consider the whole geodesic sphere or the part that constitutes the Zeiss dome). It is also important to highlight the fact that in the lowest levels the increase of accuracy is more important: building a geodesic dome level 16 or level 25 does not involve a great increase in the accuracy but represents a really important problem in terms of assembly due to the high number of elements.

The complete list of values is in the *Annex 5.2*.

2.1.3.4 Design tool

We will conclude this first part of the study with a graphic (figure **2.22**) which summarizes the most important elements concerning the geodesic spheres that have been analyzed. It is only by means of such an overview that we can understand all the elements contributing to the complexity of this structure and, thus, **decide** which is the more appropriate level when conceiving a geodesic dome. We have adopted a maximal value of n=50 as the analysis is the same for higher values.
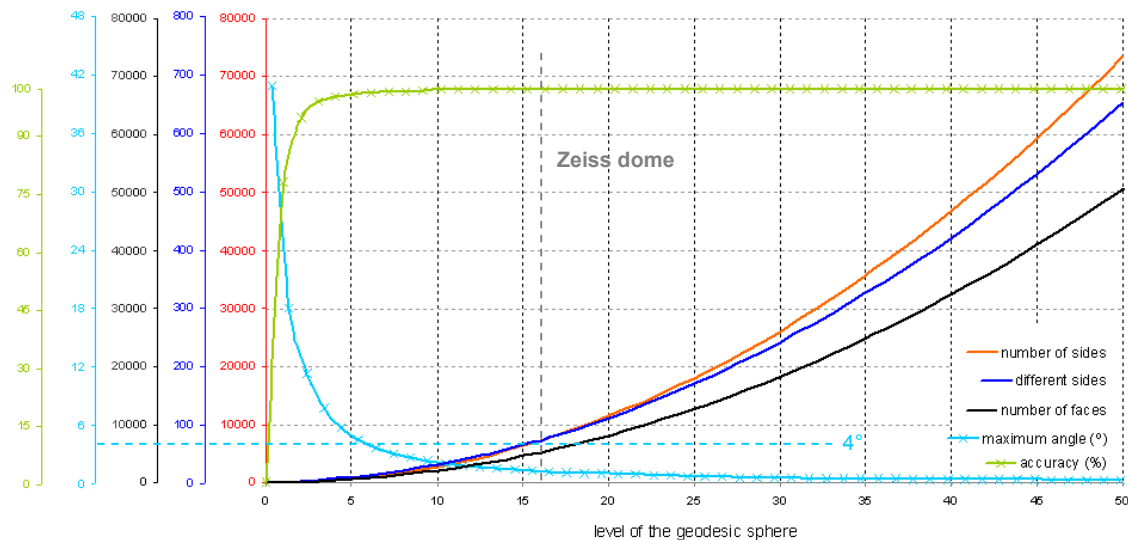
Figure 2.22: *Graphic showing the main properties of a geodesic sphere according to its level.*

As we could already deduce from the analytical expressions, the number of sides, the number of different sides and the number of faces have a **quadratic growth**. The curves for the accuracy and the maximal angle are an interpolation of the values found thanks to the script. The complete list of values is in the *Annex 5.2*.

These geometrical aspects are related to the way in which the Zeiss dome was designed and built. It is in this sense that we will describe the construction method, even if we do not know all the details as the structure was built in 1922.

2.1.4 CONSTRUCTION METHOD

The description of the construction method will be only **qualitative** and quite intuitive as there are no documents detailing the whole process. We have used some drawings and pictures from the Carl Zeiss Archive in Jena to deduce how the structure was built and we have elaborated other figures to explain it clearly.

As the dome was built on the roof of an existing factory, the first step was to conceive a **concrete ring** in which to support the structure. It was a good way of assuring the correct transmission of forces and fixing the inferior part of the structure. This concrete ring was fixed in the existing concrete beams of the factory.

The second step consisted of building the **steel mesh**. We retrieved some information concerning this part of the process in other domes using the same system but many differences exist. In our case of study, they began to assemble the zenithal bars of the dome. A framework system allowed them to gradually elevate the completed structure and proceed to the next level. Thus, it was unnecessary to install falseworks and workers could do their job in comfortable conditions on the roof of the factory (figure **2.23**). The fact that the existing factory could not support a big overload was probably at the origin of this decision as in the other structures of the same type the assembly of the bars was done in the inverse direction.
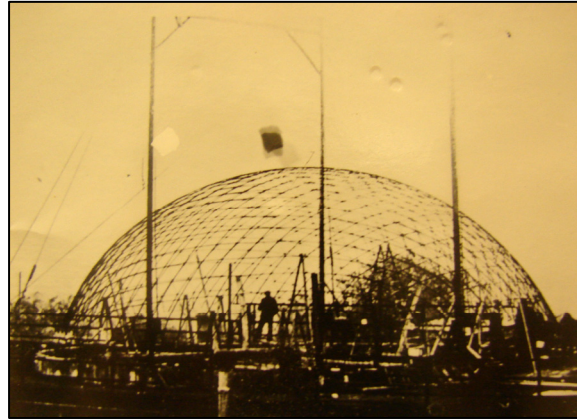
Figure 2.23: *Assembly of the steel mesh with the framework elevator system.*

This process was completed thanks to the shown node system and with an appropriate assembly plan detailing the position of the 72 different bar types. The precision of the elements and the assembly was fundamental to reach the desired structure shape. With the correct assembly of the bars we automatically obtain the conceived dome.

The construction of the **concrete shell** is also a very delicate stage. The idea was to install wood formworks of approximately 3 m x 3 m in the internal part of the dome, from the lower part to the higher and in rings. Once the formworks were installed, a thin layer (3 cm) of shot-fast hardening concrete was applied on the surface. The formworks could be used more than once as the curvature of a sphere is constant.

The last step consisted in covering the concrete shell with an appropriate **roofing** (figure **2.24**), in this case with metallic plates.
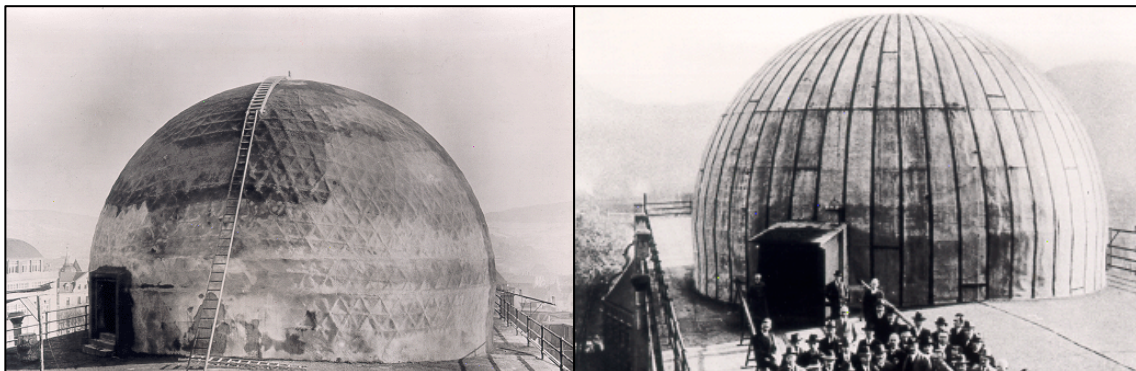
Figure 2.24: *On the left, a view of the completed concrete shell; we can still appreciate the presence of the steel structure due to the shot concrete method. On the right, the finished structure the day of its inauguration.*

Below are pictures intended to illustrate the different stages of the construction method (figure **2.25**).
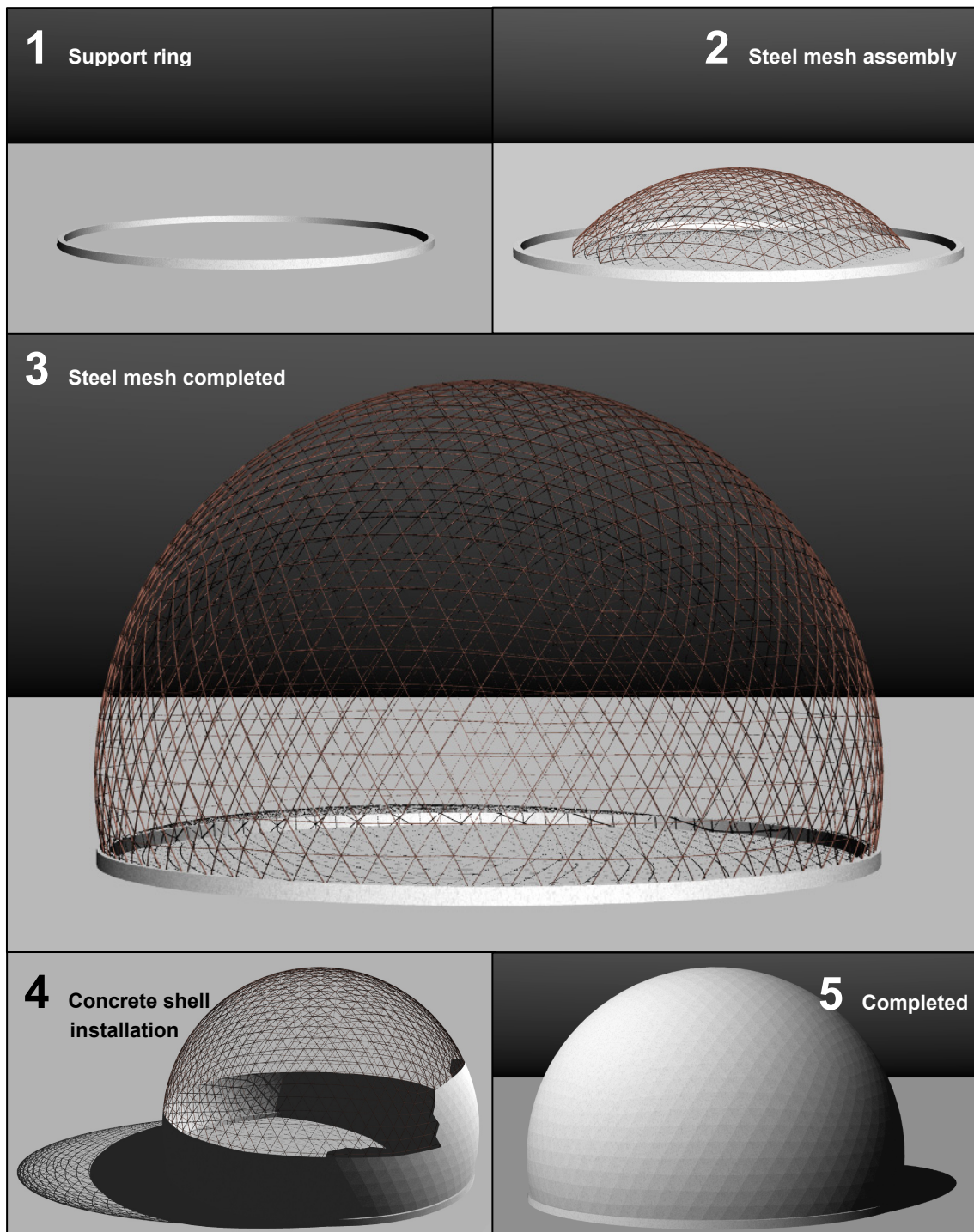
Figure 2.25: *Five render views showing the construction stages of the Zeiss dome.*

We have also produced a **video** to show how the structure was integrated into its environment. It helps to have a general overview of the factory in which the dome was

built, its final aspect and how the nodes were connected. We have joined some render views of the video which illustrate its most important parts (figure **2.26**).

We have used the 3D modeling software *Google Sketch Up 7.0* and *Autodesk 3D Studio Max 9.0*.
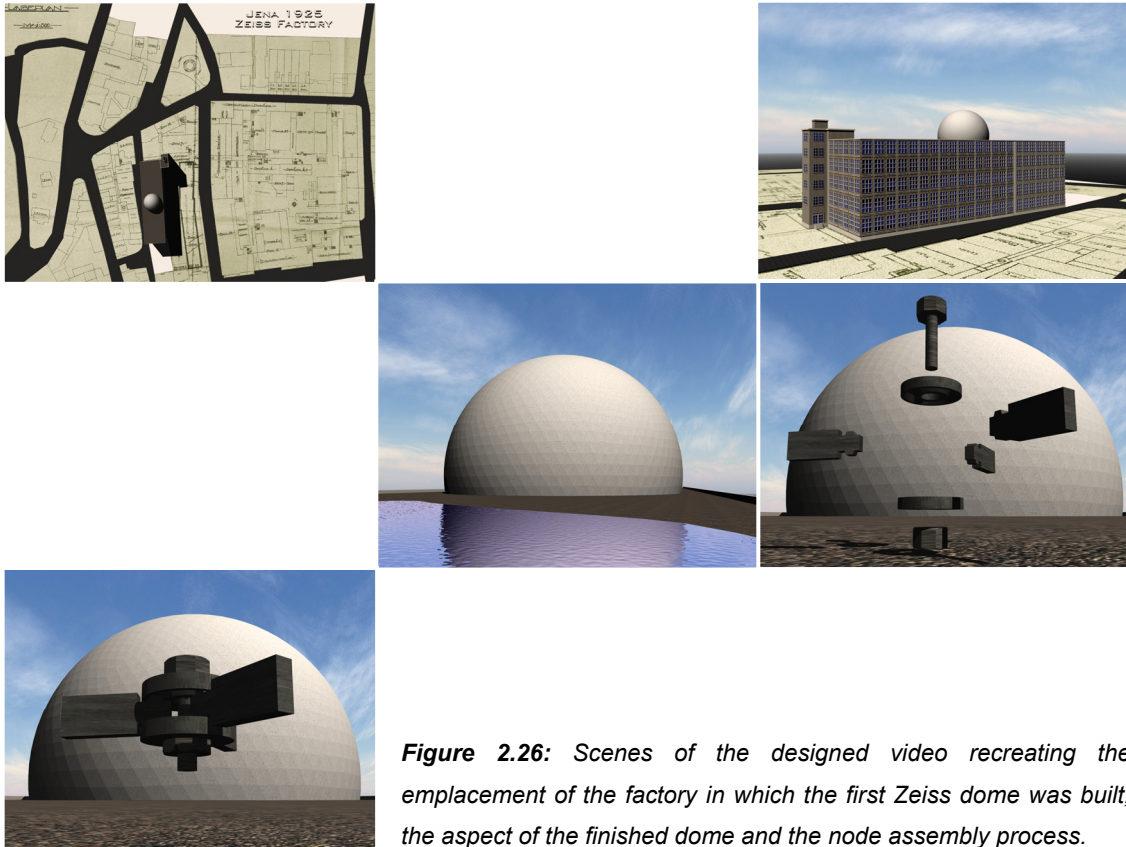
Figure 2.26: Scenes of the designed video recreating the emplacement of the factory in which the first Zeiss dome was built, the aspect of the finished dome and the node assembly process.

Finally, it is important to highlight the fact that the execution of such a process requires a previous theoretical reasoning, presented in the following chapter, justifying the dome stability.

2.2 Theoretical approach by means of the shell theory

As this is not intended to be a deep study centered upon the shell theory, which merits more time and dedication, we will present in this chapter some of its results without following the entire deductive process. The aim is to obtain some analytical results which can be compared to the results obtained using the finite-element calculation, keeping in mind the theoretical background.

Another important decision at this point was the choice between the approaches to the shell theory. On the one hand, we could have presented the whole basis of the theory using **differential geometry** (Bisch, 1997), in order to understand the essential role of the curvature of the surfaces in its structural behavior. However, this approach requires a lengthy mathematical development, which, although truly fascinating, is too wide and powerful for our case study.

On the other hand, we can *easily* deduce how a dome structure behaves by looking at one part of it and establishing some balance equations (Girkmann, 1978). Conceptually, it does not provide such a general approach, but is nevertheless quite efficient and practical for our study. Thus, we have decided to retain this approach, which is presented below.

Surfaces with single or double curvature will be referred to as shells. Loads in these structures are mainly equally distributed in the wall thickness, parallel to the middle surface active interior force (extension force), until they reach the supports. Other more complete works concerning the shell theory aim to present a complete representation of the final equations, valid for all coordinate systems and shapes. In this sense, they normally proceed so as to reach an application, doing without the geometry approach. Thus, we will consider **some special shell shapes** that can be *easily* calculated using simple mathematical resources. We will work with the *Kirchhoff-Love* theory.

The analytic approach will allow to compare its results to those obtained with the finite-element calculation. As the dome has both a concrete and a steel structure, we will be able to analyze the different models and to understand how both parts contribute in the static behavior.

2.2.1 SHELLS

We will assume the following facts (Girkmann, 1978) so as to calculate shells in a simplified way:

- The shell thickness is small compared to the other dimensions of the shell.
- The shell deflection is small compared to his thickness.

- Points that lie in a perpendicular line to the middle surface before a change in the shape of the shell remain in a deformed line that is always perpendicular to the deformed middle surface.

- The normal stresses perpendicular to the middle surface can be neglected.

In the following figure **2.27** we have a $\delta = 2h$ thick element limited perpendicularly to the middle surface by the $x = constant$ and $y = constant$ sections (x,y curvilinear coordinates). The associated radii of rotation are r_y and r_x. In the side $x = constant$ we can find the stress components σ_x, τ_{xy} and τ_{xz} and in the side $y = constant$ σ_y, τ_{yx} and τ_{yz}. The magnitude of these variables is related to the distance z from the middle surface. We can also appreciate the considered forces and moments.
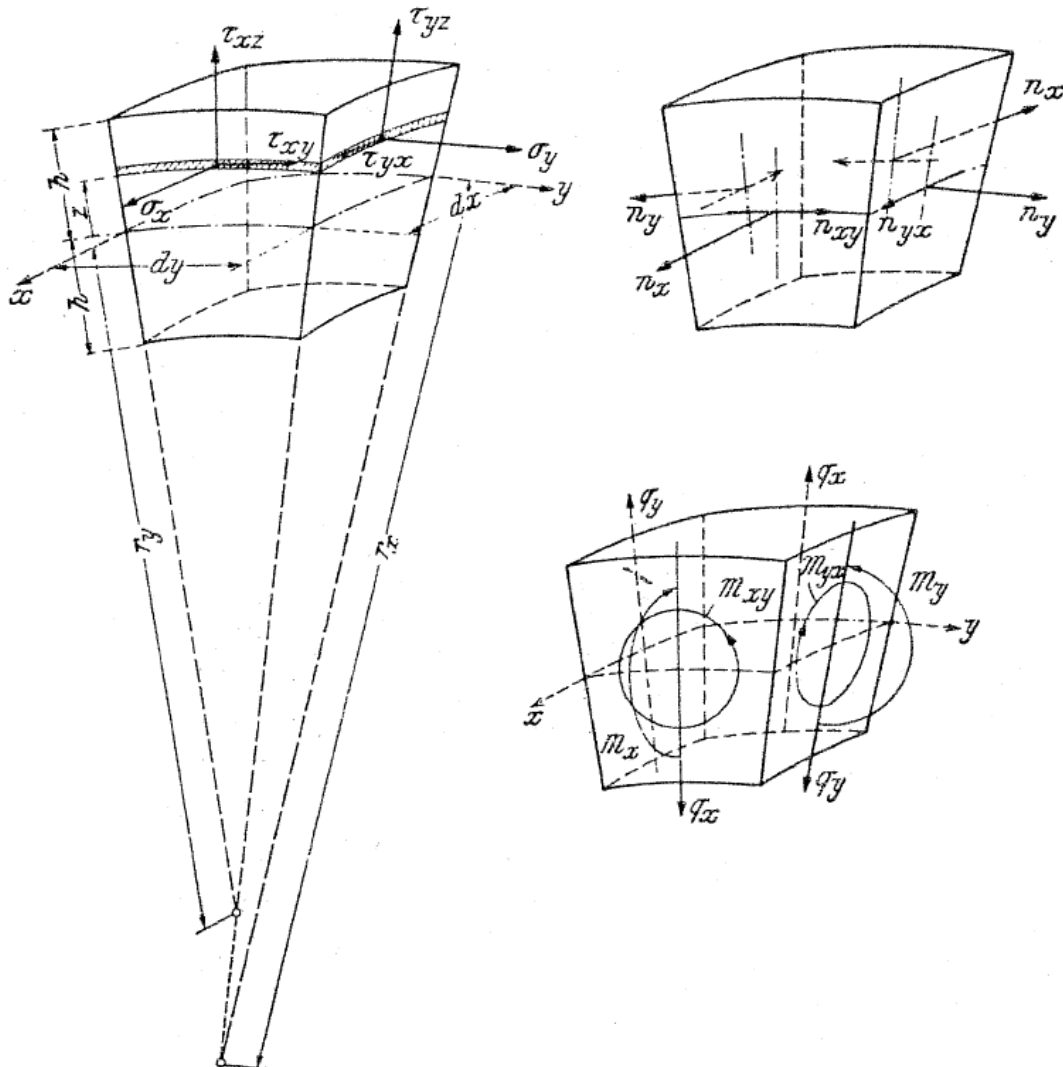
Figure 2.27: *View of the element and the stresses and forces acting in it.*

The width of the sides of the considered element is variable. For, respectively, *c = constant* and *y = constant*, the width *w* is, in *z = 0,* equal to:

$$w_x = \frac{r_y + z}{r_y} \qquad\qquad w_y = \frac{r_x + z}{r_x}$$

Thus, we can deduce (Girkmann, 1978) the **expressions of the forces and moments** acting in our section:

$$n_x = \int_{-h}^{+h} \sigma_x (1 + \frac{z}{r_y}) \mathrm{d}z \qquad\qquad n_y = \int_{-h}^{+h} \sigma_y (1 + \frac{z}{r_x}) \mathrm{d}z \tag{1}$$

$$n_{xy} = \int_{-h}^{+h} \tau_{xy} (1 + \frac{z}{r_y}) \mathrm{d}z \qquad\qquad n_{yx} = \int_{-h}^{+h} \tau_{yx} (1 + \frac{z}{r_x}) \mathrm{d}z \tag{2}$$

$$m_x = -\int_{-h}^{+h} \sigma_x (1 + \frac{z}{r_y}) z\,\mathrm{d}z \qquad\qquad m_y = -\int_{-h}^{+h} \sigma_y (1 + \frac{z}{r_x}) z\,\mathrm{d}z \tag{3}$$

$$m_{xy} = -\int_{-h}^{+h} \tau_{xy} (1 + \frac{z}{r_y}) z\,\mathrm{d}z \qquad\qquad m_{yx} = -\int_{-h}^{+h} \tau_{yx} (1 + \frac{z}{r_x}) z\,\mathrm{d}z \tag{4}$$

$$q_x = -\int_{-h}^{+h} \tau_{xz} (1 + \frac{z}{r_y}) \mathrm{d}z \qquad\qquad q_y = -\int_{-h}^{+h} \tau_{yz} (1 + \frac{z}{r_y}) \mathrm{d}z \tag{5}$$

The sign of n_x and n_y is positive for a traction. The positive sign of the other magnitudes is shown in figure **2.27**. Positive moments give (for a positive *z*) negative normal stresses and positive shear forces produce negative shear stresses.

As the sides of the element are perpendicular between them, we obtain:

$$\tau_{xy} = \tau_{yx}$$

The shear forces n_{xy} and n_{yx} and the torsional moments m_{xy} and m_{yx} are equal only when $r_x = r_y$.

Finally, we could assume that, as the width of the studied element depends on *z*, the stress components parallel to the middle surface are not linearly distributed along the shell width. However, as *h* and *z* are small compared to r_x and r_y, we can assume rectangular sides and that the normal stresses and the stresses parallel to the middle surface are linear all along the shell width.

2.2.2 MEMBRANES

In many cases, we have to assume that the middle surface stresses are equally distributed in the shell thickness $\delta = 2h$. In this case, the stress components no longer depend on z, and we obtain, from (1), (2), (3), and (4):

$$n_x = \sigma_x\delta \qquad n_y = \sigma_y\delta \qquad n_{xy} = n_{yx} = \tau_{xy}\delta = \tau_{yx}\delta \tag{6}$$

$$m_x = m_y = m_{xy} = m_{yx} = 0 \tag{7}$$

For the same reason, q_x and q_y are eliminated so as to obtain forces parallel to the middle surface. This state free of moments in the shell is called **membrane stress condition**. In this way, the middle surface only suffers a deformation and a shear force induced by the curvature. The bending stress, then, can be neglected.

The stress state of a shell can be seen as bending free when the following conditions are present (Girkmann, 1978):

- The shell has a constant curvature.

- The shell thickness does not suddenly change.

- The loads are constant in their spatial distribution and magnitude.

- The border forces are tangent to the middle surface.

- The support structure impedes the deformation of the structure creating only tangential forces.

2.2.3 REVOLUTION MEMBRANES

Since we seek to study the behavior of a dome, we are interested in the revolution shells. The middle surface of a **revolution membrane** is obtained by rotating a planar curve (meridian) around an axis that is in the same plane. The points of the middle surface are determined by means of the angle θ of the meridian plane and the angle φ that forms the normal of the shell at that point and the rotation axis. The radii of the main curvatures (meridian and transverse curvatures) are called r_1 and r_2 and that of the parallel is called r_0.

We analyze an element of the shell which has the middle surface between the meridians θ and $\theta + d\theta$ and the parallels $\varphi + d\varphi$. The forces in the section are represented by n_θ, n_φ, $n_{\theta\varphi} = n_{\varphi\theta}$. When considering a load p in this element, we will decompose it into the parallel tangent direction, the meridian tangent direction and the normal of the shell plane (components X, Y and Z). X and Y are positive in the sense of θ and φ and Z is positive in the inside direction.

In general, the stresses and the forces acting in the sections vary from a point to another. For this reason, the stresses must be expressed as functions of θ and φ. We can then write:

$$n_\theta + \mathrm{d}n_\theta = n_\theta + \frac{\partial n_\theta}{\partial \theta}\mathrm{d}\theta + \ldots$$
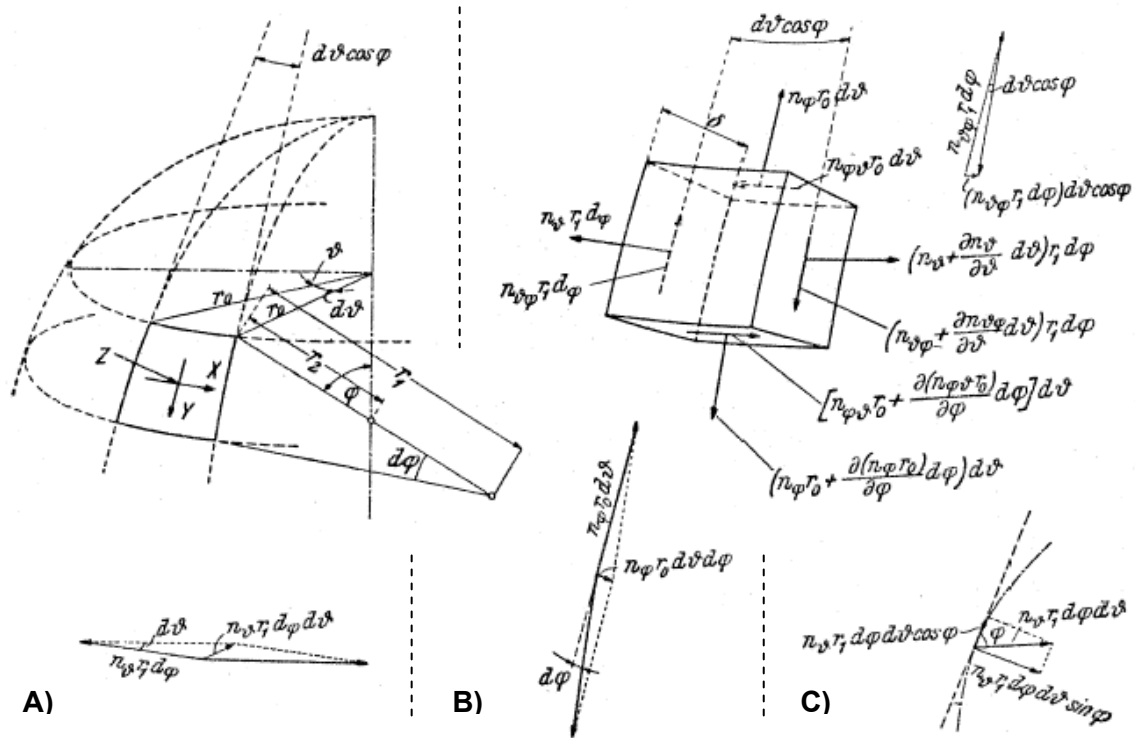
Figure 2.28: *View of the analysis of a rotation membrane. The A, B and C segments show the details of the projections.*

However, if we analyze the meridian direction, it is not only the force but also the length of the section that changes: *r₀+dr₀*. These variations result in the following expression in the side *φ +dφ* for the initial value *(n_φr₀) dθ* in the side *φ*:

$$\left((n_\varphi r_0) + \frac{\partial (n_\varphi r_0)}{\partial \varphi}\mathrm{d}\varphi \right)\mathrm{d}\theta$$

In order to clarify the notation and the reasoning, we have included the schema of figure **2.28**, which will help to establish the **balance conditions** for the membrane. We will consider the three directions of our system of reference and, for each one, we will take all the acting forces into account by projecting them in the right direction (see

figure **2.28**, details A, B and C). We can then obtain (Girkmann, 1978) the three equations, for X,Y and Z directions respectively, that follow:

$$\frac{\partial n_\theta}{\partial \theta} r_1 + \frac{(\partial n_{\varphi\theta} r_0)}{\partial \varphi} + n_{\theta\varphi} r_1 \cos\varphi + X r_0 r_1 = 0 \tag{8}$$

$$\frac{\partial n_{\theta\varphi}}{\partial \theta} r_1 - n_\theta r_1 \cos\varphi + \frac{(\partial n_\varphi r_0)}{\partial \varphi} + Y r_0 r_1 = 0 \tag{9}$$

$$\frac{n_\theta}{r_2} + \frac{n_\varphi}{r_1} = -Z \tag{10}$$

where $n_{\theta\varphi} = n_{\varphi\theta}$ and $r_0 = r_2 \sin\varphi$.

2.2.4 ROTATION-SYMMETRICAL LOAD IN A MEMBRANE

We will now integrate the resulting equations considering that we have a rotation-symmetrical load: $X = 0$, so $n_{\theta\varphi} = n_{\varphi\theta} = 0$. Equation number (8) is accomplished and for (9) and (10) we obtain:

$$n_\theta r_1 \cos\varphi - \frac{(\mathrm{d}n_\varphi r_0)}{\mathrm{d}\varphi} = Y r_0 r_1 \qquad \frac{n_\theta}{r_2} + \frac{n_\varphi}{r_1} = -Z \tag{11}$$

So

$$n_\theta = -r_2\left(Z + \frac{n_\varphi}{r_1}\right) \tag{12}$$

And, from (11),

$$-n_\varphi r_2 \cos\varphi - \frac{\mathrm{d}(n_\varphi r_0)}{\mathrm{d}\varphi} = Y r_0 r_1 + Z r_1 r_2 \cos\varphi$$

We then multiply by -sin φ and use that $r_0 = r_2 \sin\varphi$:

$$n_\varphi r_2 \sin\varphi \cos\varphi + \frac{\mathrm{d}(n_\varphi r_2 \sin\varphi)}{\mathrm{d}\varphi} \sin\varphi = -r_1 r_2 (Y \sin\varphi + Z \cos\varphi)\sin\varphi$$

By observation,

$$\frac{\mathrm{d}}{\mathrm{d}\varphi}(n_\varphi r_2 \sin^2\varphi) = -r_1 r_2 (Y \sin\varphi + Z \cos\varphi)\sin\varphi$$

We just need to integrate in terms of φ :

$$n_\varphi = -\frac{1}{r_2 \sin^2\varphi}\left(\int r_1 r_2 (Y \sin\varphi + Z \cos\varphi)\sin\varphi \mathrm{d}\varphi + C\right) \tag{13}$$

where C depends on the boundary conditions. We can then deduce n_θ from (12).

Another approach involves establishing a vertical balance of the whole structure, as shown in figure **2.29**.

If P_φ is the resultant of all the loads that are applied to the dome, we have:

Figure 2.29: Forces and geometry details in a revolution membrane.

$$P_\varphi + (n_\varphi \sin \varphi) 2\pi r_0 = 0$$

So, we can find the following expression:

$$n_\varphi = -\frac{P_\varphi}{2\pi r_0 \sin \phi} \tag{14}$$

Once again we can then deduce n_θ from (12).

We have seen how, thanks to the balance equations, we can deduce the **forces** acting in the shells. We can now for this rotation-symmetrical problem write the equations that link the **strain** with the displacements and the strain with the forces acting in the shell (from the properties of the material). Thus, we will be able to obtain the **displacements** in terms of these forces.

The results that we present now are the final part of a development done following the mechanics of solids and the strength of materials. The complete explanations can be found in Bisch (1997). We must also keep in mind that we are still in our rotation-symmetrical problem and that, from now on, $r_1 = r_2 = a$.

We consider now a local reference system in the surface of the shell, with the x-axis following the meridian direction, the y-axis in the parallel direction and the z-axis in the direction of the normal to the surface, positive to the outside. Thus, the vector of displacements can be written as *(u,v,w)*. With **small displacements** and in its linear version, the strain tensor, constant in the shell thickness (Kirchhoff-Love), has the following aspect (Bisch, 1997):

$$\varepsilon_{11} = \frac{\mathrm{d}u}{a\mathrm{d}\varphi} + \frac{w}{a} \tag{15}$$

$$\varepsilon_{12} = \frac{1}{2}\left(\frac{\mathrm{d}v}{a\mathrm{d}\varphi} - \frac{v}{a}\cot\varphi\right) \tag{16}$$

$$\varepsilon_{22} = \frac{w}{a} + \frac{u}{a}\cot\varphi \tag{17}$$

Considering a linearly **elastic, homogeneous and isotropic material** (where *e* is the thickness of the shell, *E* is the modulus of elasticity and *v* is the Poisson ratio) we can write, if we look only at the purely elastic part (Bisch, 1997):

$$\varepsilon_{11} = \frac{1}{Ee}\left(n_\varphi - \nu n_\theta\right) \tag{18}$$

$$\varepsilon_{12} = \frac{1}{Ee}\left((1-\nu)n_{\varphi\theta} - \nu(n_\varphi + n_\theta)\right) \tag{19}$$

$$\varepsilon_{22} = \frac{1}{Ee}\left(n_\theta - \nu n_\varphi\right) \tag{20}$$

Finally, we would like to comment on some aspects of the **assumptions of the membrane theory**. It is very important to remember that two conditions are required to establish balance in a membrane. On the one hand, the exterior forces applied on the shell must be compatible with the balance equations: the surface must be free of moment and the reaction in the boundary must be tangent to the surface.

On the other hand, the strains must be compatible with the different parts of the shell and the exterior. Some incompatibilities may arise due to thickness or curvature discontinuities, concentrated forces, or inappropriate kinematic boundary conditions.

In order to respect the way the dome of study was built, we will be forced not to accomplish certain of these conditions. For instance, even if the tangent to the surface at the boundary is not vertical, we will set up horizontal support plates. This procedure will lead to slightly different results for the parts of the shell near the boundary, where a local bending will appear.

2.2.5 DEAD LOAD ON A DOME SHELL

The dome has thickness *δ* and we assume a constant uniformly distributed dead load *g*. The load has the following components in terms of *φ* (Girkmann, 1978):

$$X = 0 \qquad Y = g\sin\varphi \qquad Z = g\cos\varphi \tag{21}$$

We use (12) and (14) so as to obtain the normal forces. The area over the *φ* parallel circle is:

$$O_\varphi = 2\pi a f = 2\pi a^2(1 - \cos\varphi)$$

The load acting in this part of the dome, then, is:

$$P_\varphi = gO_\varphi = 2\pi g a^2(1 - \cos\varphi)$$

Thus, we obtain from (14):

$$n_\varphi = -\frac{2\pi g a^2 (1 - \cos\varphi)}{2\pi r_0 \sin\varphi}$$

with

$$r_0 = a \sin\varphi$$

and

$$n_\varphi = -ga\frac{1 - \cos\varphi}{\sin^2\varphi} = -\frac{ga}{1 + \cos\varphi} \tag{22}$$

As we have $r_1 = r_2 = a$, we can use (12):

$$n_\theta = -a\left(Z + \frac{n_\varphi}{a}\right) \tag{23}$$

Finally, using (15) and (16) we can write:

$$n_\theta = -ga\left(\cos\varphi - \frac{1}{1 + \cos\varphi}\right) \tag{24}$$

The following figure **2.30**: is a representation of the normal forces induced by this load case. It is important to highlight the fact that the circular normal force over the angle $\varphi = 51°\ 49'$ is negative (compression) and positive under it (traction).
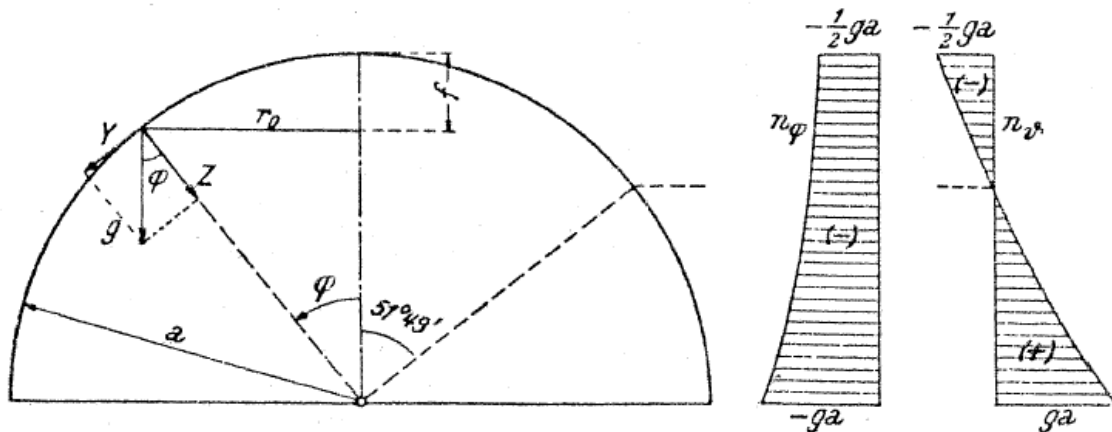
Figure 2.30: *Tangential and circular normal forces induced by the dead load in a dome shell.*

Using the preceding results and expressions (15) and (18) we can write, as any force is applied in the direction perpendicular to the radius ($n_{\varphi\theta} = 0$, $\varepsilon_{12} = 0$):

$$\frac{du}{ad\varphi} + \frac{w}{a} = \varepsilon_{11} = \frac{1}{Ee}(n_\varphi - \nu n_\theta) = -\frac{ga}{Ee}\left(\frac{1 + \nu(1 - \cos\varphi - \cos^2\varphi)}{1 + \cos\varphi}\right) \tag{25}$$

$$\frac{w}{a} + \frac{u}{a}\cot\varphi = \varepsilon_{22} = \frac{1}{Ee}(n_\theta - \nu n_\varphi) = \frac{ga}{Ee}\left(\frac{1 + \nu - \cos\varphi - \cos^2\varphi}{1 + \cos\varphi}\right) \tag{26}$$

If we subtract these expressions and integrate them, we deduce the displacement *u(φ)*. We then impose the boundary condition of no displacement in the support plates *u(φ=102,18°)=0*, obtaining the constant of integration *C₁=-1,67*. We have used (26) to write the expression of w(φ). Obviously, *v=0*.

$$u(\varphi) = -\frac{ga^2(1+\nu)}{Ee}\sin\varphi\left(-1,67 + \log\left(\frac{2}{1+\cos\varphi}\right) + \frac{1}{1+\cos\varphi}\right) \tag{27}$$

$$w(\varphi) = \frac{ga^2}{Ee}\left(\frac{1 + \nu - \cos\varphi - \cos^2\varphi}{1 + \cos\varphi}\right) + \dots$$

$$\dots + \frac{ga^2(1+\nu)}{Ee}\cos\varphi\left(-1,67 + \log\left(\frac{2}{1+\cos\varphi}\right) + \frac{1}{1+\cos\varphi}\right) \tag{28}$$

As the boundary condition is only imposed for the *u* displacement, we obtain an expression of *w* which is not null at *φ=102,18°* (support plates). Therefore, a local bending will appear. It is small, however, as we can observe in *2.3* (*Ideal shape's finite-element calculation*).

2.2.6 SNOW LOAD ON A DOME SHELL

We consider the following constant uniformly distributed snow load *p* with components (Girkmann, 1978):

$$X = 0 \qquad Y = p\sin\varphi\cos\varphi \qquad Z = p\cos^2\varphi \tag{29}$$

Over the parallel *φ* we have a load of:

$$P_\varphi = pr_0^2\pi = pa^2\pi\sin^2\varphi$$

We obtain, from (14):

$$n_\varphi = -\frac{pa^2\pi\sin^2\varphi}{2\pi a\sin^2\varphi} = -\frac{1}{2}pa \tag{30}$$

Finally, using (17) and (19) we deduce:

$$n_\vartheta = -\frac{1}{2}pa\cos 2\varphi \tag{31}$$

The following figure **2.31** shows a representation of the normal forces induced by this load case. This time, the transition between the negative and positive circular normal force is for an angle $\varphi = 45°$.
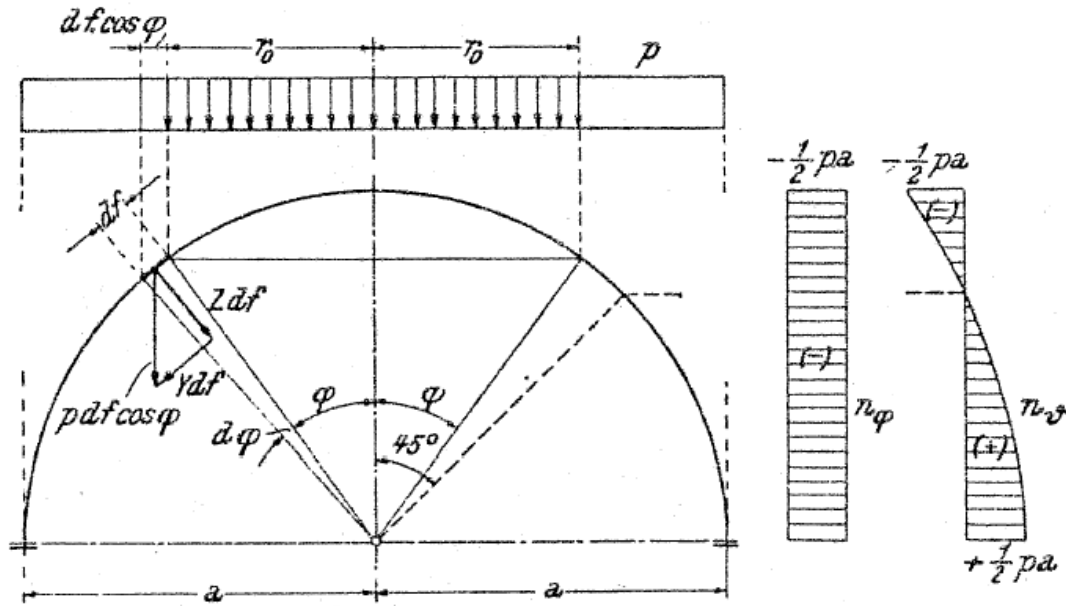
Figure 2.31: Tangential and circular normal forces induced by the snow load in a dome shell.

Using the preceding results and expressions (15) and (18) we can write, as any force is applied in the direction perpendicular to the radius ($n_{\varphi\theta} = 0$, $\varepsilon_{12}=0$):

$$\frac{du}{ad\varphi} + \frac{w}{a} = \varepsilon_{11} = \frac{1}{Ee}\left(n_\varphi - \nu n_\theta\right) = \frac{pa}{2Ee}\left(-1 + \nu\cos 2\varphi\right) \tag{32}$$

$$\frac{w}{a} + \frac{u}{a}\cot\varphi = \varepsilon_{22} = \frac{1}{Ee}\left(n_\theta - \nu n_\varphi\right) = \frac{pa}{2Ee}\left(-\cos 2\varphi + \nu\right) \tag{33}$$

If we subtract these expressions and integrate them, we deduce the displacement $u(\varphi)$. We impose then the boundary condition of no displacement in the support plates $u(102,18°)=0$, obtaining the constant of integration $C_2=0,481$. We have used (33) to write the expression of w(φ). Obviously, *v=0*.

$$u(\varphi) = \frac{pa^2}{2Ee}\sin\varphi\left(0,481 + 2(\nu+1)\cos\varphi\right) \tag{34}$$

$$w(\varphi) = \frac{pa^2}{2Ee}\left(-\cos 2\varphi + \nu\right) - \frac{pa^2}{2Ee}\cos\varphi\left(0,481 + 2(\nu+1)\cos\varphi\right) \tag{35}$$

As the boundary condition is only imposed for the *u* displacement, we obtain an expression of *w* which is not null at *φ=102,18°* (support plates). Therefore, a local bending will appear.

Finally, we would like to draw attention to the fact that the theoretical development for a **wind load** on a dome shell will not be done. It can be found in the literature (Girkmann, 1978) and requires a previous study of skew-symmetrical loads in a membrane. However, we will present the results computed with the finite-element model so as to see the behavior of the Zeiss dome.

2.3 Ideal shape's finite-element calculation

Thanks to the geometrical description we will now be able to build our model and, taking into account the structural details, import it into a finite-element calculation program.

2.3.1 SCRIPTING THE GEODESIC SPHERE

The first step is to obtain the **3D geometry** of the studied dome. However, we may want to study geodesic domes in a more general way, so an efficient way to work would consist in conceiving an algorithm that generates a R radius geodesic sphere of level *n*. This will not only be a good starting point for further research but also an easy way to define the Jena dome: we will only have to fix R = 8 m and *n* = 16 and trim the useless part of the sphere.

In this first approach, we will design a **script** by means of the computing interface offered by *Rhinoceros 4.0*, a 3D NURBS modeling software (Rutten, 2009). NURBS are B-spline curves with a nonuniform knot vector, being B-splines freedom curves that consist of Bézier curve segments of the same degree and that are knotted together at their endpoints with the highest possible smoothness (Pottmann et al., 2007). The main language is Visual Basic, but the program offers specific commands that allow visualization and graphical work with the mathematical objects stored in variables. We will work with a *Rhino 3D Visual Basic Script file* (*.rvb*),

Even if we only present the final script, there were of course **many other versions** as many problems occurred during this process. On the one hand, we wanted to obtain the geodesic sphere by only building one of the projected faces of the icosahedron and

then copy it by means of geometrical transformations so as to find the whole sphere. However, because an icosahedron's vertices have irrational coordinates and that *Rhino* works with floats, some **accuracy problems** occurred: the assembly of the original triangles was not accurate enough (figure **2.32**). The solution was to give the 12 point coordinates of the icosahedron as an input and then build the 20 faces one per one. It is obviously a slower process but solves the problem.
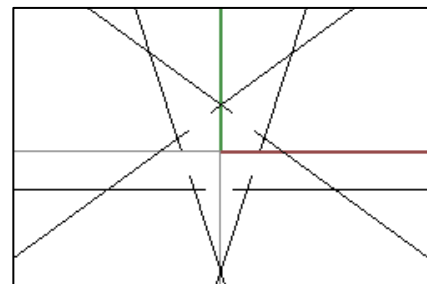
Figure 2.32: Accuracy problem in the dome zenith: vertices do not meet in the same point

On the other hand, the problem was related to the **means of dividing** the icosahedron faces and projecting the resulting intersection points. The first method consisted in simply dividing the edges, tracing the lines that define the division of the face, finding the intersection between those lines, and projecting the beginning and end points of each of the resulting lines into a *R* radius sphere. We used many *Rhino*

commands to perform these operations and this fact made the script slower; furthermore, we obtained the geometry of the geodesic sphere, but without any information on the faces that define the sphere.

A much better approach to our problem uses **vectors**. All the operations that have been described can easily and efficiently be performed using vector commands, which are contained in the *Scripting Library version 1.10* by Stylianos Dritsas (see the *Annex 5.1* for more details). Knowing the three vertices that define the icosahedron face, we know also the vectors that define its edges. It is by rescalating these vectors and by doing simple operations between them that we can build the partitioned face of the icosahedron. The fact of projecting the icosahedron face into the sphere is easily made by *rescaling* the vector that goes from the origin to the newfound vertices giving it length R. We are working with each face of the future geodesic sphere; thus, we only have to define, for each face, a mesh element that will be recognized when exporting the model. The resulting script and its analysis is as follows:

```
1    Option Explicit
2    'Script written and copyrighted by <Raül Vinyes Raso>
3    'Script version Spring 2009
4
5    Dim intLevel, dblRadius, arrObjects
6
7    Call Main()
8    Sub Main()
9
10     Call Rhino.EnableRedraw(False)
11
12     Dim arrCenter, dblA, dblB, dblT, dblx,dbly, arrP(11)
13     intLevel = Rhino.GetReal("Level", 16, 1, 100)
14     dblRadius = Rhino.GetReal("Radius of the sphere", 8, 1, 100)
15
16     dblT = (1+(5)^(1/2)) / 2
17     dblA = dblRadius*( ((dblT)^(1/2)) / ((5)^(1/4)) )
18     dblB = dblradius*( 1 / ( (5^(1/4)) * ((dblT)^(1/2)) ) )
19
20     arrP(0)=Array(0,dblA,dblB) : arrP(1)=Array(dblB,0,dblA)
21     arrP(2)=Array(dblA,dblB,0) : arrP(3)=Array(0,-dblA,dblB)
22     arrP(4)=Array(-dblB,0,dblA) : arrP(5)=Array(-dblA,dblB,0)
23     arrP(6)=Array(0,dblA,-dblB) : arrP(7)=Array(dblB,0,-dblA)
24     arrP(8)=Array(dblA,-dblB,0) : arrP(9)=Array(0,-dblA,-dblB)
25     arrP(10)=Array(-dblB,0,-dblA) : arrP(11)=Array(-dblA,-dblB,0)
26
27     Face arrP(0),arrP(1),arrP(2) : Face arrP(0),arrP(5),arrP(6)
28     Face arrP(11),arrP(5),arrP(10) : Face arrP(3),arrP(11),arrP(9)
29     Face arrP(3),arrP(1),arrP(8) : Face arrP(4),arrP(0),arrP(5)
30     Face arrP(4),arrP(5),arrP(11) : Face arrP(4),arrP(11),arrP(3)
31     Face arrP(4),arrP(3),arrP(1) : Face arrP(4),arrP(1),arrP(0)
32
33     Face arrP(8),arrP(9),arrP(3) : Face arrP(9),arrP(10),arrP(11)
34     Face arrP(10),arrP(6),arrP(5) : Face arrP(2),arrP(6),arrP(0)
35     Face arrP(2),arrP(8),arrP(1) : Face arrP(7),arrP(8),arrP(9)
36     Face arrP(7),arrP(9),arrP(10) : Face arrP(7),arrP(10),arrP(6)
37     Face arrP(7),arrP(6),arrP(2) : Face arrP(7),arrP(2),arrP(8)
```
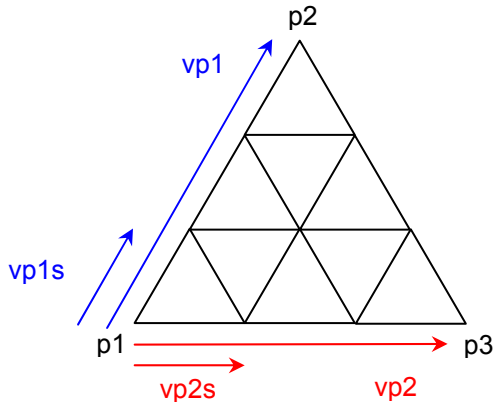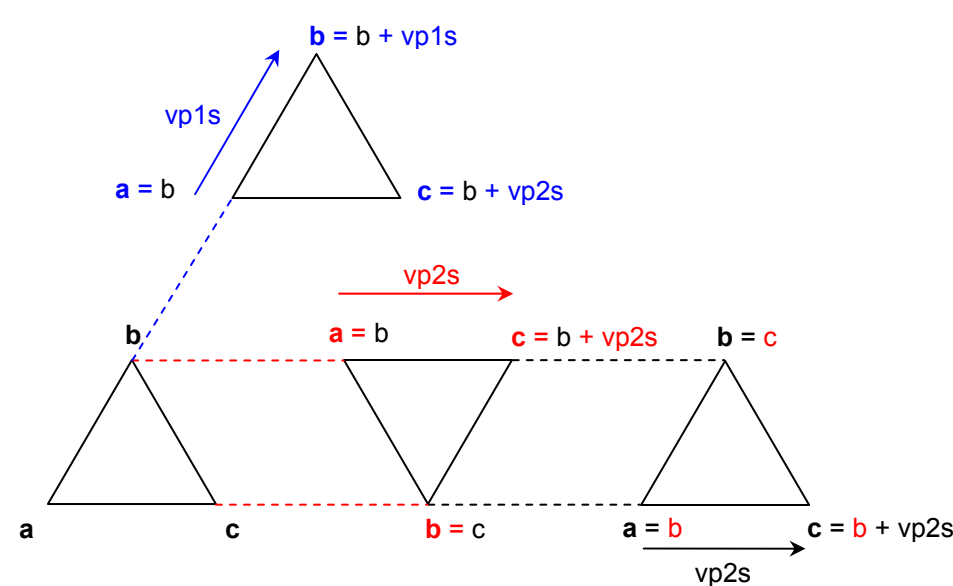
```
38     dblx =1 / ( (dblT*((5)^(1/2)))^(1/2) )
39     dbly = 180 * ( Atn( dblx / ((-dblx * dblx + 1)^(1/2)) ) ) / Pi
40     arrObjects = Rhino.AllObjects
41     Rhino.RotateObjects arrObjects,Array(0,0,0),dbly,Array(0,1,0)
42
43     Call Rhino.EnableRedraw(True)
44
44 End Sub
46
47
48 Function Face (p1,p2,p3)
49
50     Dim i,j,p1bis,vp1,vp2,vp1s,vp2s,a,b,c,va,vb,vc,strPl
51
52     p1bis=p1
53     vp1 = vector_create (p1,p2)
54     vp2 = vector_create (p1,p3)
55     vp1s = vector_scale (vp1,1/intlevel)
56     vp2s = vector_scale (vp2,1/intlevel)
57
58     For i=1 To intlevel
59         a = p1bis
60         b = vector_add(p1bis,vp1s)
61         c = vector_add(p1bis,vp2s)
62         va = vector_create (array(0,0,0),a)
63         vb = vector_create (array(0,0,0),b)
64         vc = vector_create (array(0,0,0),c)
65         va = vector_rescale (va,dblRadius)
66         vb = vector_rescale (vb,dblRadius)
67         vc = vector_rescale (vc,dblRadius)
68
69         For j=1 To (2*(intlevel-i)+1)
70             strPl = Rhino.AddPolyline (array(va,vb,vc,va))
71             Rhino.MeshPolyline strPl
72             Rhino.DeleteObject strPl
73
74             a = b : b = c : c = vector_add(a,vp2s)
75             va = vb : vb = vc : vc = vector_create (array(0,0,0),c)
76             vc = vector_rescale (vc,dblRadius)
77         Next
78         p1bis=vector_add(p1bis,vp1s)
79     Next
80
81 End Function
```

Line	Description
	Main
12...14	Input of the radius and the level of the geodesic sphere.
20...25	Coordinates of the 12 vertices of the inscribed icosahedron.
27...37	Subdivision and projection into a R radius sphere of the 20 faces.
38...41	Rotation of the sphere so as to place an original vertex in the z-axis.

	Function face
53...56	Vectors defining two of the face sides (vp1,vp2) and vectors defining the subdivision in the same directions (vp1s,vp2s) :

58...79	Loop traveling across all face-subdivisions.
59...61	Points (a,b,c) defining each sub-face.
65...67	Projection of the points into the sphere.
70...72	Creation of the mesh defined by the three projected points.
74...78	Coordinates of the next sub-face :

2.3.2 EXPORT OF THE GEOMETRIC MODEL

We have managed to obtain our geometry for a geodesic sphere, as we can see in figure **2.33**. Thus, we only have to trim the sphere in order to keep 11 subdivisions for the lateral faces of the dome, as shown in the drawings and pictures of the structure. The model can be **exported** from an *OpenNURBS 3D Model file* (.*3dm*) to an *AutoCAD drawing exchange file (.dxf)*; all the planar objects will be converted to polylines and the meshes written as 3D planes.
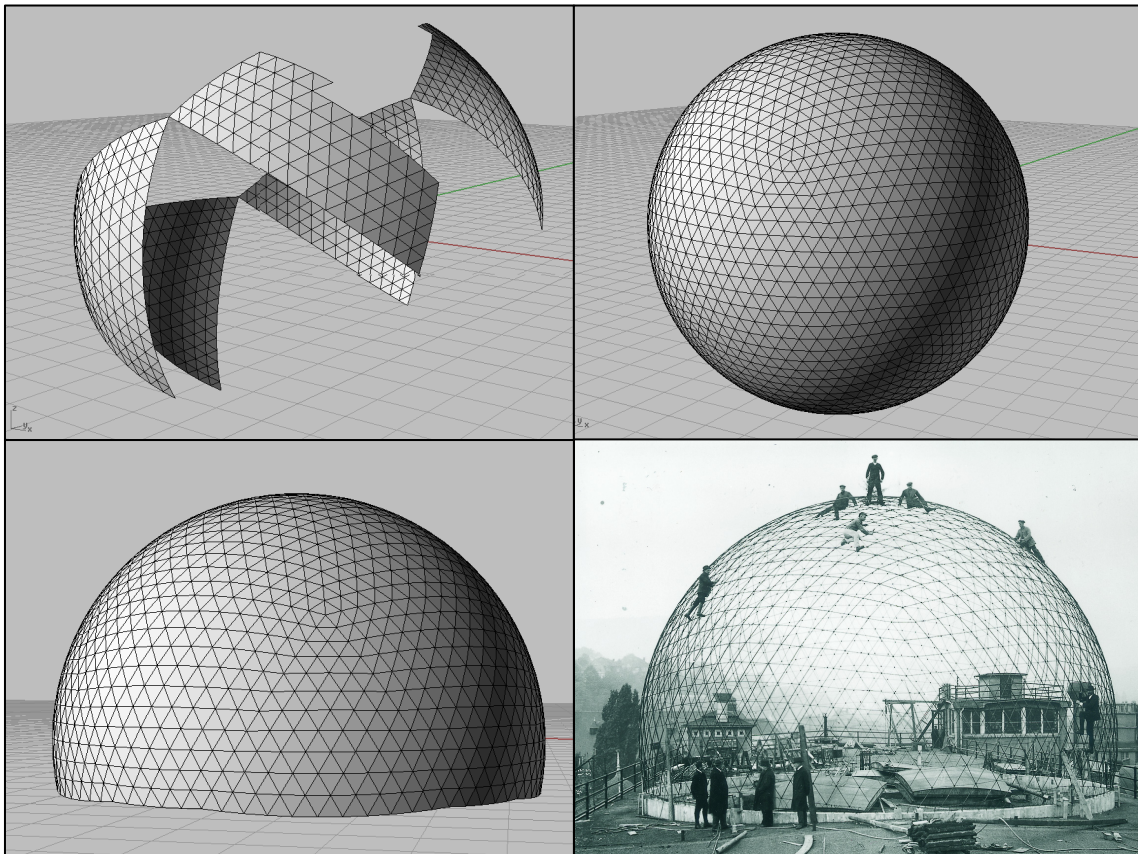
Figure 2.33: In the upper part of the composition we can see how the geometry is built and how it looks when the script is over. In the lower part we see the obtained geometry after trimming the geodesic sphere and the modeled original structure, both with exactly the same mesh subdivision.

The next step is to **import** this file to a *Dlubal RFEM 3.0* file (.*rf3*). *Dlubal RFEM 3.0* is a finite-element software for 3D structural calculations. With this software we can calculate beams, shells and volumes; those structures are decomposed into smaller parts (finite-elements) and, for each part, the balance equations are set up (Vogl et al., 2008).

1D-elements are assumed to have a section that remains planar after deformation. Each element has 12 degrees of freedom, 6 for each endpoint. For a linear calculation, compression, tension and torsion are also assumed to be linear on the x axis of the beam, independently from deflection and shear forces. Those are approximated with a third degree polynomial in *x*, taking into account the effect of shear stresses.

2D-elements are normally described with square elements and conditions at nodes are the same as those for 1D-elements. The basis of plane surfaces constitute the **Mindlin/Reissner** theory (keep in mind that we used the Kirchhof-Love theory in our analytical approach). A quadratic reference system is chosen to ensure a direct link with beams. Based on a mixed interpolation of the transversal displacement, the rotation of the section and the transversal shear strain, **MITC4-elements** (Mixed Interpolation of Tensorial Components) are employed (Dvorkin, 1984).

The transferred information appears as nodes, lines and planes. Table **2.6** summarizes those properties; for more details see the *Construction methods chapter 2.1.4*.

Number of nodes	1561
Number of planes	3040
Number of bars	4600
Mean of the bars length *l* (mm)	604,9
Different values of *l*	72

Table 2.6: Global statistics of the generated geometry exported to the statics program.

2.3.3 STRUCTURAL PROPERTIES

We must now introduce all of the described **structural** properties into the FE-model, which are summarized in the following table **2.7**.

Bars' section and class	Rectangular section of 8 x 20 mm *Truss* : bar accepting only a normal stress
Concrete shell	Plane surfaces Thickness: 30 mm
Materials	**Steel :** tensile strength of 370 MN/m^2 **Concrete :** compressive strength of 20 MN/m^2 and tensile strength of 2,5 MN/m^2

Support plates	Locked displacement in x, y, z axis
	Locked rotation around the z axis
	Support plates located in the base nodes
Load cases	**LC1 : Dead load** = 0,815 kN/m^2
	LC2 : Snow : vertical load of s = 0,68 kN/m^2
	LC3 : Wind : horizontal load of q = 0,94 kN/m^2
Load groups	**LG1 : Deformation load group** = LC1 + LC2 + LC3
	LG2 : Design load group = 1,35*LC1 + 1,5*LC2 + 1,5*LC3

Table 2.7: *Structural details introduced in* Dublal RFEM 3.0 in order *to reproduce the conditions of the Carl Zeiss dome in Jena.*

Concerning the **bars** section (table **2.8** and figure **2.34**), it is important to highlight the fact that it is not symmetrical. This means that we have to orient all the bars of the model in such a way that the centered normal of the faces having two 8 mm sides passes through the center of the dome. We have used *trusses* as they reproduce the way bars work in the structure, only accepting a normal stress. A more detailed model with *beams* (bars having bending strength) produces identical results, confirming our hypothesis.

Section properties				
Width	b	8,0	mm	
Depth	h	20,0	mm	
Cross-section area	A	1,60	cm^2	
Shear area	A_y	1,33	cm^2	
Shear area	A_z	1,33	cm^2	
Moment of inertia	I_y	0,53	cm^4	
Moment of inertia	I_z	0,09	cm^4	
Governing radius of rotation	r_y	5,80	Mm	
Governing radius of rotation	r_z	2,30	Mm	
Weight	W_t	1,30	kg/m	
Surface	A_{Surf}	0,056	m^2/m	
Torsional constant	J	0,26	cm^4	
Elastic section modulus	$S_{y,max}$	0,53	cm^3	
Elastic section modulus	$S_{y,min}$	-0,53	cm^3	
Elastic section modulus	$S_{z,max}$	0,21	cm^3	
Elastic section modulus	$S_{z,min}$	-0,21	cm^3	
Statical moment of area	Q_y	0,40	cm^3	
Statical moment of area	Q_z	0,16	cm^3	
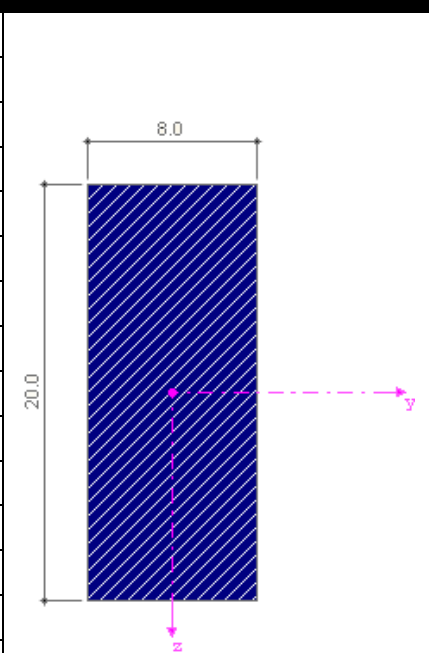
Table 2.8: *Properties and schema of the section.*
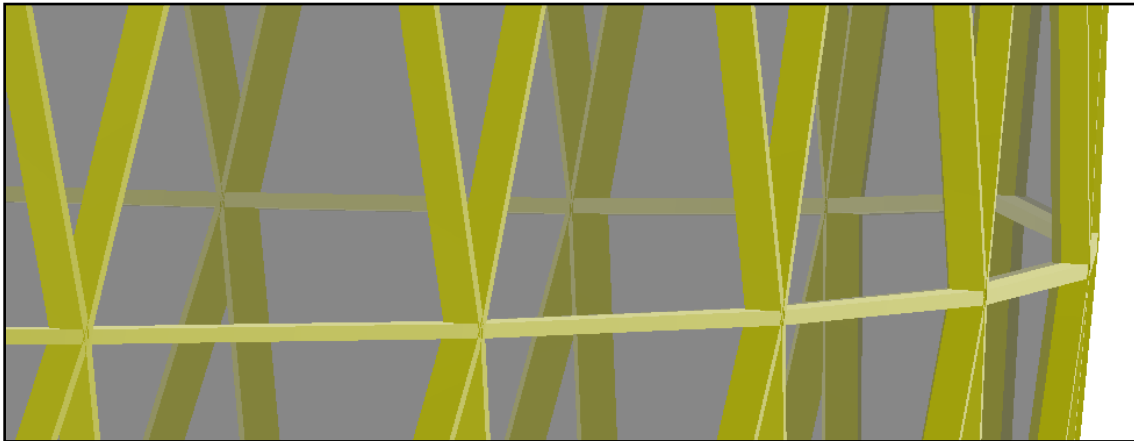
Figure 2.34: *Detail of the orientation of the bars in the structure.*

We have used **plane surfaces**, which are defined in *Dlubal RFEM 3.0* as surfaces accepting all forces and moments. This is a good way to verify that the shell acts as a membrane, as we will find very small and localized (near the support plates) moments (*see 2.3.5 Analysis of the results*).

The **materials** used have the following detailed description (tables **2.9** and **2.10**):

Steel mesh properties			
Unit weight	γ	78,5	kN/m^3
Modulus of elasticity	E	210000	MN/m^2
Shear modulus	G	81000	MN/m^2
Poisson ratio	v	0,30	
Yield strength	f_y	370	MN/m^2
Ultimate tensile strength	f_u	490	MN/m^2

Table 2.9: *Properties of the **steel** used for the bars.*

Unit weight	γ	25,0	kN/m^3
Modulus of elasticity	E	21100	MN/m^2
Shear modulus	G	9000	MN/m^2
Poisson ratio	v	0,12	
Characteristic cube compressive strength	$f_{ck,cube}$	20,0	MN/m^2
Mean axial tensile strength	f_{ctm}	2,5	MN/m^2

Table 2.10: *Properties of the **concrete** used for the shell.*

Furthermore, the **support plates** (figure **2.35**) have been disposed horizontally in the base nodes. Even if we considered inclining them in such a way that their normal is tangent to the dome surface as required for the shell theory, the support structure in the documents from the Carl Zeiss Archive is closest to the chosen option.
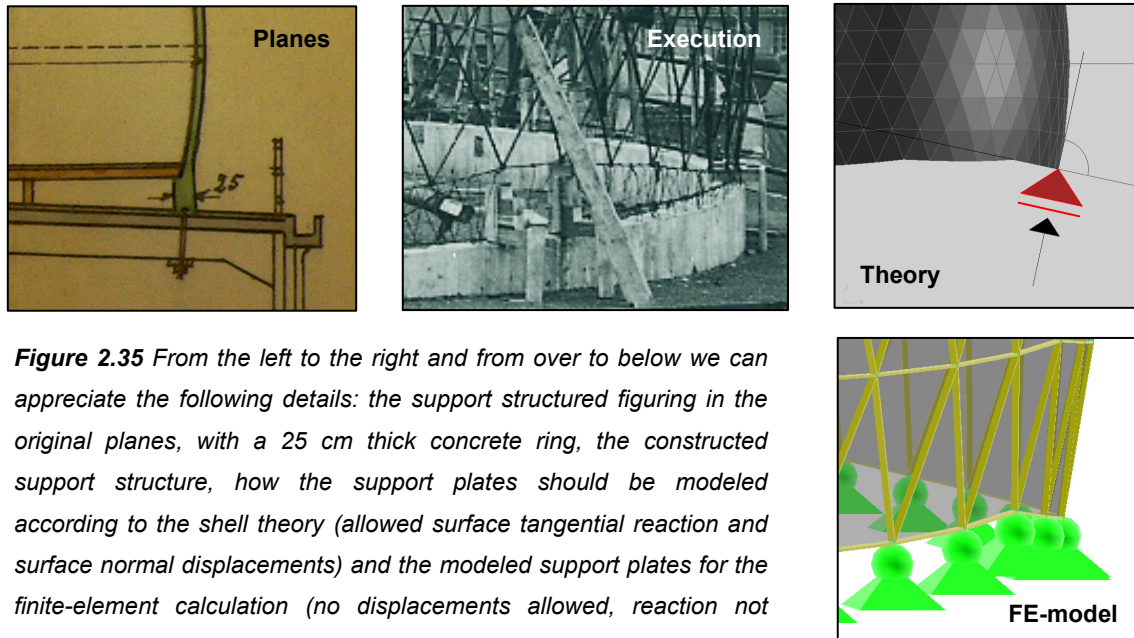
Figure 2.35 From the left to the right and from over to below we can appreciate the following details: the support structured figuring in the original planes, with a 25 cm thick concrete ring, the constructed support structure, how the support plates should be modeled according to the shell theory (allowed surface tangential reaction and surface normal displacements) and the modeled support plates for the finite-element calculation (no displacements allowed, reaction not tangent to the surface).

Finally, in order to obtain the values of the snow (figure **2.36**) and wind (figure **2.37**) loads we have followed the German norm (DIN 1055-4 and DIN 1055-5).
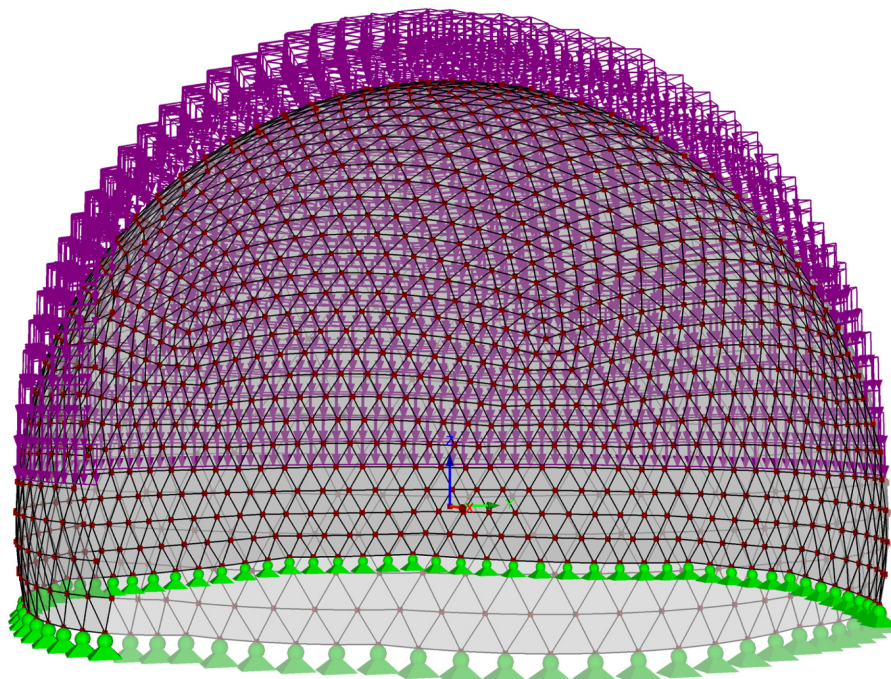
Figure 2.36: Snow load (in violet) applied to the structural model.

Concerning the **snow load**, we should consider that this load is only effective in the part of the roof which forms an angle smaller than 60° with the horizontal, but we will do it for the whole hemisphere in order to compare the results with the theoretical solution. Furthermore, we are only going to consider the symmetrical case, with a load of $0,8 * s_k$, where s_k represents the characteristic snow load on the ground. The German snow map gives us the value of s_k for Jena (zone 2), which is $s_k = 0,25 + 1,91 * ((A + 140) / 760)^2 \geq 0,85$ with $A = 155\ m$ (Jena's altitude). Thus, we obtain $s_k = 0,85\ kN / m^2$ and p = 0,8 * 0,85 = 0,68 kN / m^2.

Taking into account that the city of Jena is in zone 2 on the German **wind** map, we have a $q_{ref} = 0,39\ kN/m^2$. The dome is built, however, on the roof of a 22 m high factory; thus, we can take $z = 26\ m$ so as to obtain an average value for q. Using the formulas given by the German norm we have $q\ (z = 26\ m) = 1,7 * q_{ref} * (z / 10)^{0,37}$, as we are in a land class III (*Binnenland*, inland) and $7\ m < z \leq 50\ m$. The resulting q is 0,94 kN / m^2.
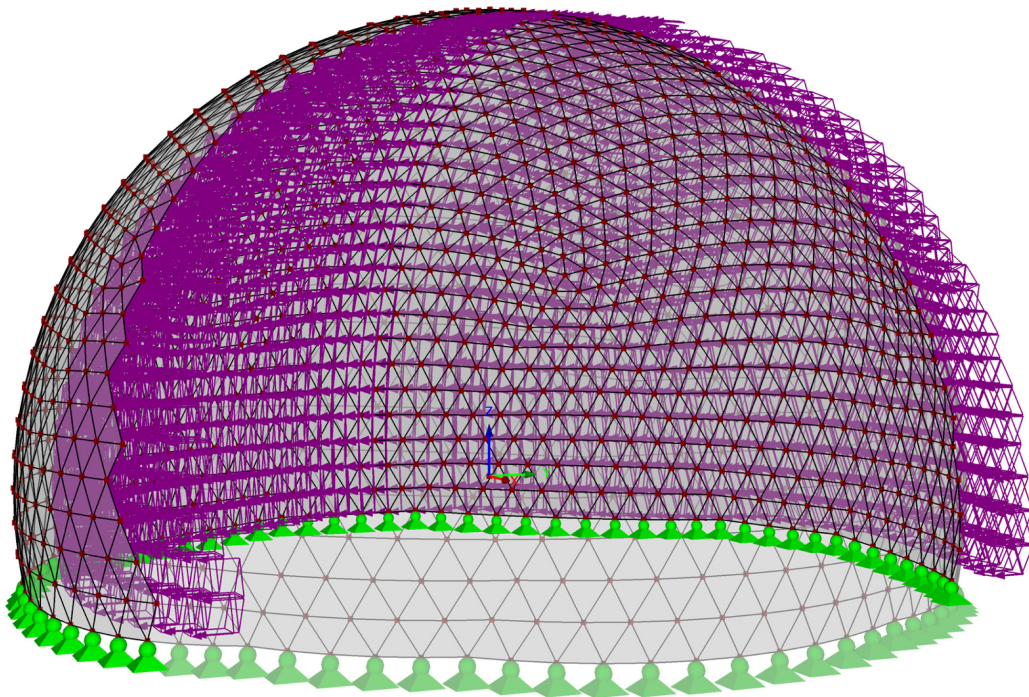
Figure 2.37: *Wind load schema (in violet) applied to the structural model.*

Figure **2.38** shows the final aspect of the model. We are ready now to run the calculations and analyze the results.
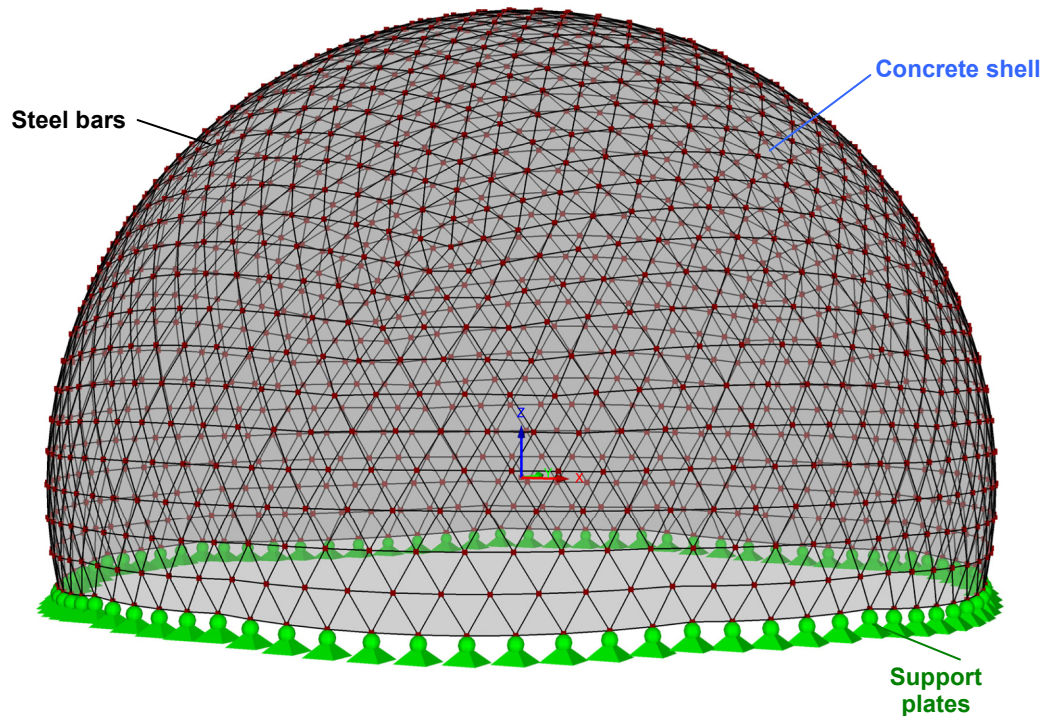
Figure 2.38: *Overview of the model including all the structural details. The load cases are not shown.*

2.3.4 LOAD CASES AND LOAD GROUPS

We have defined the **dead load case** and the **snow load case** to compare the FE-model results with the theoretical approach. Furthermore, the **wind load case** will show how the structure behaves in such a case. Finally, the **deformation load group** will give us the maximal deformation of the structure and with the **design load group** we will be able to obtain the maximal stresses in it. We will always show the detailed results in the same **control section named S**.

2.3.4.1 Dead load case

By means of the following figures and tables we will present the **results** of the described structure and its further **analysis**. When we compute the dome under a dead load, we can produce the following figures **2.39** to **2.47**. We can already see one of the most interesting aspects of the structure behavior: the extremely small deformations.

LC1: Dead load
u

Against Y-direction
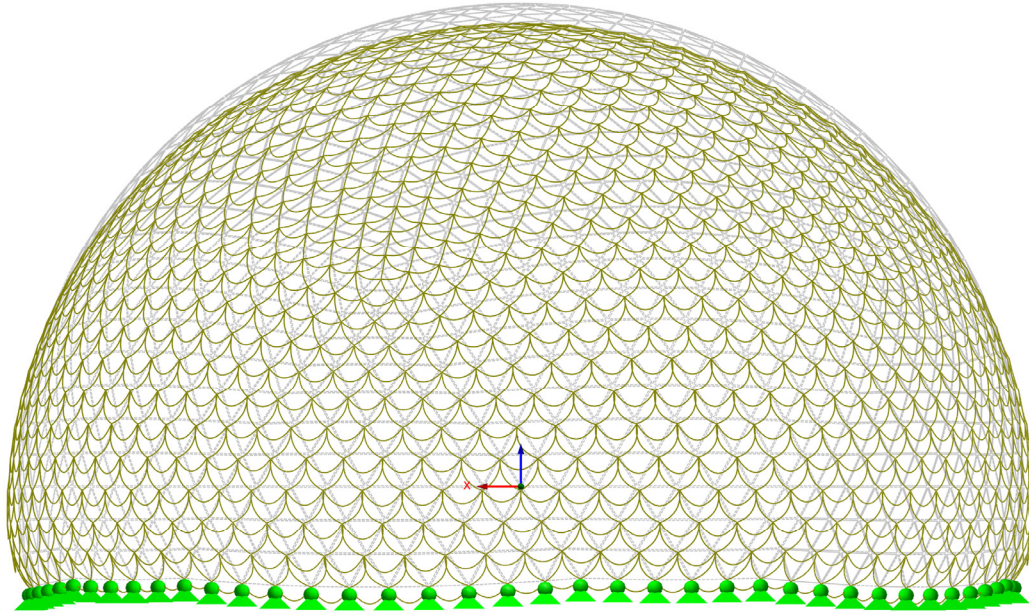
Max u: 0.200, Min u: 0.000 [mm]
Factor of deformations: 2000.00

Figure 2.39: *Deformation of the steel structure under the dead load (complete FE-model).*

LC1: Dead load
u

Against Y-direction

Section S

Deformation
|u| [mm]

0.162
0.147
0.133
0.118
0.103
0.088
0.074
0.059
0.044
0.029
0.015
0.000

Max :   0.162
Min :   0.000
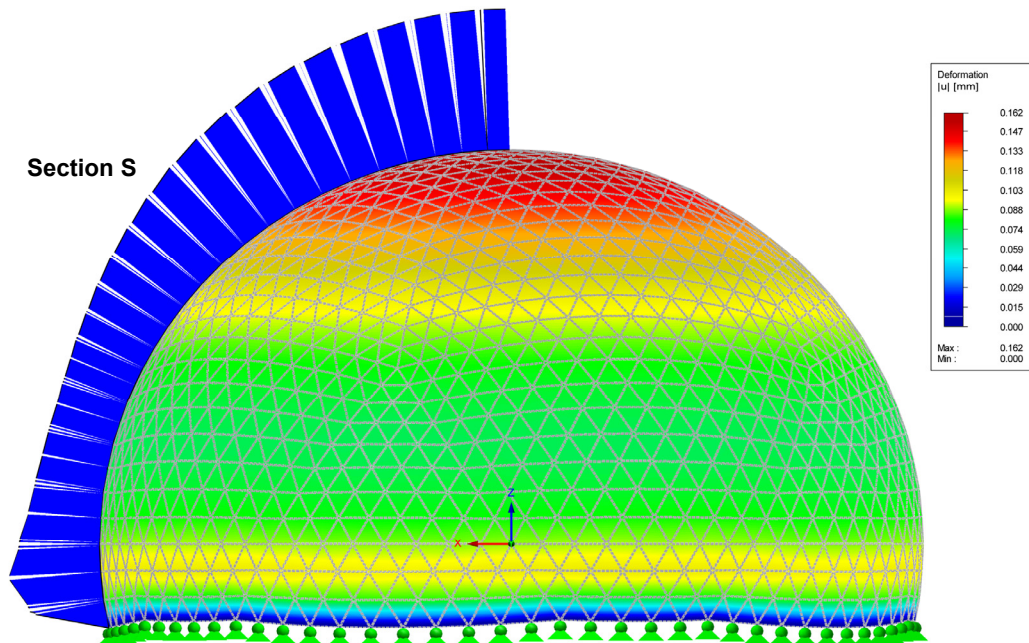
Max u: 0.162, Min u: 0.000 [mm]
Factor of deformations: 0.00

Figure 2.40: *Deformation of the concrete shell under the dead load, with the detail of section **S** (complete FE-model).*

LC1: Dead load
u

Isometric
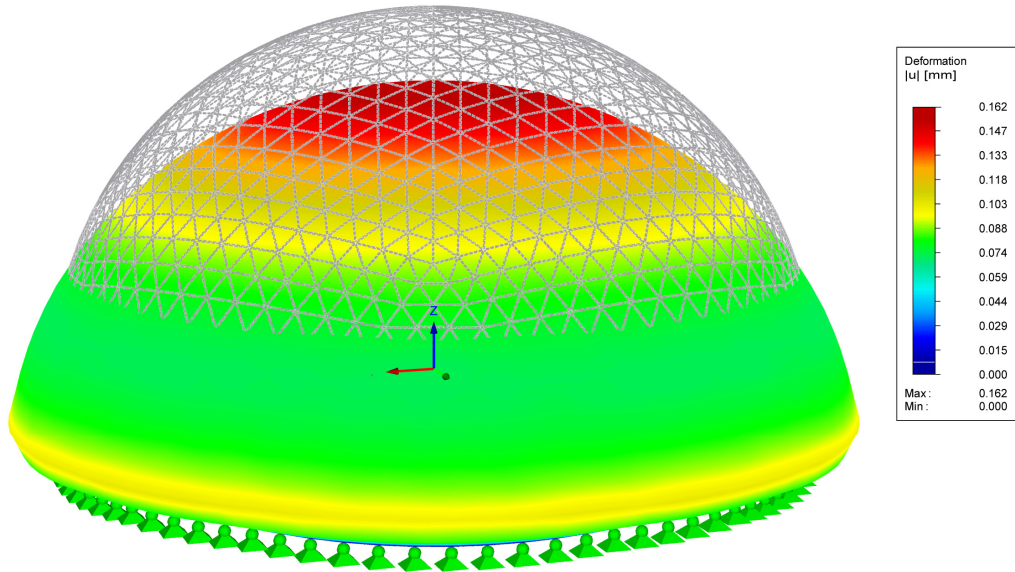
Max u: 0.162, Min u: 0.000 [mm]

Figure 2.41: *3D view of the deformation of the concrete shell under the dead load (complete FE-model).*

LC1: Dead load
Members N

Against Y-direction
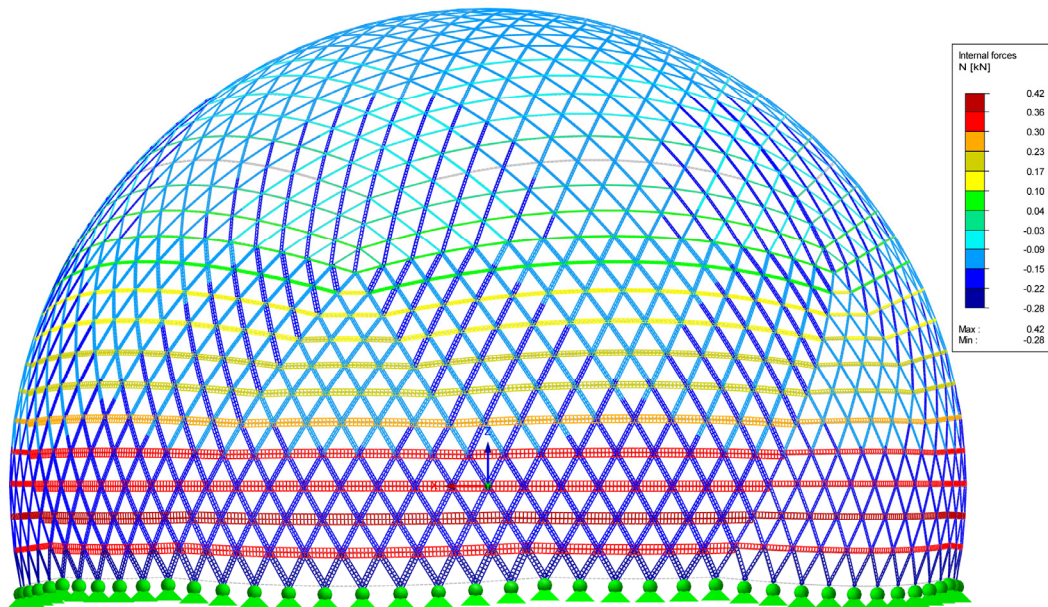
Members Max N: 0.42, Min N: -0.28 [kN]

Figure 2.42: *Normal force in the steel structure under the dead load (complete FE-model).*

LC1: Dead load
Surfaces n-1

Against Y-direction

compression

Section S

tesion

51,6 °

Principal values
n₁ [kN/m]

| 8.71 |
| 7.66 |
| 6.60 |
| 5.55 |
| 4.50 |
| 3.45 |
| 2.40 |
| 1.35 |
| 0.30 |
| -0.75 |
| -1.80 |
| -2.85 |

Max : 8.71
Min : -2.85

Surfaces Max n-1: 8.71, Min n-1: -2.85 [kN/m]

Figure 2.43: *Internal circular normal force in the concrete shell under the dead load, with the detail of section S (complete FE-model).*

LC1: Dead load
Surfaces n-2

Against Y-direction

compression

Section S

Principal values
n₂ [kN/m]

| -2.82 |
| -3.32 |
| -3.81 |
| -4.30 |
| -4.80 |
| -5.29 |
| -5.78 |
| -6.28 |
| -6.77 |
| -7.27 |
| -7.76 |
| -8.25 |

Max : -2.82
Min : -8.25

Surfaces Max n-2: -2.82, Min n-2: -8.25 [kN/m]
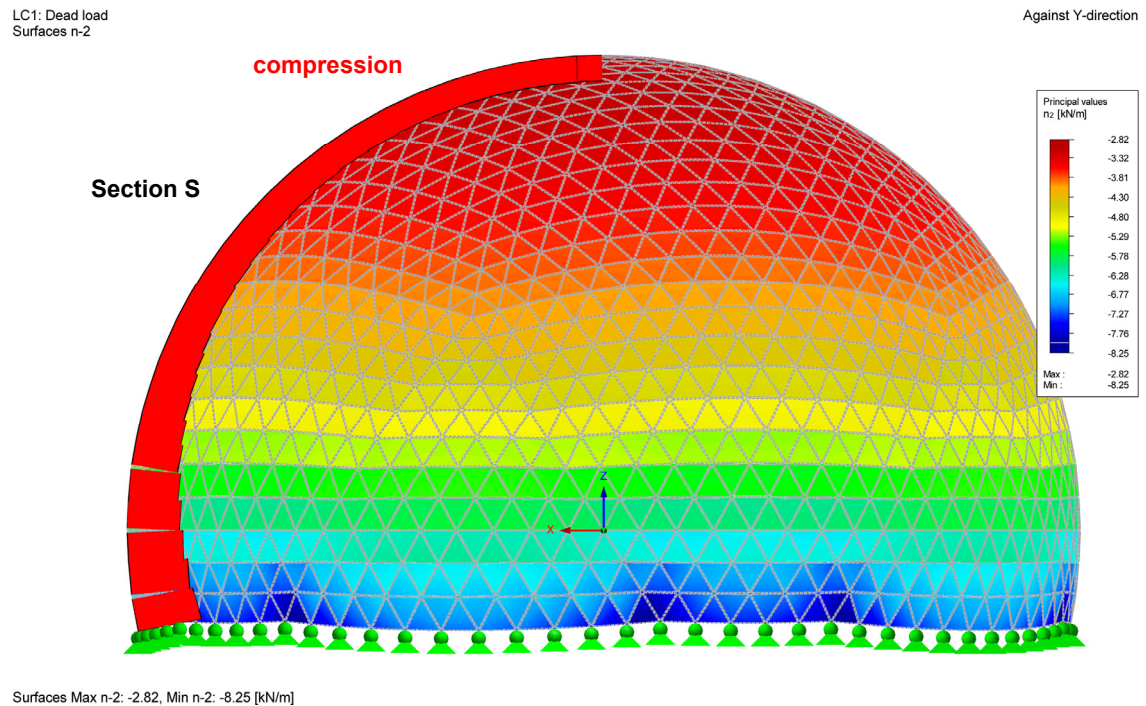
Figure 2.44: *Internal tangential normal force in the concrete shell under the dead load, with the detail of section S (complete FE-model).*
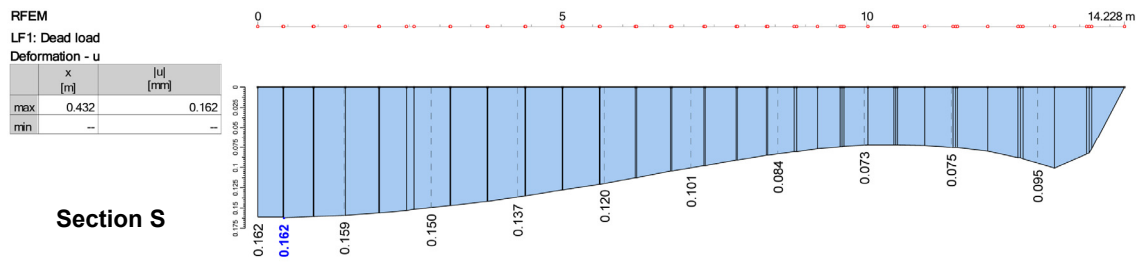
Figure 2.45: *Deformation of the concrete shell under the dead load in **S** (FE-model).*
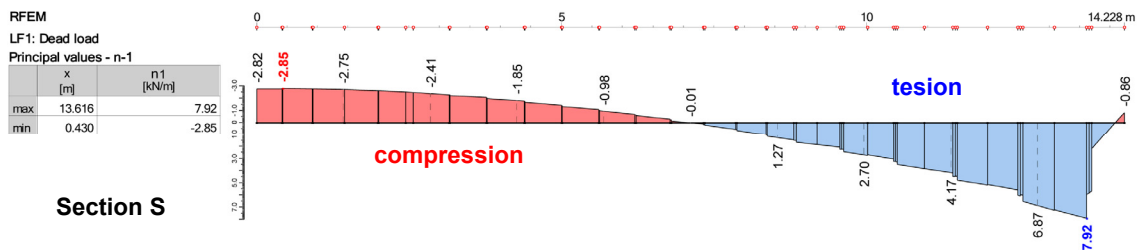
Figure 2.46: *Internal circular normal force in the concrete shell under the dead load in **S** (FE-model).*
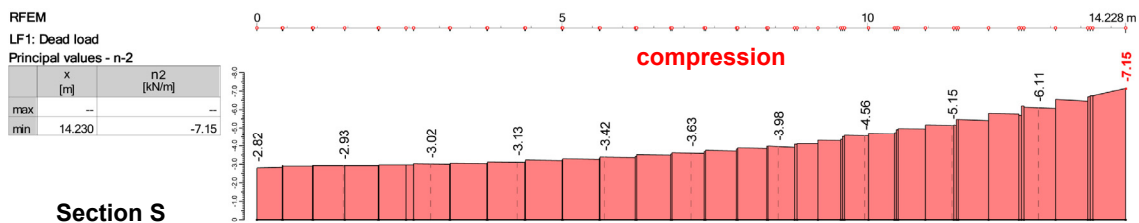
Figure 2.47: *Internal tangential normal force in the concrete shell under the dead load in **S** (FE-model).*

Although the results are very interesting and self-explanatory on their own, we would like to comment on the relationship between the solution obtained with the **finite-element model** and the **theoretical solution calculated *by hand***, both in the **dead load case and in the snow load case**. For the other load cases and load groups we will only present the complete FE-model solution. We continue to present the results in the same control section S as before and using the *Excel* worksheets detailed in the *Annex 5.3*.

We thus have four different solutions to our problem, resulting from four different approaches. On the one hand, we can obtain some results thanks to our FE-model. We can compute the whole structure (concrete shell + steel mesh, approach A) or we can simply compute the concrete shell with an additional load equivalent to the steel mesh dead load (approach B). Thus, we will be able to compare our results more accurately and extract some interesting conclusions.

On the other hand, the theoretical solution can be calculated assuming that we only have a concrete shell but applying the dead load of both the concrete and the steel structure (approach C). We can also proceed in the inverse way, assuming that

we only have a steel shell and applying the same load as before (approach D). In this case the thickness of the steel shell is taken as the volume of steel divided by the surface of the dome; this procedure was followed by engineer Finsterwalder in 1923 in his Final Year Project (Finsterwalder, 1923). He obtained overestimated deformations.

Finally, another way to consider both the steel mesh and the concrete shell would be to use a homogenization approach. We can learn more about this subject in Meschke-Rumanus (2008) and Kaminski (2005).

We summarize the four approaches in the following table **2.11**:

Approach	FE-model	Theory	Concrete shell	Steel mesh
A	✔	✘	✔	✔
B	✔	✘	✔	✘
C	✘	✔	✔	✘
D	✘	✔	✘	✔

Table 2.11 *Description of the four different approaches to our problem in the dead load case and in the snow load case.*

The values of the parameters used in expressions (22), (24), (27), (28), (30), (31), (34), (35) are the same as those used in the finite-element model, as we can see in table **2.12**.

Theoretical model parameters		
Radius of the dome (m)	R	8
Area of the dome (m^2)	A	487
Maximum value of φ (°)	φ_{max}	102,18
Concrete's modulus of elasticity (MN/m^2)	E_c	21100
Concrete's Poisson ratio	v_c	0,12
Steel's modulus of elasticity (MN/m^2)	E_s	210000
Steel's Poisson ratio	v_s	0,30
Weight of the whole structure (kN)	W	397
Volume of steel (m^3)	M_s	0,445
Dead load (kN/m^2)	g	0,82
Snow load (kN/m^2)	p	0,68

Table 2.12: *Values of the parameters used in the theoretical model.*

In the following figures **2.48** to **2.50** we can see how the results of the four models look. Curves A and B have been softened.

The differences between A and C can be explained by the **mechanical role of the steel bars**, which has not been taken into account in the theoretical approach (the steel bars, as we can see when we compare A and B models, take a part of the circular and tangential normal forces of the concrete shell). Furthermore, we have made many **approximations** in our theoretical model that are not always the same done in the finite-element model and that can help to explain the small differences in terms of displacements between B and C, which should produce the same results.

The differences between C and D are only in terms of displacements. We can conclude that approximating the displacements of the structure by only considering a concrete shell is the best way to obtain similar results to the complete FE-model (A). Thus, the displacement behavior of the concrete shell predominates over that of its steel counterpart.

We will show the same sort of figures for the snow load case, holding the preceding analysis valid. It is necessary to highlight the fact that, for this load case, the displacements for B and C are nearly equal.
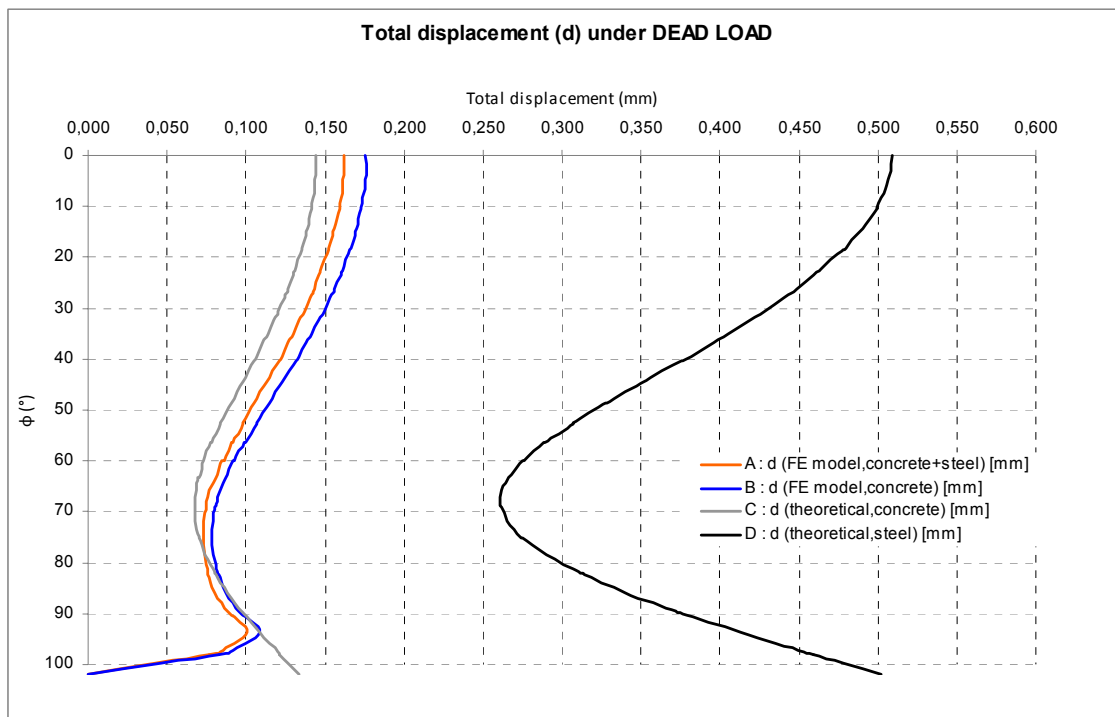
Figure 2.48: *Comparison between the finite-element calculation and the theoretical one of the deformation of the concrete shell under the dead load in section **S**.*
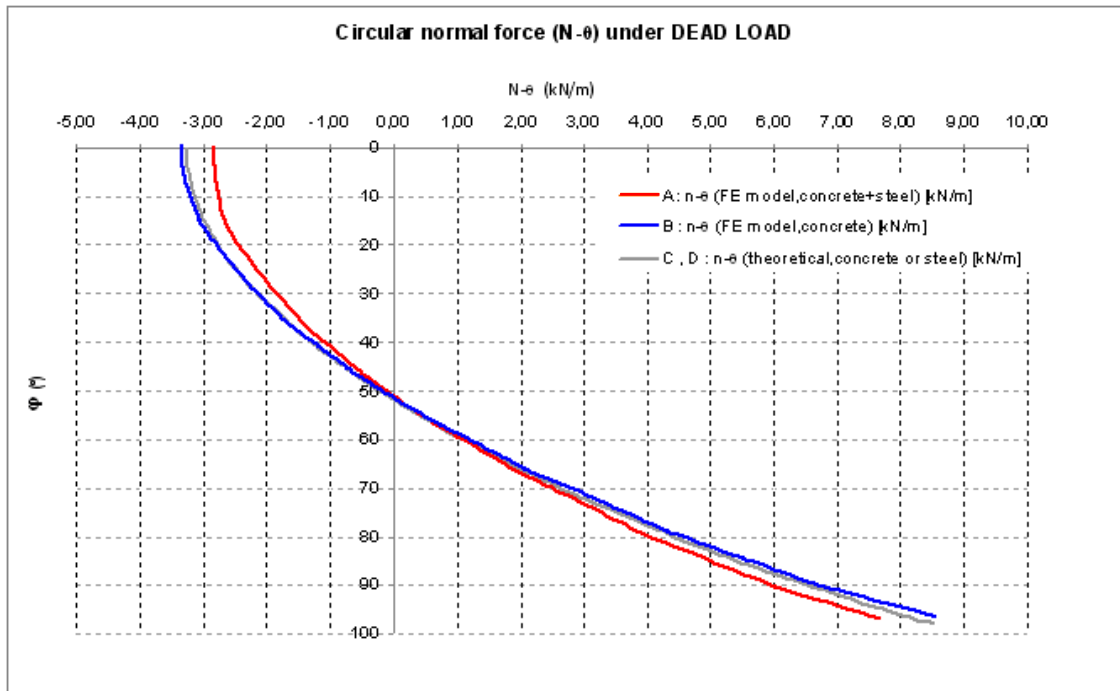
Figure 2.49: *Comparison between the finite-element calculation and the theoretical one of the internal circular normal force in the concrete shell under the dead load in section **S**.*
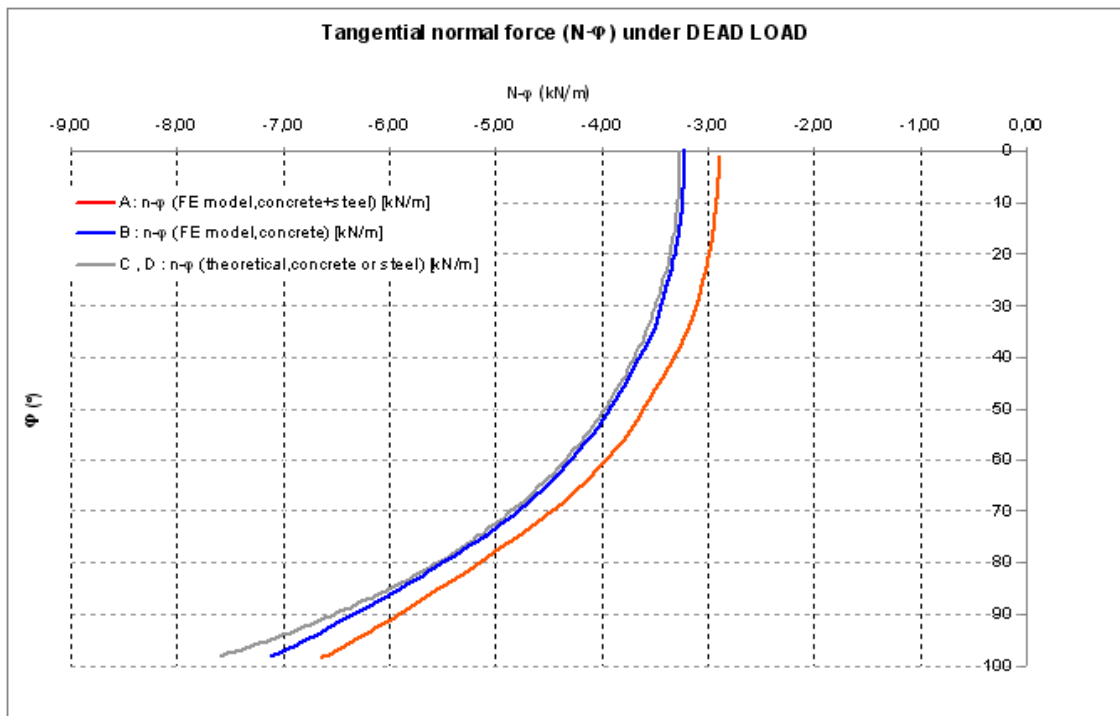
Figure 2.50: *Comparison between the finite-element calculation and the theoretical one of the internal tangential normal force in the concrete shell under the dead load in section **S**.*

2.3.4.2 Snow load case

The snow load also produces an interesting effect in the dome (figures **2.51** to **2.59**):
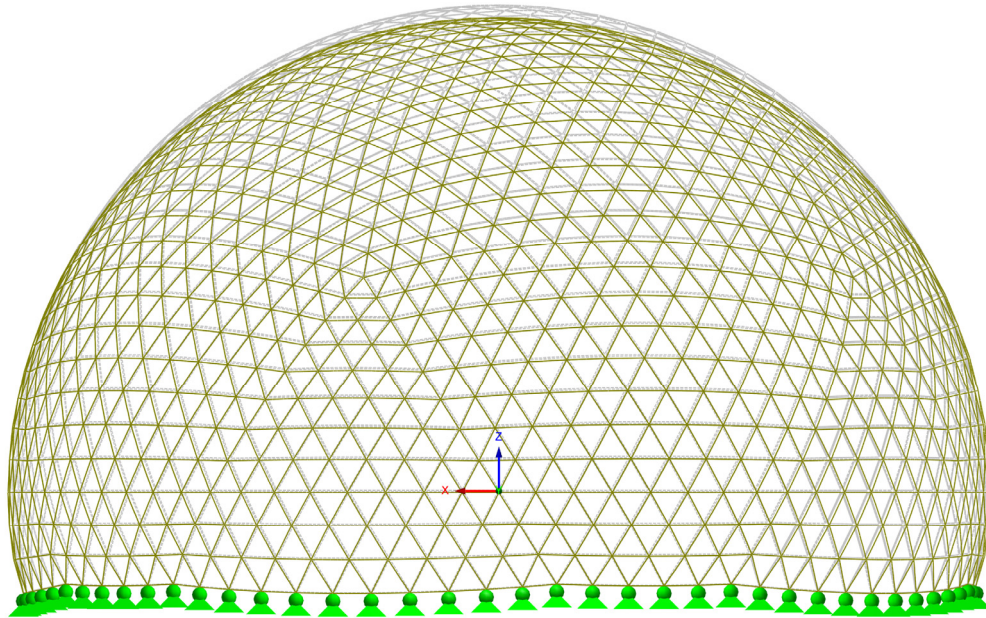
Figure 2.51: *Deformation of the steel structure under the snow load (complete FE-model).*
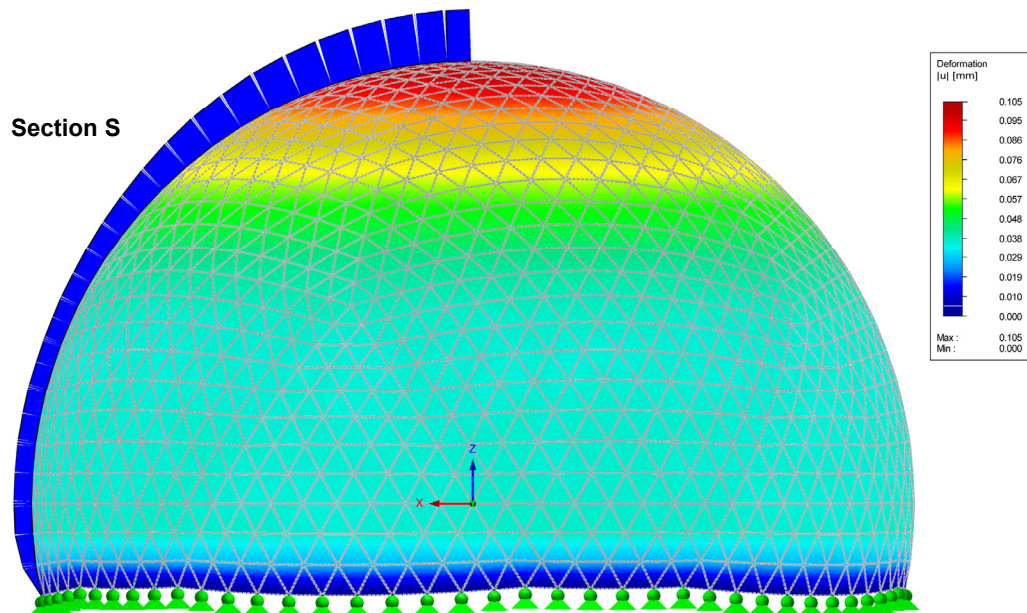
Figure 2.52: *Deformation of the concrete shell under the snow load, with the detail of section S (complete FE-model).*

LC3: Snow
u

Isometric
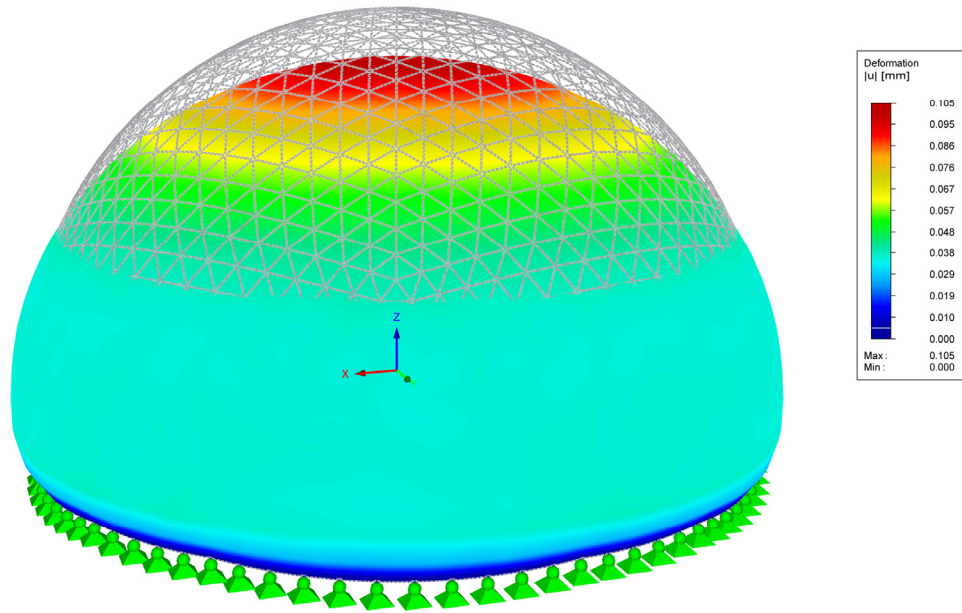
Max u: 0.105, Min u: 0.000 [mm]

Figure 2.53: *3D view of the deformation of the concrete shell under the snow load (complete FE-model).*

LC3: Snow
Members N

Against Y-direction
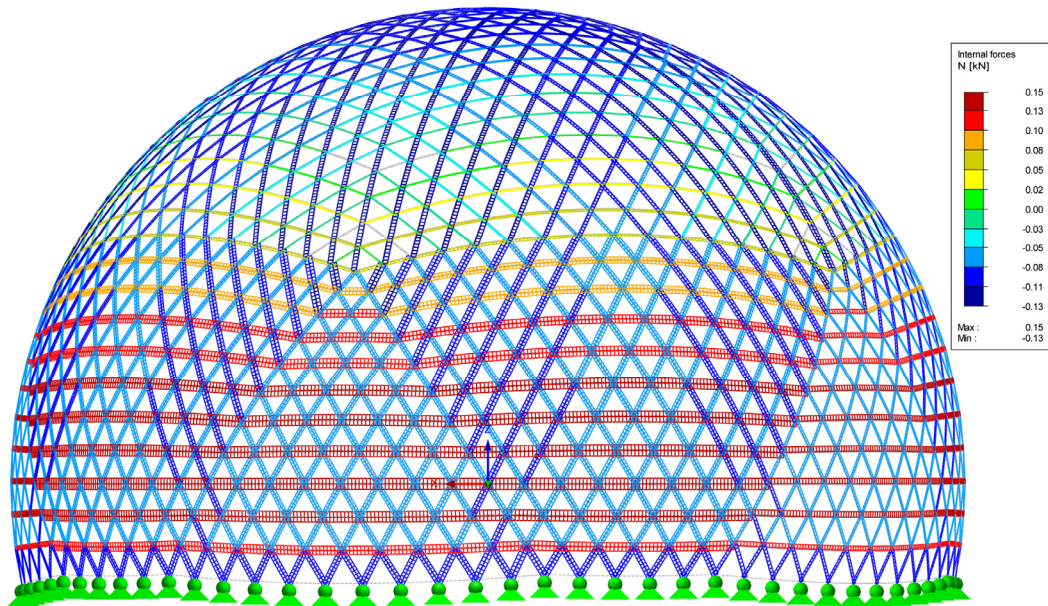
Members Max N: 0.15, Min N: -0.13 [kN]

Figure 2.54: *Normal force in the steel structure under the snow load (complete FE-model).*
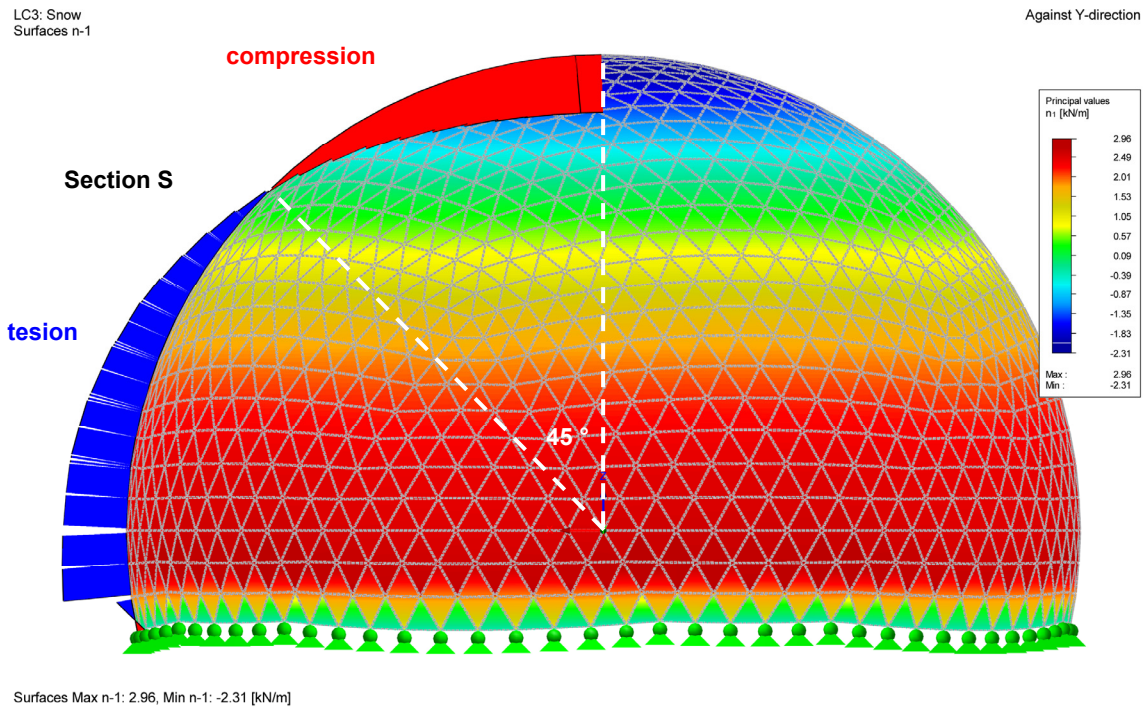
Figure 2.55: *Internal circular normal force in the concrete shell under the snow load, with the detail of section S (complete FE-model).*

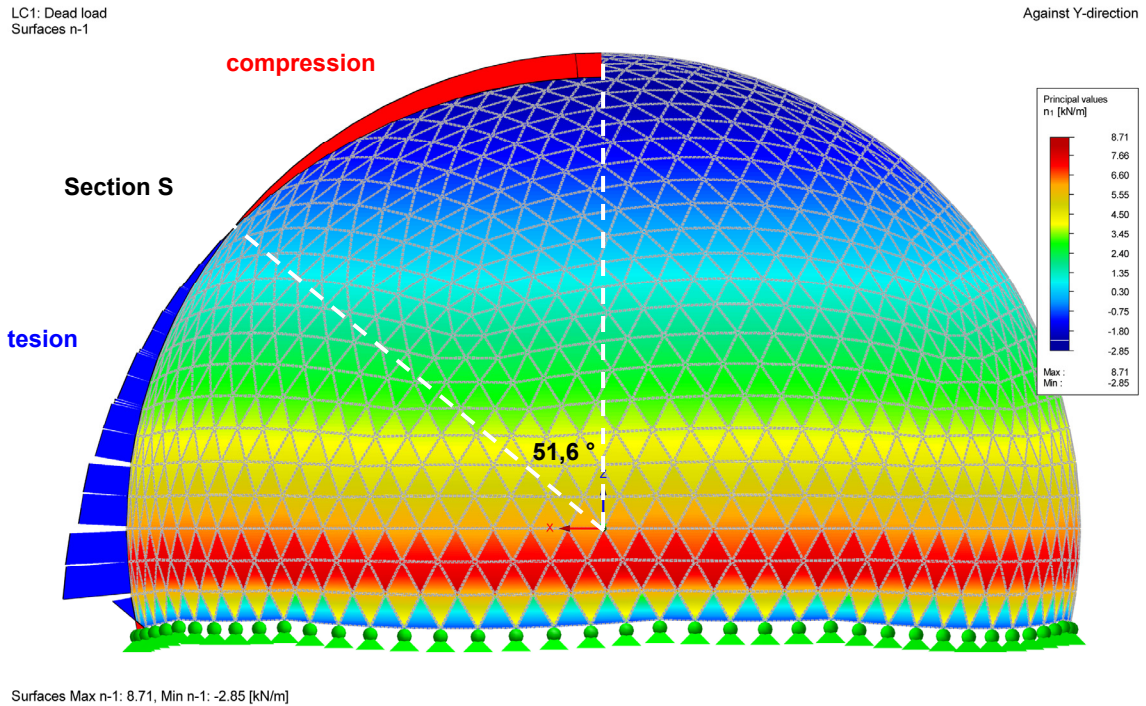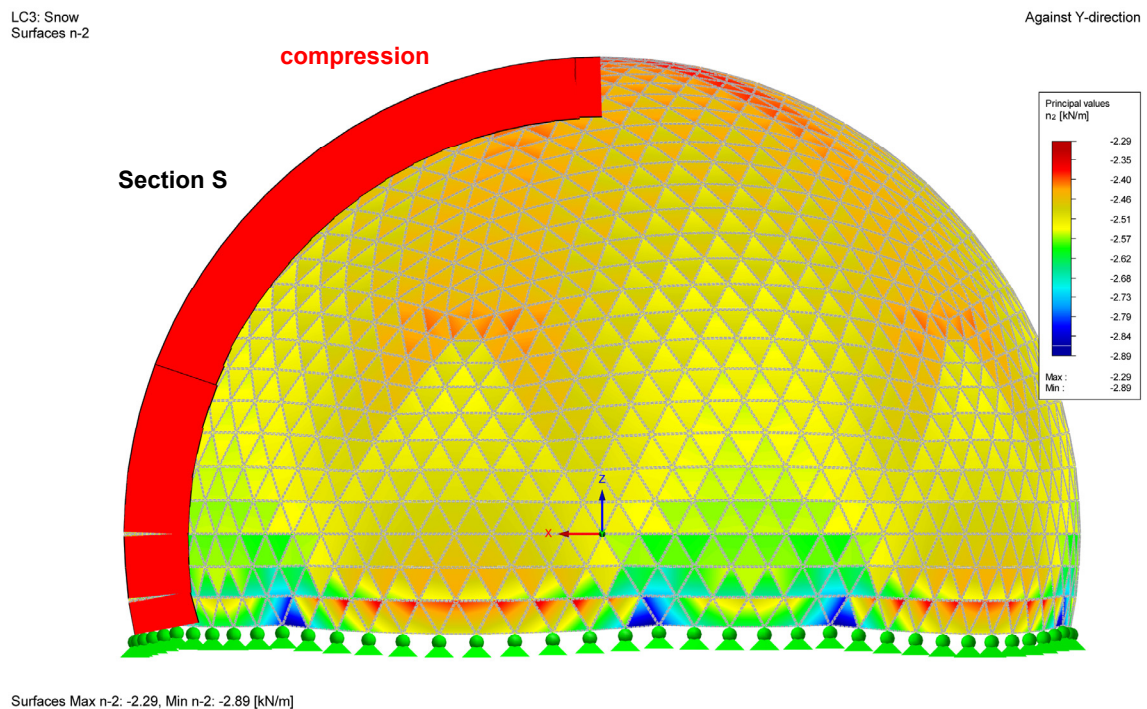Figure 2.56: *Internal tangential normal force in the concrete shell under the snow load, with the detail of section S (complete FE-model).*
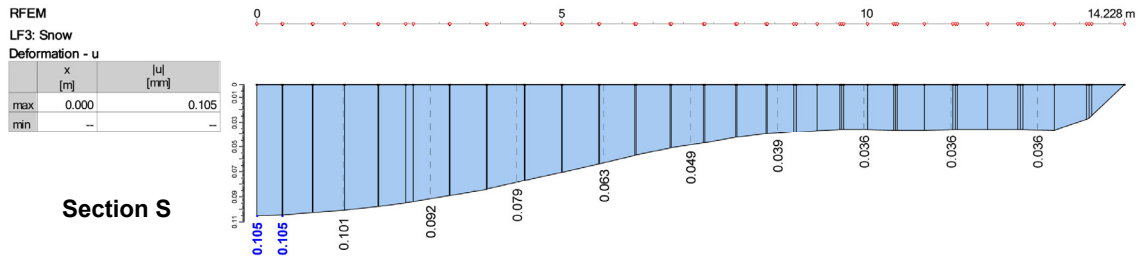
Figure 2:57: *Deformation of the concrete shell under the snow load in S (FE-model).*
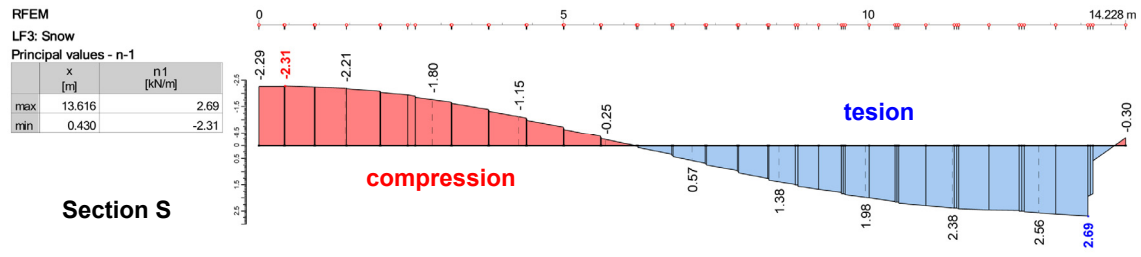
Figure 2.58: *Internal circular normal force in the concrete shell under the snow load in S (FE-model).*
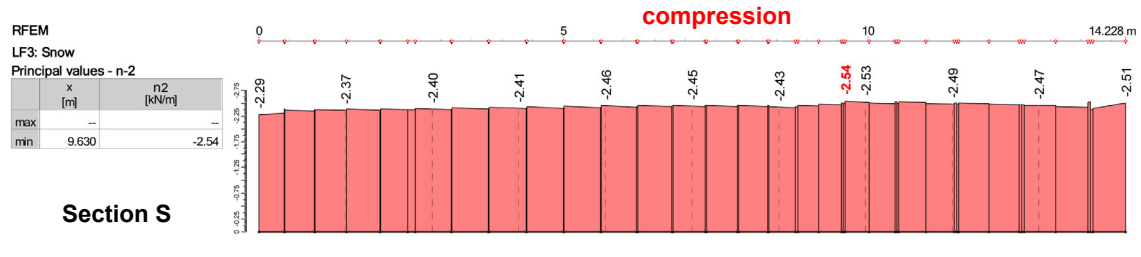
Figure 2.59: *Internal tangential normal force in the concrete shell under the snow load in S (FE-model).*

We can already see with the preceding figures that some of the predictions of the theoretical model are confirmed. However, a deeper analysis is necessary to compare the different models. Once again, we obtain the expected results and the comments on the dead load case are also validated for this load case (figures **2.60** to **2.62**).
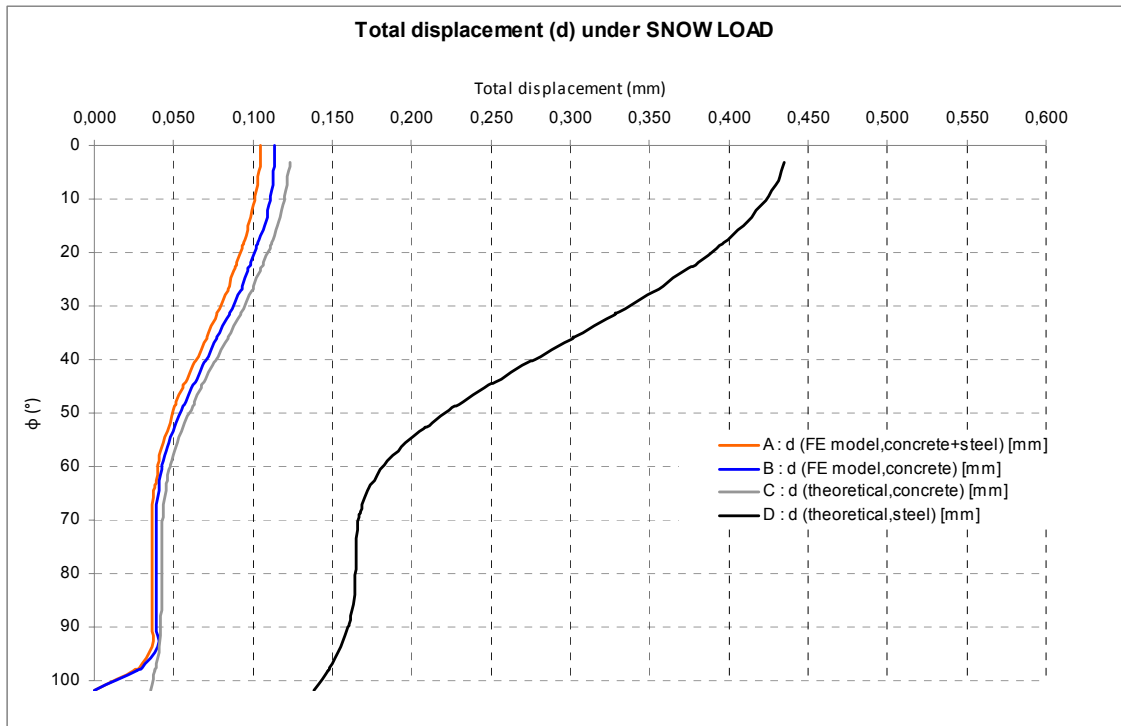
Figure 2.60: *Comparison between the finite-element calculation and the theoretical one of the deformation of the concrete shell under the snow load in section **S**.*
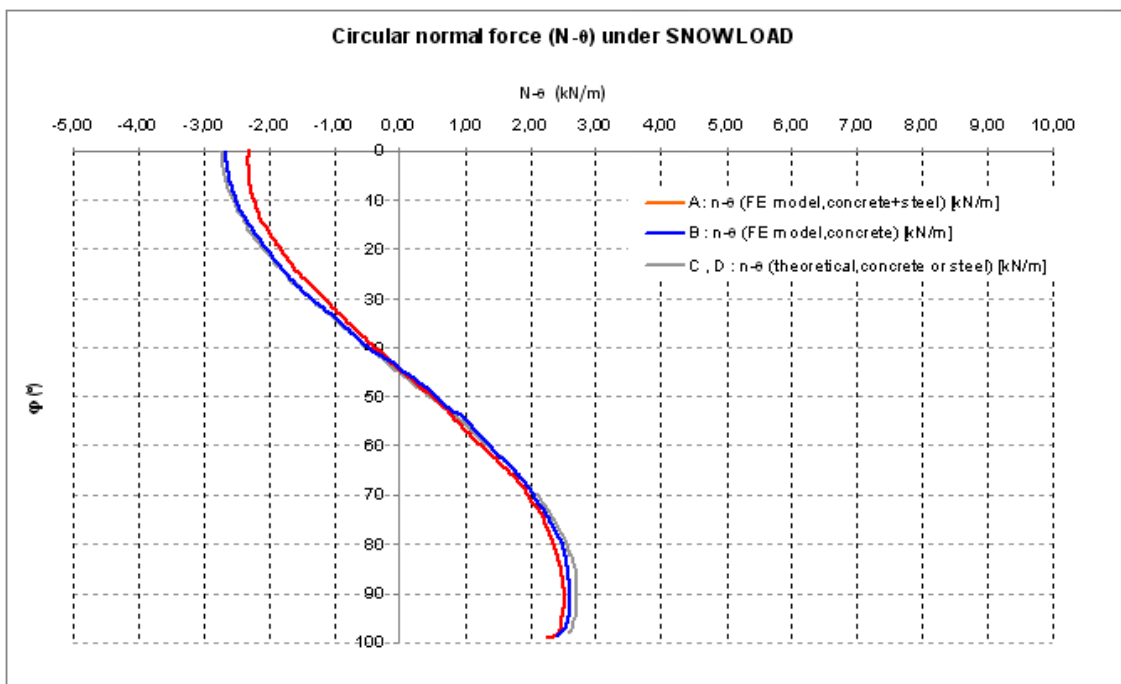
Figure 2.61: *Comparison between the finite-element calculation and the theoretical one of the internal circular normal force in the concrete shell under the snow load in section **S**.*
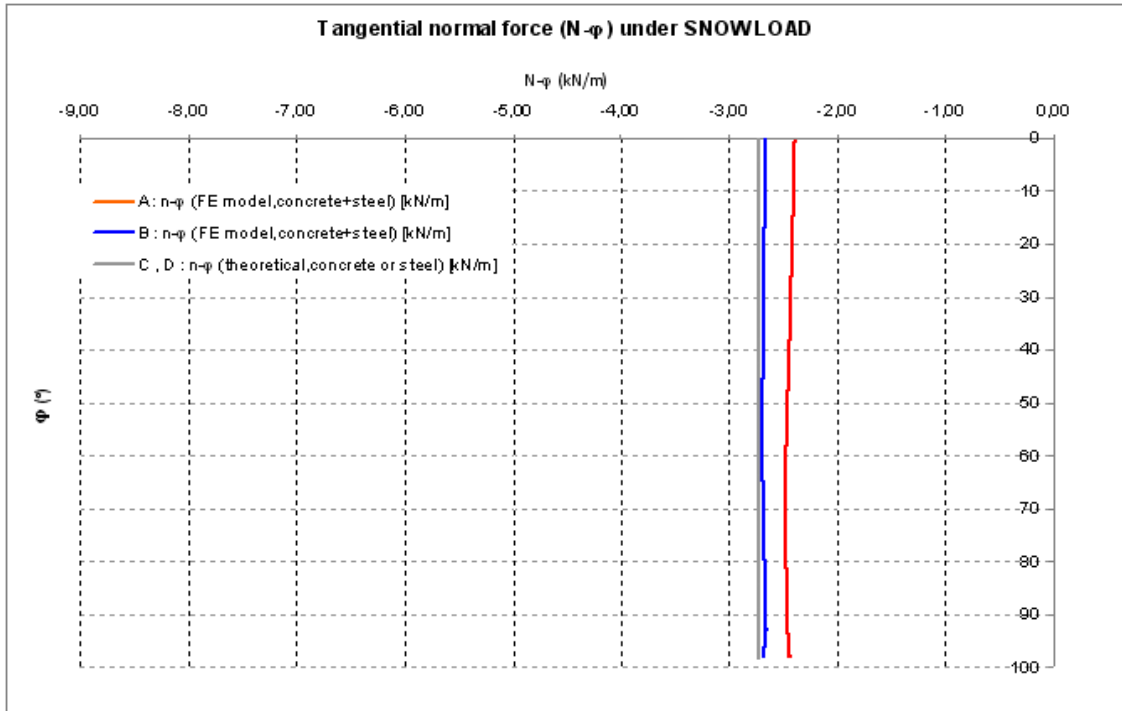
Figure 2.62: *Comparison between the finite-element calculation and the theoretical one of the internal tangent normal force in the concrete shell under the snow load in section **S**.*

2.3.4.3 Wind load case

These are the effects of the **wind load** (figures **2.63** to **2.71**).
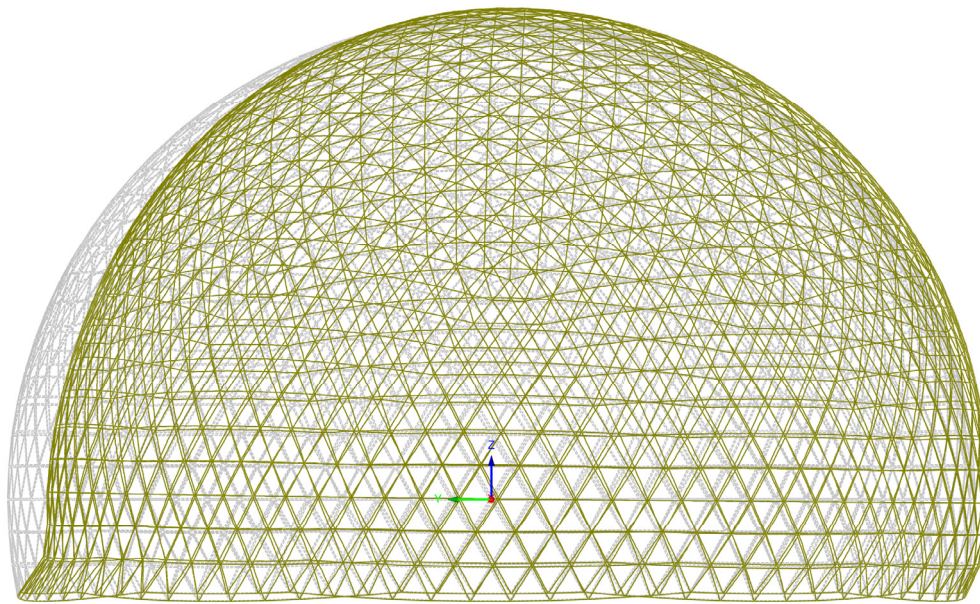
Figure 2.63: *Deformation of the steel structure under the wind load (complete FE-model).*

LC2: Wind
u

Against Y-direction

Section S

Max u: 0.152, Min u: 0.000 [mm]
Factor of deformations: 5000.00
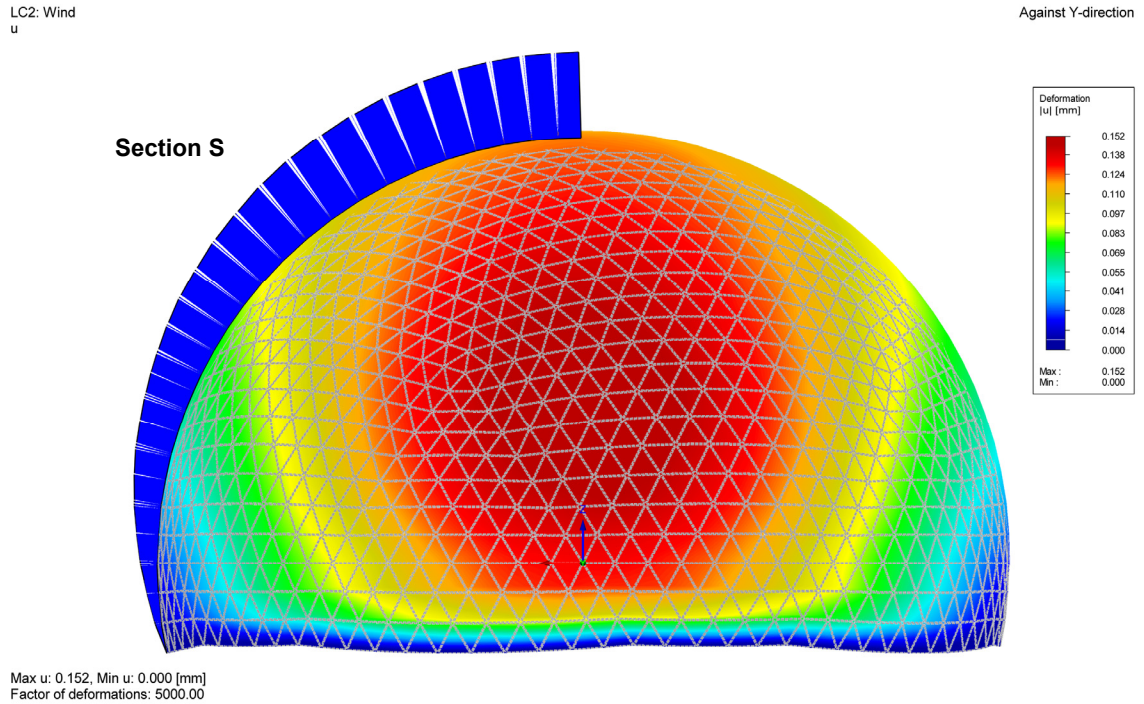
Figure 2.64: *Deformation of the concrete shell under the wind load, with the detail of section **S** (complete FE-model).*

LC2: Wind
u

Isometric

Section S

Max u: 0.152, Min u: 0.000 [mm]
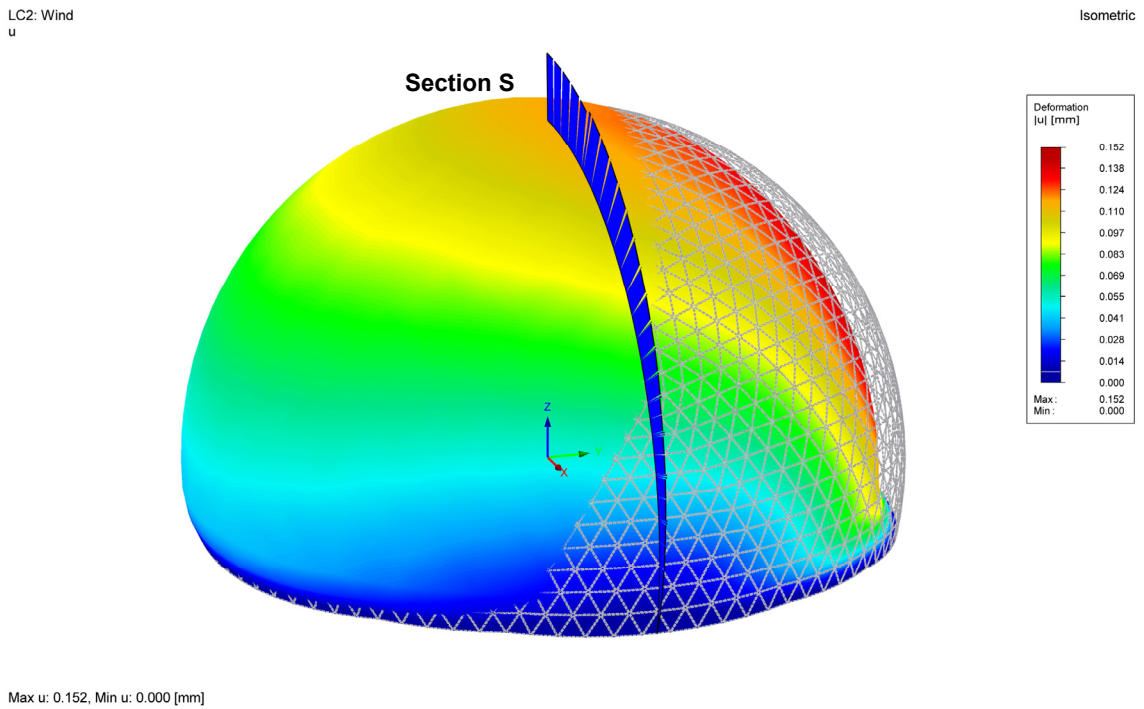
Figure 2.65: *3D view of the deformation of the concrete shell under the wind load, with the detail of section **S** (complete FE-model).*

LC2: Wind
Members N

In X-direction
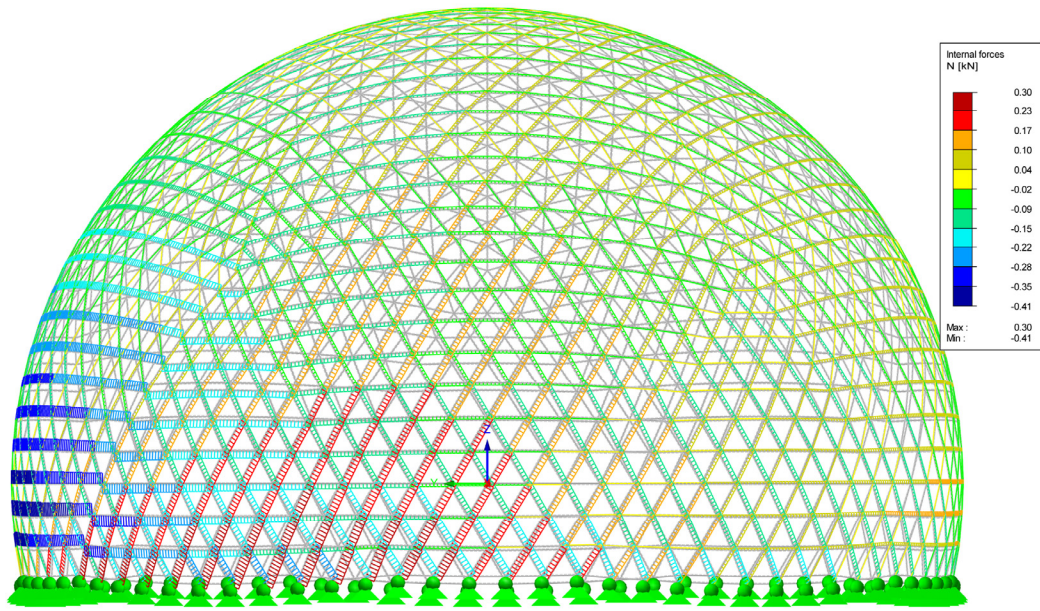
Members Max N: 0.30, Min N: -0.41 [kN]

Figure 2.66: *Normal force in the steel structure under the wind load (complete FE-model).*

LC2: Wind
Surfaces n-1

Isometric

tesion
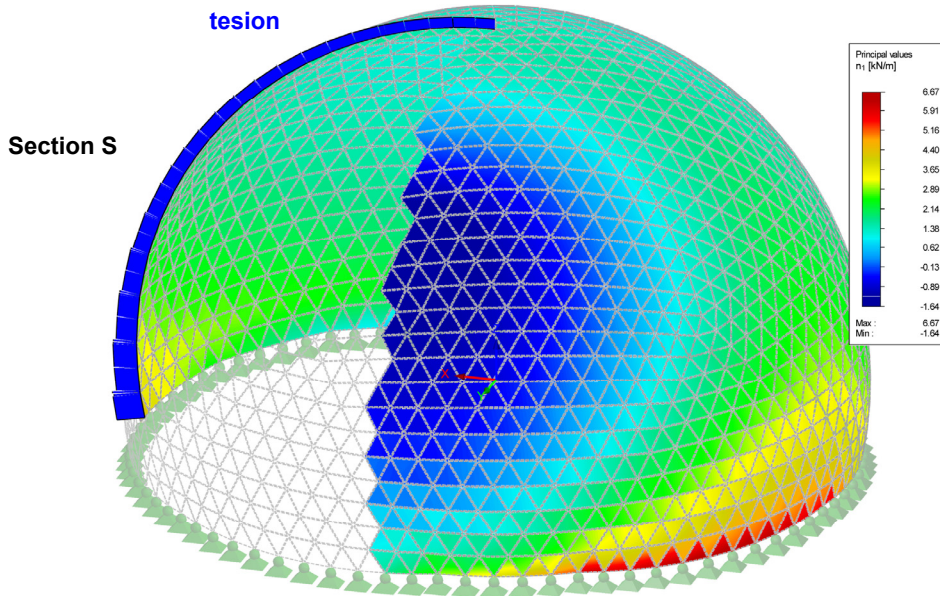
Section S

Surfaces Max n-1: 6.67, Min n-1: -1.64 [kN/m]

Figure 2.67: *Internal circular normal force in the concrete shell under the wind load, with the detail of section S (complete FE-model).*
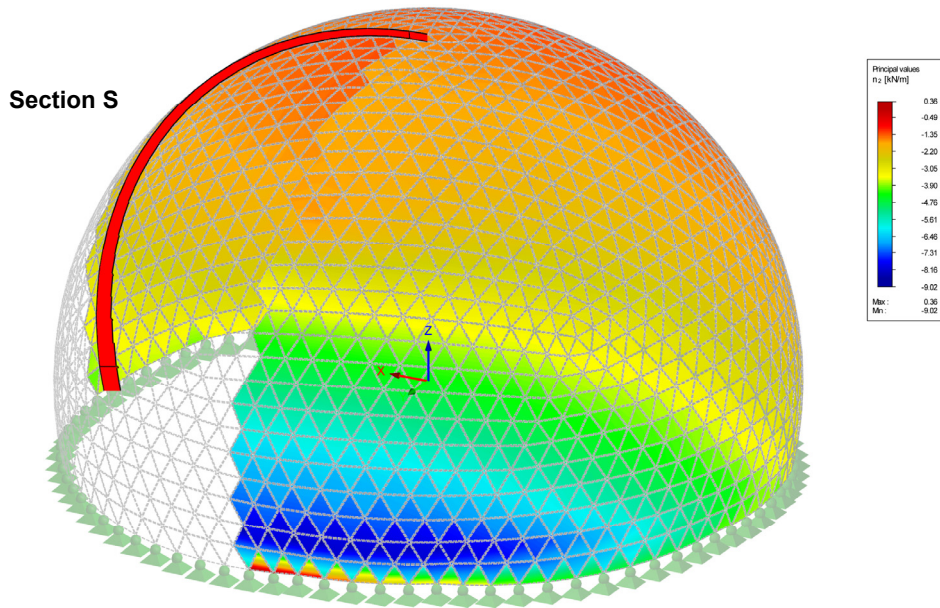
Surfaces Max n-2: 0.36, Min n-2: -9.02 [kN/m]

Figure 2.68: *Internal tangential normal force in the concrete shell under the wind load, with the detail of section S (complete FE-model).*
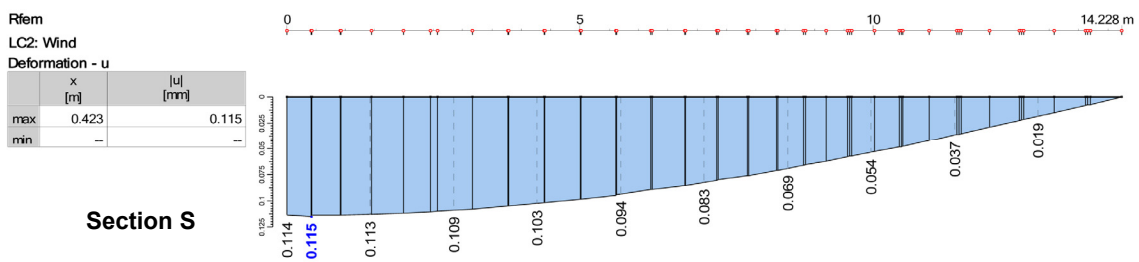
Figure 2.69: *Deformation of the concrete shell under the wind load in S (FE-model).*
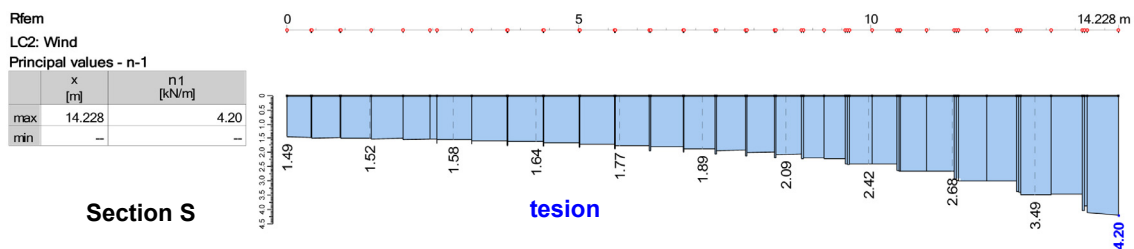
Figure 2.70: *Internal circular normal force in the concrete shell under the wind load in S (FE-model).*
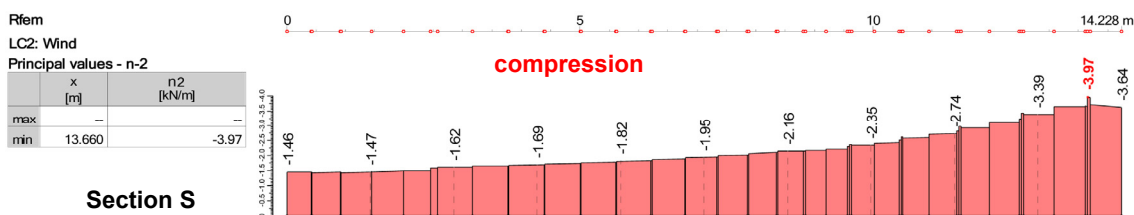
Figure 2.71: *Internal tangential normal force in the concrete shell under the wind load in S (FE-model).*

Even if it is more difficult to analyze the wind load case as we do not have a theoretical model to work with, we see that the induced deformation and normal forces are slightly bigger but spatially distributed in a different way. The steel mesh has, probably, a more important role with this kind of skew-symmetrical load case.

2.3.4.4 Deformation load group

We have also considered a load group so as to evaluate the **deformations**, which consists in the sum of the dead load, the snow load and the wind load (figures **2.72** and **2.73**). Once again we obtain extremely small values.
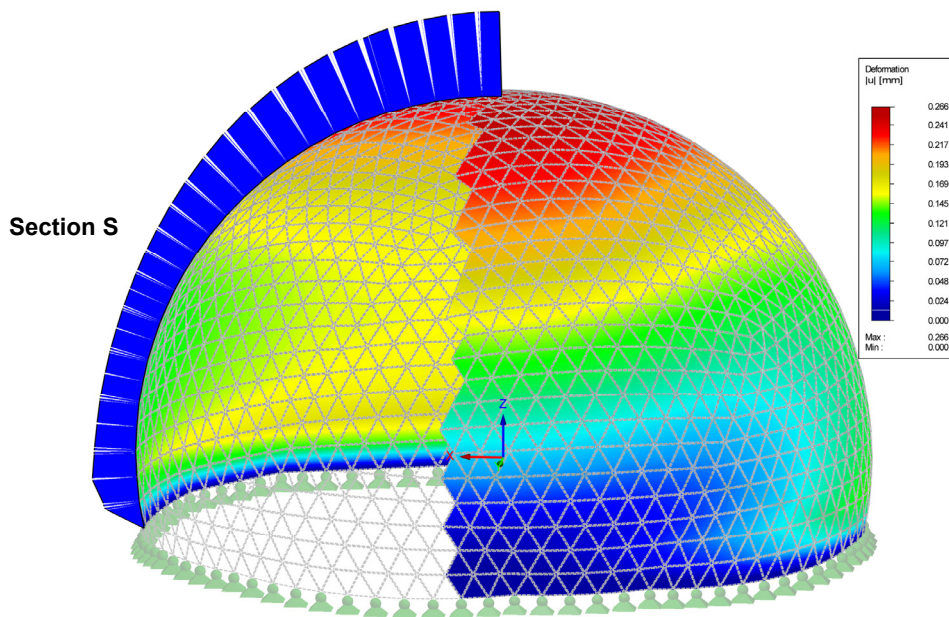
Figure 2.72: *Deformation of the concrete shell under the deformation load group, with the detail of section S (complete FE-model).*
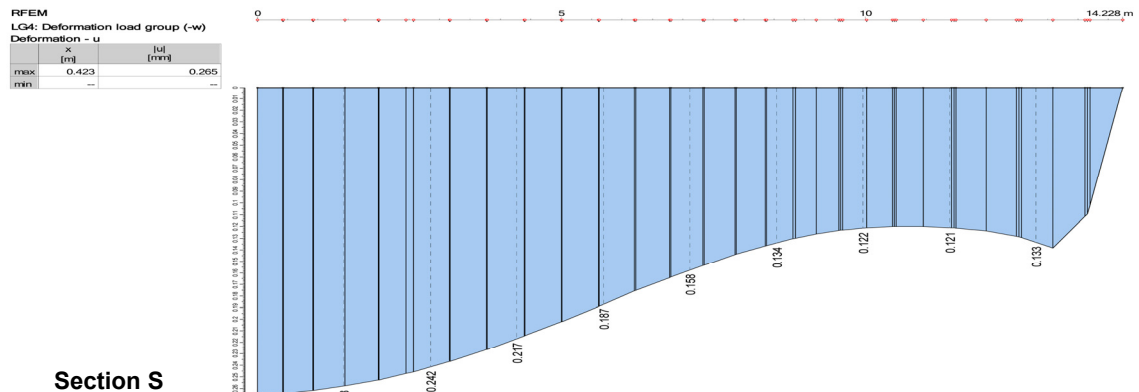
Figure 2.73: *Deformation of the concrete shell under the deformation load group in section S (complete FE-model).*

2.3.4.5 Design load group

We also have a load group for the **design phase**, which is defined as 1,35 times the dead load plus 1,5 times the snow and wind loads. In this case it is important to look at the stresses (figures **2.73** to **2.77**), which are minimal.
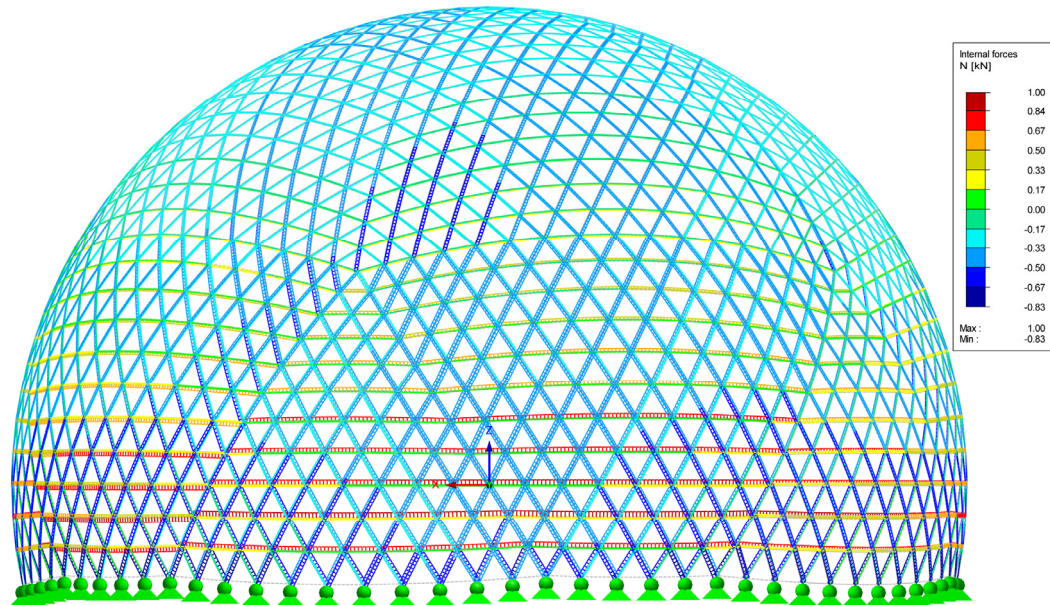
Members Max N: 1.00, Min N: -0.83 [kN]

Figure 2.74: *Normal force in the steel structure under the design load group (complete FE-model).*
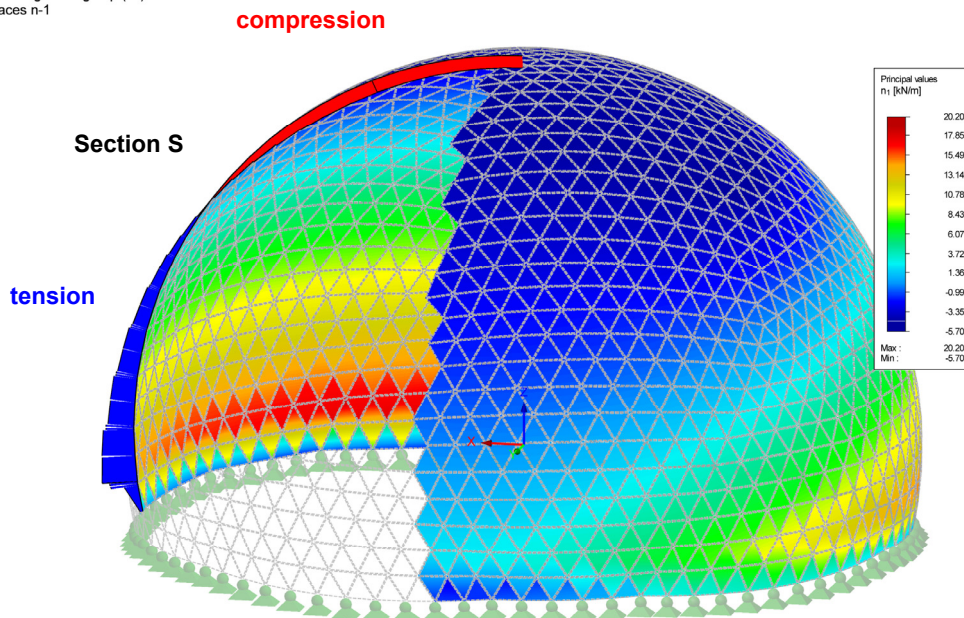
Surfaces Max n-1: 20.20, Min n-1: -5.70 [kN/m]

Figure 2.75: *Internal circular normal force in the concrete shell under the design load group, with the detail of section S (complete FE-model).*
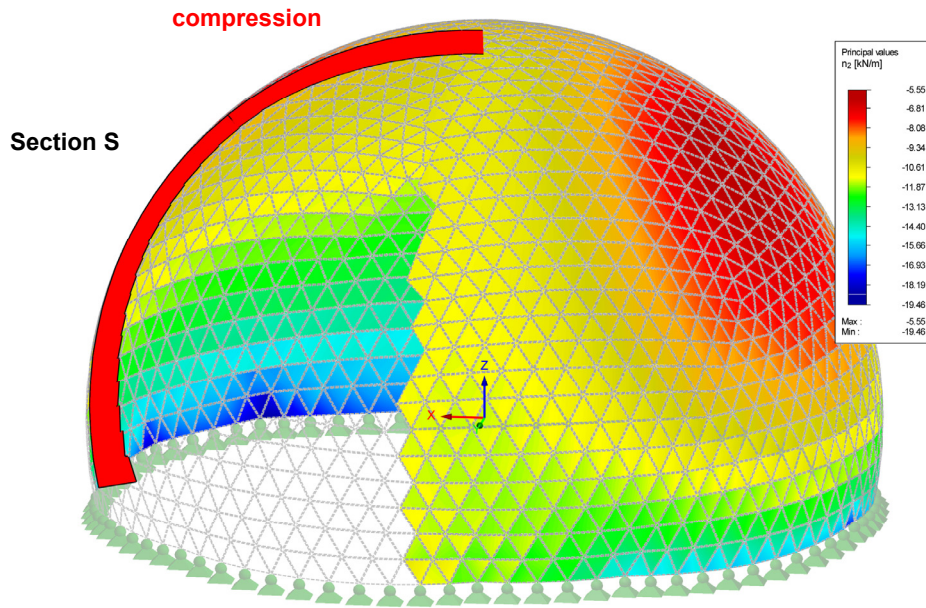
Surfaces Max n-2: -5.55, Min n-2: -19.46 [kN/m]

Figure 2.76: *Internal tangential normal force in the concrete shell under the design load group with the detail of section S (complete FE-model).*
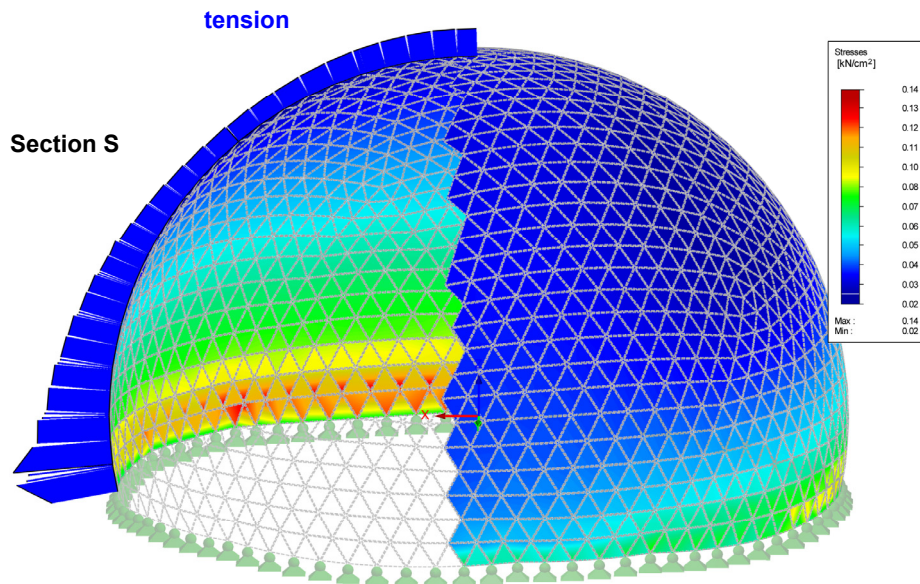
Surfaces Max Sigma-eqv,max,Mises: 0.14, Min Sigma-eqv,max,Mises: 0.02 [kN/cm^2]

Figure 2.77: *Stresses in the concrete shell under the design load group, with the detail of section S (complete FE-model).*

All of these results are analyzed in the following chapter, although we can already glimpse the outstanding behavior of the structure just from observing the stresses on both the concrete shell and stabs (table **2.13**). As we can appreciate in the results of the FE-model, the **stresses** in the concrete shell remain very small, since they are distant from the tensile and compressive strengths. The same phenomenon occurs in the bars: we can calculate the stress in them by dividing the normal force by its known section. We obtain once again small values relative to the yield strength. We have taken, in each case, the extreme value even if it does not occur at the same point.

To obtain a stress value that takes into account both the shell and the bars, we assume that the force acting in the bars is *distributed* in its surrounding concrete shell. Thus, we assume a mean bar length of 0,60 m, 0,67 m apart in the tangential direction and 0,60 m in the circular direction. Furthermore, when we calculate the stress in the tangential direction we must take into account two inclined bars at approximately 60°.

In the concrete shell			
Max **compressive** stress (σ_{Mises})	1,4 < 20,00	MN/m^2	Fig. **2.77**
Max circular **compressive** stress	0,0057 / (0,03) = 0,19	MN/m^2	Fig. **2.75**
Max tangential **compressive** stress	0,0195 / (0,03) = 0,65	MN/m^2	Fig. **2.76**
Max circular **tensile** stress	0,0202 / (0,03) = 0,68	MN/m^2	Fig. **2.75**
Max **compressive** stress in the bars	0,00083 / (0,02*0,008) = 5,2 <370	MN/m^2	Fig. **2.74**
Max **tensile** stress in the bars	0,001 / (0,02*0,008) = 6,3 < 370	MN/m^2	Fig. **2.74**
Max circular **compressive** stress	0,19 + 0,00083 / (0,03*0,67) = 0,23	MN/m^2	Fig. **2.75 + 2.74**
Max tangential **compressive** stress	0,65 + 0,00083 * 3$^{0.5}$ / (0,03*0,6) = 0,73	MN/m^2	Fig. **2.76 + 2.74**
Max circular **tensile** stress	0,68 + 0,001 / (0,03*0,67) = 0,73	MN/m^2	Fig. **2.75 + 2.74**

Table 2.13: *Extreme values for stresses both in the concrete shell and in the bars for the design load case.*

2.3.5 ANALYSIS OF THE RESULTS

At this point, it is important to try to explain the **role of the steel bars** in this structure. First of all, we have seen that the differences in the results between the complete model (FE-model A) and the theoretical model C, which takes only into account the concrete shell, can be explained by the forces acting in the bars, even if it constitutes only a small part of the total forces generated by the studied load cases. Comparing models A and B, we can also deduce that the steel mesh helps to retain the

displacements. Those bars, then, have a mechanical role and could, with larger loads, support the tension that eventually the concrete would be unable to resist; the steel structure could also help to resist the effects of the local bending near the support plates. Bars can also have a more important role in skew-symmetrical load cases such as wind. Furthermore, we have to remember that it is thanks to the construction of the steel mesh that we can achieve the desired spherical shape; without the geometric study of geodesic spheres it would be impossible to approximate such a shape. Finally, the existence of the mesh allows for the installation of the formworks and the construction of the concrete shell. Thus the steel mesh has **mechanical**, **geometrical** and **constructive** roles.

However the **concrete shell plays a role as well**, apart from the already known and studied mechanical behavior. On the one hand, it covers the structure, which is a problem that appears in all the framework structures. On the other, it also helps to avoid the deflection of the steel bars: small angles between the bars can create this phenomenon. Finally, we have verified that the concrete shell acts as a membrane when the moments are zero, confirming our hypothesis; only small moments appear near the support plates. Figure **2.78** shows the value of m_x; we obtain similar results for m_y and m_{xy}.
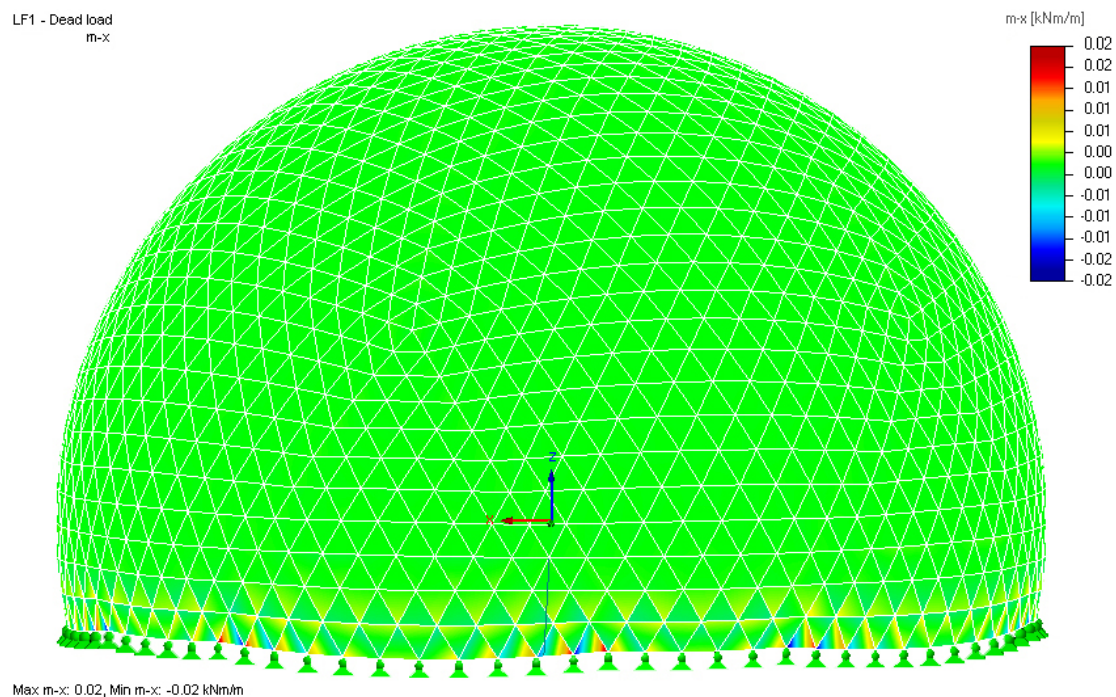
Figure 2.78: *Moment m_x in the concrete shell under the dead load case (complete FE-model).*

In addition, it is important to comment on the differences that appear between the theoretical and finite-element models near the **support plates** ($\varphi=102,18°$). We discussed a local bending in this part of the structure resulting from the imposed null displacement, which does not fit the theory assumptions; in fact, the natural deformation of the dome is to expand its radius, but this is impeded by the use of a concrete ring that connects the dome and the roof of the building. Furthermore, these support plates are disposed horizontally, obtaining a reaction that is not tangential to the shell (once again, the theory assumptions are not locally accomplished).

This fact explains the differences between both models, as well as the small problems that may appear during and after the construction of the dome, such as cracks near the support plates. However, the deformations are very small compared to the thickness of the shell, so we will not encounter major problems.

As a final comment, we should highlight the **general behavior of the structure**. Even if the thickness of the concrete shell is small and we have a mesh of extremely thin bars, the deformations suffered by the structure are always less than 1 mm. Unfortunately, we cannot compare these results with experimental observations since the structure was demolished some years after.

There are obviously other factors that can degrade this situation: on the one hand, the bars are actually less performing as we have not taken into account the connection between them. On the other, we have not considered the geometric imperfections and the influence of non-uniform material properties, which are factors with a potentially notable negative influence on the behavior of the structure.

Thus the dome is not over dimensioned at all (in any case, a 3 cm shell is not excessive as we also have to take into account constructive aspects), but certainly very stable. It is precisely thanks to its dome shape that the forces are so highly efficiently distributed in the structure, leading to minimal deformations. We can now understand from the **static** point of view why domes have been used so frequently throughout our history. But there are certainly other criteria, such as **aesthetics**. Let us see how we can factor in these additional criteria.

2.4 Script design : connecting creativity to statics

It would be unfair to conclude this project without highlighting the main role that *scripting* has played in many areas. On the one hand, we used it to analyze bar length, to compute angles between bars and to obtain the area of a geodesic sphere level *n*. Such a precise study would have been impossible without this tool, as we are dealing with structures that can have over one thousand elements.

On the other hand, we displayed all of these results in a self-explanatory manner: bars and planes are labeled and color-coded according to their properties in order to clearly illustrate the assembly process.

Finally, we built the 3D model of the Zeiss dome and exported it to the FE-calculation software. It is thanks to this connection that we were able to go one step further and establish a connection with static concepts.

Thus, we are talking about a very powerful tool which allows us to **analyze**, **show,** and **create**. We are limited only by our creativity as we need only translate our thoughts into commands. We could go so far as to say that scripting helps us to boost our design possibilities, and offers at the same time, a soft transition to the structural calculation.

It is precisely for this reason that we have even **more ideas** on how to improve the study of the Zeiss dome, but much more time would be required to develop them appropriately. Therefore, we will show only two more examples of how to use the script tool in the design process.

2.4.1 SCRIPTING THE IMPERFECTIONS

The first example is related to the study of the effects that **imperfections** would have in the Zeiss dome. A practical way to do it would be to slightly modify the coordinates of the geodesic dome vertices, by introducing a *random* variation in the vector length when projecting the new vertices into the ideal sphere (the new vertices are at a distance of *R * (1 - r)* from the center of the sphere, with *r* being a random value *0 ≤ r ≤ ε*).

We present the new geometry in the following figure **2.79**. We assume that the bars of the structure were produced with an accuracy of ε = 0,6 % (a deviation of 0,05 mm was accepted in the original structure, 8 mm being the smallest principal dimension of the bars). Imperfections are shown in figure **2.79** with a factor 7 and bars have been colored with a gradient color going from red to blue proportional to the value of the displacement respect to the original position. We would only have to export the new geometry into the FE-calculation software to obtain the structural solution.
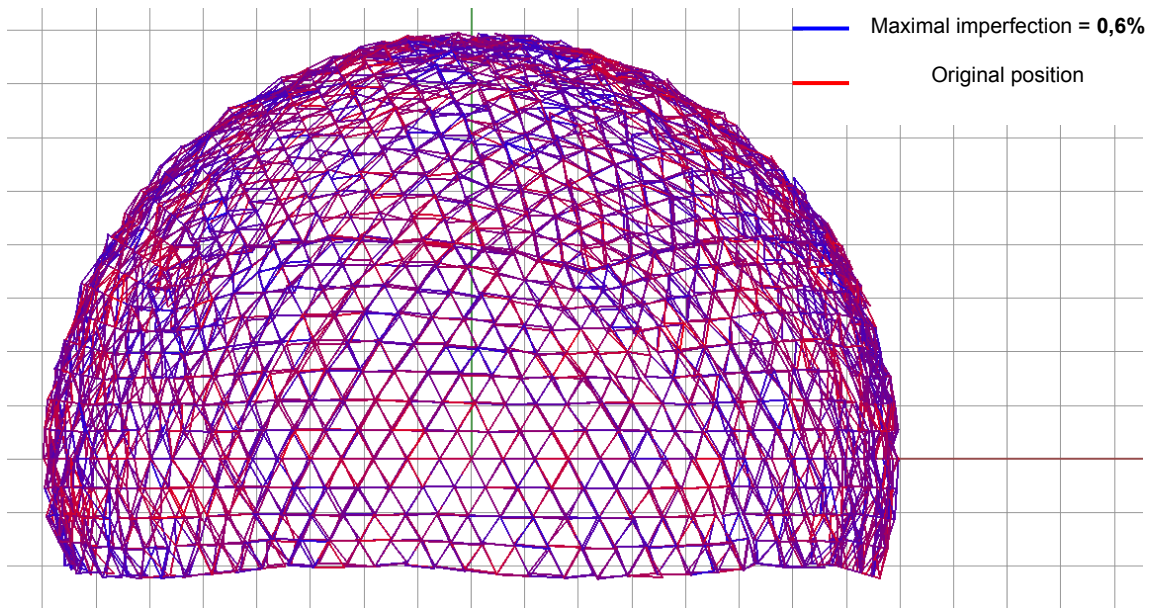
Figure 2.79: *Random generated imperfections in the steel structure, shown with a factor 7 and colored depending on their value (blue for maximal imperfections, red for minimal ones).*

However, we can predict that such a deformed structure would produce an anomaly in terms of deflection, being the membrane theory invalidated.

2.4.2 SCRIPTING THE DESIGN

The second example has to do with **design**. It is commonplace to add some holes on the roofing, either to improve the illumination of the interior spaces or simply for aesthetic reasons. But how would this variation influence the static behavior?
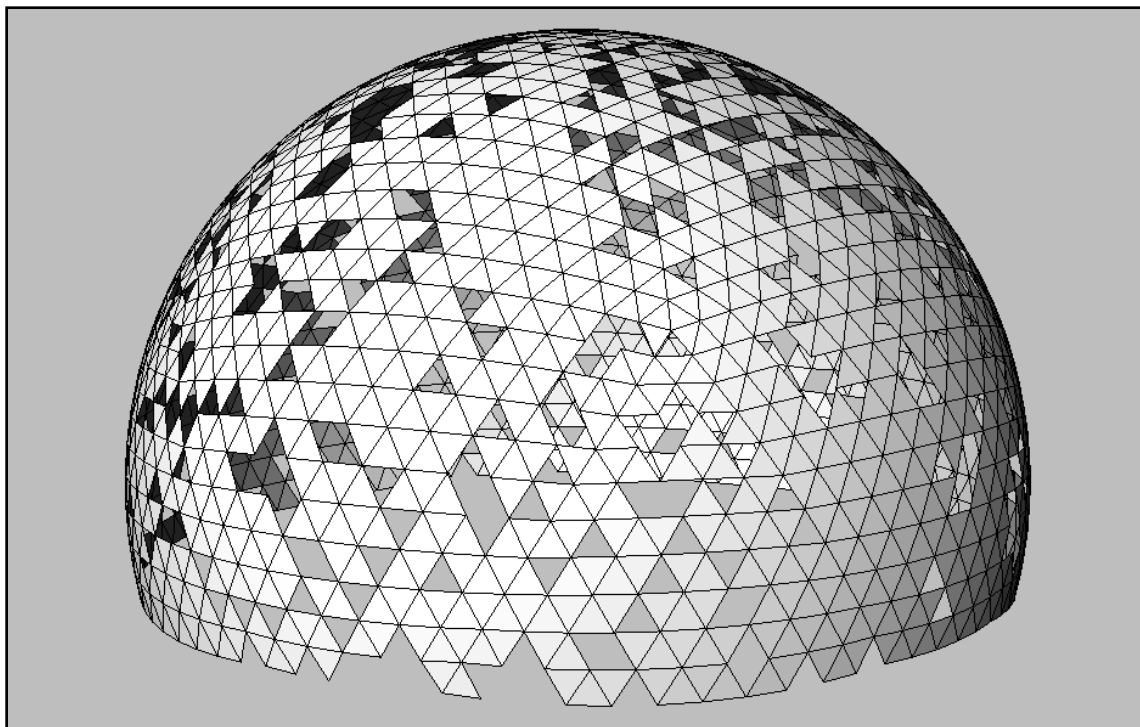
Figure 2.80: *Zeiss dome with random generated holes representing 20% of the original dome area.*

The preceding figure **2.80** shows how this modified geodesic dome could look, with random holes on its roof. The holes represent, in this case, 20% of the original dome area, but we can modify this parameter depending on our preferences. Figure **2.81** shows a more accurate view of the design.
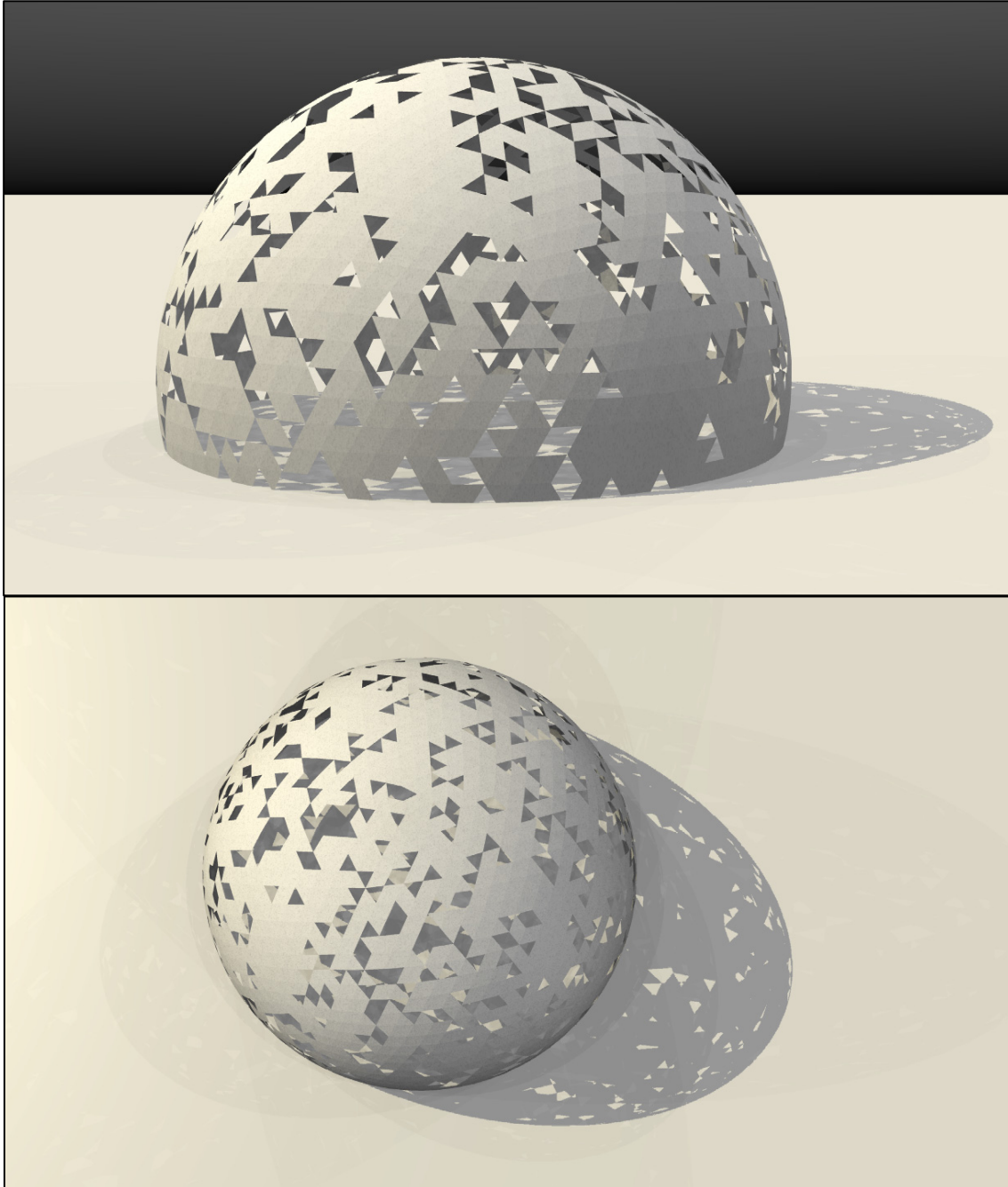
Figure 2.81: Render views of the script-designed structure.

We can go one step farther by showing the effects of such a modification of the structure under the dead load. We have built three new geometrical models to study the behavior of a dome with circular, tangential, and random openings (these represent approximately 5% of the original dome area). We can already guess that the

membrane behavior will disappear due to a local deflection around the openings and, as we will no longer have the dome-shape effect, we should expect larger displacements (30% larger, as indicated by figure **2.82** and table **2.14**). The radial normal forces and tangential normal forces must now find a new path, creating a local anomaly around the openings (with a radius measuring approximately two times the width of the openings) that is even more significant near the support plates (figure **2.83**).
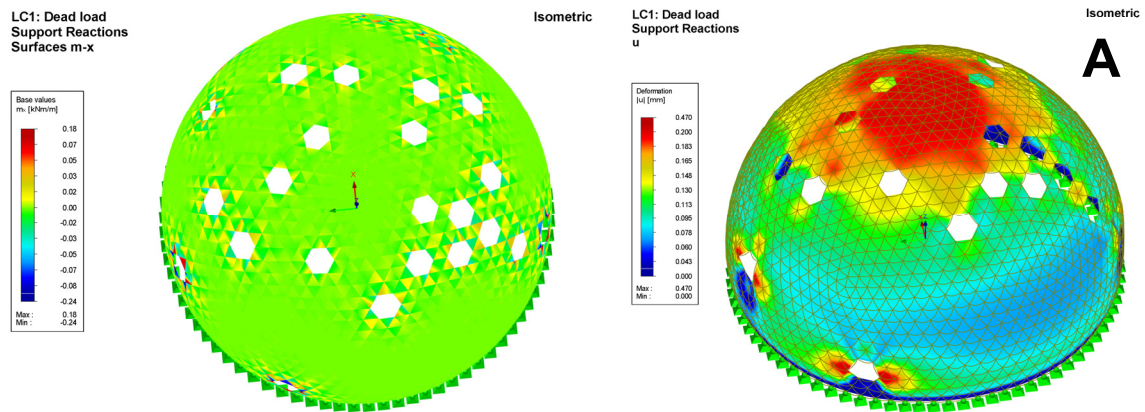
Figure 2.82: *Moment m_x and deformation of the concrete shell with random openings (dead load).*
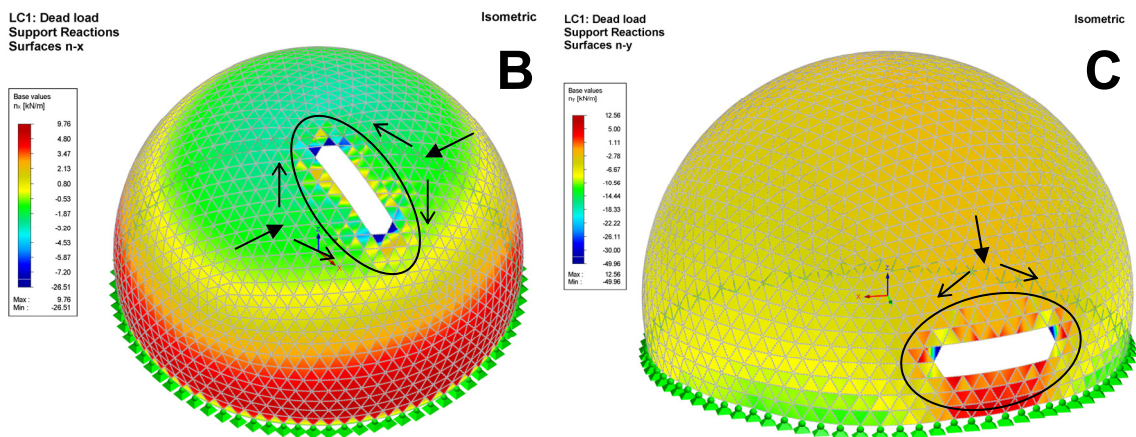
Figure 2.83: *Internal circular normal force and internal tangential normal force in the concrete shell with, respectively, a tangential opening and a circular opening (dead load).*

Models	Zeiss dome	Open dome A	Open dome B	Open dome C
Zenith displacement	0,16 mm	0,21 mm	0,13 mm	0,21 mm
Local max. displacement (openings)	-	0,47 mm	2,1 mm	2,5 mm
Normal force max. anomaly (op.)	-	+ 21 kN / m	- 24 kN / m	- 40 kN / m

Table 2.14: *Comparison of the displacements and the normal force maximal anomaly around the openings in the different models (dead load).*

First, it is important to highlight that such a modification in the structure provides the basis for the preceding **reasoning process**. Careful study of the original dome enables us to predict the general behavior of the open dome. Second, the study of the modified structure represents a link between the *old* obstacles concerning standard shell structures and the **new challenge** that openings represent.

In this case, we are restricted by the function of the structure. However, there are more generic examples in which the idea of scripting a shape can be applied. Freeform surfaces are widely used today and such an approach not only simplifies the calculations but also gives the designer a greater degree of freedom

Finally, as a future work, we could even think about a more advanced way of understanding the connection between aesthetics and statics. We could set up a dialogue between both approaches of the object and define an optimizing criterion thanks to the parametric model of the geometry that is compatible with both a 3D design program and a 3D statics program. This would produce a structure that not only fits into the given geometry but also has an internal framework that induces minimum stress: the so-called **shape-stress or topological optimization**.

We can now draw a number of conclusions. However, we can already say that in this reasoning process we have attempted to include some stages of the conception process: in other words, we have sought to be ***creative designers***.

3 CONCLUSIONS

"It is pertinent to ask what qualities and attitudes mark the sort of engineer who is willing to break through the many constraints and do something different (…). Obviously, there must be a strong motivation. Ambition is an important factor, but there must be much more: a sense of mission (…), a lively sense of curiosity and fascination with structures and objects; and dissatisfaction with conventional ways of doing things"

Alan Holgate, Holgate (1997)

Jena, 1922. A group of engineers conceive a new system that allows for the construction of incredibly thin concrete shells. Frankfurt am Main, 2009. The same system is studied, trying to provide new reasoning elements. Eighty-seven years have passed but something has not changed. The aim of doing *something new, something different*.

Aside from the intermediate conclusions developed in the preceding chapters, this work strives to demonstrate that a multiple and intertwined approach to a given problem is much more useful than many different independent approaches, because they cannot take into account the connection that always exists between them.

For example, the **historical research** concerning the Zeiss dome was fundamental to explain how the structure was understood in its time and allowed us to build the **parametric geometrical model**. The unique flexibility of this model, that can be adapted to many different needs, permitted a permanent dialogue between **both aesthetics and statics issues**.

The main goal of the project was to answer to the following question: why are we separating the functions of architects and engineers? It would be certainly naïve to think that all engineers can have an aesthetic sensibility, or that all architects want to work with complex structural problems. But tools such as *scripting* and an open mind can make them work together, contributing both parts in all stages of a project and creating a much richer solution. This idea can of course be broadened and applied to many other fields.

Finally, we should highlight the fact that this study does not claim to be exhaustive but rather to show certain tools that can aid in the exploration of boundless possibilities. This particular interest of the presented work, is precisely what drives us **to go farther every day**, with curiosity, illusions, and expectations. But why? Baudelaire may have the answer. We have only shown some of the paths, now feel free to enjoy *your own* trip.

Nous voulons, tant ce feu nous brûle le cerveau,	*This fire burns our brains so fiercely, we wish to plunge*
Plonger au fond du gouffre, Enfer ou Ciel,qu'importe?	*To the abyss' depths, Heaven or Hell, does it matter?*
Au fond de l'Inconnu pour trouver du nouveau!	*To the depths of the Unknown to find something new!*
Charles Baudelaire*, « Le voyage »,* extract.	**Charles Baudelaire "The Voyage"** *(« Le voyage »),* extract. Translated by William Aggeler (1954), *The Flowers of Evil* , Academy Library Guild, Fresno.

4 REFERENCES

4.1 Bibliography

Bargmann, H. (1993), Historische *Bautabellen : Normen und Konstruktionhinweise 1870 bis 1960*, Werner-Verlag, Düsseldorf.

Bisch, P. (1997), *Plaques et Coques*, publication of a course in the École des Ponts Paristech, Paris.

Dischinger, F. (1925), *Deutsche Bauzeitung: Fortschritte im Bau von Massivkuppeln*, Reg.-Baumeister a.D. Fritz Eiselen, Berlin.

Dischinger, F. and Finsterwalder, U. (1932), *Beton und Eisen : Die weitere Entwicklung der Schalenbauweise „Zeiss-Dywidag"*, Reg.-Baumeister a.D. Fritz Eiselen, Berlin.

Dvorkin, E.N. (1984), *A continuum mechanics based four-node shell element for nonlinear analysis*, In: Eng. Comput., vol.1, pp.77-88.

Finsterwalder, U. (1923), *Statische Berechnung der Zeisskuppel*, Dilpomhauptprüfung from the Technischen Hochschule München, München.

Girkmann, K. (1978), *Flächentragwerke*, Springer Verlag, Wien.

Heinle, E. and Schlaich, J. (1996), *Kuppeln aller Zeiten – aller Kulturen*, Deutsche Verlags-Anstalt, Stuttgart.

Holgate, A. (1997), *The art of Structural Engineering. The work of Jörg Schlaich and his Team*, Edition Axel Menges, Stuttgart.

Kaminski, M. (2005), *Computational Mechanics of Composite Materials: Sensitivity, Randomness and Multiscale Behaviour*, Edition Springer, Berlin.

Kurze B. (2006), *Industriearchitektur eines Weltunternehmens : Carl Zeiss 1880-1945*, E.Reinhold Verlag, Altenburg.

Meschke, G. and Rumanus, E. (2008), *Modelling of reinforced concrete by means of homogenization approach including steel-concrete interactions*, Institute for structural mechanics, Ruhr University Bochum, Bochum

Mörsch, E. (1923), *Der Eisenbetonbau*, Verlag von Konrad Wittwer, Stuttgart.

Müller-Wulckow, W. (1975), *Architektur der Zwanziger Jahre in Deutschland*, Druckhaus Rombach+Co GmbH, Freiburg im Breisgau.

Pottmann, H., Asperl, A., Hofer, M., Kilian, A. (2007), *Architectural Geometry*, Bentley Institute Press, Exton.

Rappaport, N. (2007), *Support and Resist. Structural engineers and design innovation*, The Monacelli Press, New York.

Vogl R., Bystrov D., Jerabék J., Kabrt L., Míchal P., Michalovic R., Nadge F., Pokorná P. (2008), *RFEM 3 Handbuch*, Ingenieur-Software Dlubal GmbH, Tiefenbach

Zeiss, C. (1922), *Verfahren zur Herstellung von Kuppeln und ähnlichen gekrümmten Flächen aus Eisenbeton*, Reichpatentamt, Germany.

Zeiss, C. (1925), *Knotenpunktverbindung für eiserne Netzwerke*, Reichpatentamt, Germany.

4.2 Institutions

- *Carl Zeiss AG*, Jena location, Corporate Archives

   Carl-Zeiss-Promenade 10, 07745 Jena

   Phone: +49 36 41/64-2759

   Fax: +49 36 41/64-3207

4.3 Internet sources

Dritsas, S. (2005), *Scripting library version 1 release 10*, public electronic publication in "http://dritsas.jeneratiff.com/scripting/library/".

Rutten, D. (2009), *Rhinoscript for Rhinoceros 4.0*, public electronic publication in "http://en.wiki.mcneel.com/default.aspx/McNeel/RhinoScript101.html".

4.4 Software

We have used the software shown in table **4.1**.

Software	Description
Adobe Photoshop 7.0	Image processing software
Autodesk 3D Studio Max 9	3D modeling software
Basic Miktex 2.7	Text and formula specialized processing software
Google SketchUp 7.0	3D modeling software
Microsoft Office Word 2003	Text processing software
Microsoft Office Excel 2003	Tables and graphics processing software
Rhinoceros 4.0	3D modeling software
Dlubal RFEM 3.0	3D finite-element calculation software
SPSS PASW Statistics 17.0	Statistics software

Table 4.1: *Used software description.*

5 ANNEX

5.1 Vectors' scripting library

The following commands are very useful when working with vectors and vertices as we avoid using the much slower *Rhino* commands. Vertices commands are also essential to build this library.

```
''#license copyright
    ''  scripting library version 1 release 10
    ''  copyright (c) 2003-2005 stylianos dritsas
    ''  license:
    ''  http://creativecommons.org/licenses/by/2.5/
    ''  contact:
    ''  dritsas [at] alum [dot] mit [dot] edu
''#endlicense

dim vector_x: vector_x = 0
dim vector_y: vector_y = 1
dim vector_z: vector_z = 2

dim vector_nl: vector_nl = vector_new( 0.0, 0.0, 0.0 )
dim vector_dx: vector_dx = vector_new( 1.0, 0.0, 0.0 )
dim vector_dy: vector_dy = vector_new( 0.0, 1.0, 0.0 )
dim vector_dz: vector_dz = vector_new( 0.0, 0.0, 1.0 )

function vector_new( x, y, z )
    vector_new = vertex_new( x, y, z )
end function

function vector_create( va, vb )
    vector_create = vector_new( _
        vb( vector_x ) - va( vector_x ), _
        vb( vector_y ) - va( vector_y ), _
        vb( vector_z ) - va( vector_z )  _
        )
end function

function vector_make( vector )
    vector_make = vector_create( _
        vector( 1 ),              _
        vector( 0 )               _
        )
end function

function vector_length( vector )
    vector_length = sqr( _
        vector( vector_x ) * vector( vector_x ) + _
        vector( vector_y ) * vector( vector_y ) + _
        vector( vector_z ) * vector( vector_z )   _
        )
end function

function vector_add( va, vb )
    vector_add = vector_new( _
        va( vector_x ) + vb( vector_x ), _
        va( vector_y ) + vb( vector_y ), _
        va( vector_z ) + vb( vector_z )  _
        )
end function

function vector_scale( vector, factor )
    vector_scale = vector_new( _
        vector( vector_x ) * factor, _
        vector( vector_y ) * factor, _
        vector( vector_z ) * factor  _
        )
end function
```

```
function vector_scalexyz( vertex, fx, fy, fz )
    vector_scalexyz = vertex_new( _
        vertex( vector_x ) * fx, _
        vertex( vector_y ) * fy, _
        vertex( vector_z ) * fz _
        )
end function

function vector_normalize( vector )
    dim length: length = vector_length( vector )
    if( length = 0.0 ) then
        vector_normalize = vector_new( 0.0, 0.0, 0.0 )
    else
        vector_normalize = vector_new( _
            vector( vector_x ) / length, _
            vector( vector_y ) / length, _
            vector( vector_z ) / length _
            )
    end if
end function

function vector_rescale( vector, length )
    dim length_: length_ = vector_length( vector )
    if( length_ = 0.0 ) then
        vector_rescale = vector_new( 0.0, 0.0, 0.0 )
    else
        vector_rescale = vector_new( _
            length * vector( vector_x ) / length_, _
            length * vector( vector_y ) / length_, _
            length * vector( vector_z ) / length_ _
            )
    end if
end function

function vector_cross( va, vb )
    vector_cross = vector_new( _
        va( vector_y ) * vb( vector_z ) - va( vector_z ) * vb( vector_y ), _
        va( vector_z ) * vb( vector_x ) - va( vector_x ) * vb( vector_z ), _
        va( vector_x ) * vb( vector_y ) - va( vector_y ) * vb( vector_x ) _
        )
end function

function vector_dot( va, vb )
    vector_dot = va( vector_x ) * vb( vector_x ) + _
        va( vector_y ) * vb( vector_y ) + _
        va( vector_z ) * vb( vector_z )
end function

function vector_equals( va, vb )
    vector_equals = ( ( va( vector_x ) = vb( vector_x ) ) and _
        ( va( vector_y ) = vb( vector_y ) ) and _
        ( va( vector_z ) = vb( vector_z ) ) )
end function

function vector_null( vector )
    vector_null = ( ( vector( vector_x ) = 0.0 ) and _
        ( vector( vector_y ) = 0.0 ) and _
        ( vector( vector_z ) = 0.0 ) )
end function

function vector_zero( vector, zero )
    vector_zero = ( abs( vector( vector_x ) <= zero ) and _
        abs( vector( vector_y ) <= zero ) and _
        abs( vector( vector_z ) <= zero ) )
end function

function vector_invert( vector )
    vector_invert = vector_new( _
        -vector( vector_x ), _
        -vector( vector_y ), _
        -vector( vector_z ) _
        )
end function
```

```
function vector_absolute( vector )
    vector_absolute = vector_new( _
        abs( vector( vector_x ) ),  _
        abs( vector( vector_y ) ),  _
        abs( vector( vector_z ) )   _
        )
end function

function vector_align( va, vb )
    vector_align = ( vector_dot( va, vb ) > 0.0 )
end function

function vector_normal( va, vb, vc )
    dim u: u = vector_create( va, vb )
    dim v: v = vector_create( va, vc )
    vector_normal = vector_normalize( vector_cross( u, v ) )
end function

function vector_reflect( vector, axis )
    dim u: u = vector_dot( vector, axis )
    vector_reflect = vector_new( _
        2.0 * u * axis( vector_x ) - vector( vector_x ), _
        2.0 * u * axis( vector_y ) - vector( vector_y ), _
        2.0 * u * axis( vector_z ) - vector( vector_z )   _
        )
end function

function vector_mirror( vector, normal )
    dim u: u = vector_dot( vector, normal )
    vector_mirror = vector_new( _
        -2.0 * u * normal( vector_x ) + vector( vector_x ), _
        -2.0 * u * normal( vector_y ) + vector( vector_y ), _
        -2.0 * u * normal( vector_z ) + vector( vector_z )   _
        )
end function

function vector_bisector( vertex, u, v )
    vector_bisector = vector_normalize( _
        vector_create( _
        vertex, _
        vertex_middle( _
        vertex_translate( vertex, u ), _
        vertex_translate( vertex, v )  _
        ) _
        ) _
        )
end function

function vector_random( )
    vector_random = vector_new( rnd( ), rnd( ), rnd( ) )
end function

function vector_dependant( va, vb, tolerance )
    dim n: n = vector_cross( va, vb )
    vector_dependant = _
        ( abs( n( vector_x ) ) ) <= tolerance ) and _
        ( abs( n( vector_y ) ) ) <= tolerance ) and _
        ( abs( n( vector_z ) ) ) <= tolerance )
end function


dim vertex_x: vertex_x = 0
dim vertex_y: vertex_y = 1
dim vertex_z: vertex_z = 2

dim vertex_null: vertex_null = vertex_new( 0.0, 0.0, 0.0 )

function vertex_new( x, y, z )
    vertex_new = array( x, y, z )
end function

function vertex_convert( vertex )
    vertex_convert = number_convert( vertex( vertex_x ) ) + "," + _
        number_convert( vertex( vertex_y ) ) + "," + _
        number_convert( vertex( vertex_z ) )
end function
```

```
function vertex_print( vertex, digits, delimiter )
    vertex_print = formatnumber( vertex( vertex_x ), digits, 0, 0, 0 ) + delimiter + _
        formatnumber( vertex( vertex_y ), digits, 0, 0, 0 ) + delimiter + _
        formatnumber( vertex( vertex_z ), digits, 0, 0, 0 )
end function

function vertex_clone( vertex )
    vertex_clone = vertex_new( _
        vertex( vertex_x ), _
        vertex( vertex_y ), _
        vertex( vertex_z ) _
        )
end function

function vertex_length( va, vb )
    dim dx: dx = va( vertex_x ) - vb( vertex_x )
    dim dy: dy = va( vertex_y ) - vb( vertex_y )
    dim dz: dz = va( vertex_z ) - vb( vertex_z )
    vertex_length = sqr( dx * dx + dy * dy + dz * dz )
end function

function vertex_equals( va, vb )
    vertex_equals = ( ( va( vertex_x ) = vb( vertex_x ) ) and _
        ( va( vertex_y ) = vb( vertex_y ) ) and _
        ( va( vertex_z ) = vb( vertex_z ) ) )
end function

function vertex_translate( vertex, vector )
    vertex_translate = vertex_new( _
        vertex( vertex_x ) + vector( vertex_x ), _
        vertex( vertex_y ) + vector( vertex_y ), _
        vertex( vertex_z ) + vector( vertex_z ) _
        )
end function

function vertex_translatexyz( vertex, dx, dy, dz )
    vertex_translate = vertex_new( _
        vertex( vertex_x ) + dx, _
        vertex( vertex_y ) + dy, _
        vertex( vertex_z ) + dz _
        )
end function

function vertex_scale( vertex, factor )
    vertex_scale = vertex_new( _
        vertex( vertex_x ) * factor, _
        vertex( vertex_y ) * factor, _
        vertex( vertex_z ) * factor _
        )
end function

function vertex_scalexyz( vertex, fx, fy, fz )
    vertex_scalexyz = vertex_new( _
        vertex( vertex_x ) * fx, _
        vertex( vertex_y ) * fy, _
        vertex( vertex_z ) * fz _
        )
end function

function vertex_rotate( vertex, origin, axis, angle )
    vertex_rotate = vertex_translate( vertex, vector_invert( origin ) )
    vertex_rotate = vertex_multiply( vertex_rotate, matrix_rotate( axis, angle ) )
    vertex_rotate = vertex_translate( vertex_rotate, origin )
end function

function vertex_interpolate( va, vb, factor )
    vertex_interpolate = vertex_new( _
        ( vb( vertex_x ) - va( vertex_x ) ) * factor + va( vertex_x ), _
        ( vb( vertex_y ) - va( vertex_y ) ) * factor + va( vertex_y ), _
        ( vb( vertex_z ) - va( vertex_z ) ) * factor + va( vertex_z ) _
        )
end function
```

```
function vertex_map( vertex, origin, vx, vy, vz )
    vertex_map = vertex_new( _
        origin( vertex_x ) + vertex( vertex_x ) * vx( vertex_x ) + _
        vertex( vertex_y ) * vy( vertex_x ) + _
        vertex( vertex_z ) * vz( vertex_x ), _
        origin( vertex_y ) + vertex( vertex_x ) * vx( vertex_y ) + _
        vertex( vertex_y ) * vy( vertex_y ) + _
        vertex( vertex_z ) * vz( vertex_y ), _
        origin( vertex_z ) + vertex( vertex_x ) * vx( vertex_z ) + _
        vertex( vertex_y ) * vy( vertex_z ) + _
        vertex( vertex_z ) * vz( vertex_z ) _
        )
end function

function vertex_local( vertex, origin, vx, vy, vz )
    dim vector: vector = vector_create( origin, vertex )
    vertex_local = vertex_new( _
        vector_dot( vector, vx ), _
        vector_dot( vector, vy ), _
        vector_dot( vector, vz ) _
        )
end function

function vertex_global( vertex, origin, vx, vy, vz )
    vertex_global = vertex_map( vertex, origin, vx, vy, vz )
end function

function vertex_multiply( vertex, matrix )
    vertex_multiply = vertex_new( _
        vertex( vertex_x ) * matrix( matrix_00 ) + _
        vertex( vertex_y ) * matrix( matrix_01 ) + _
        vertex( vertex_z ) * matrix( matrix_02 ) + _
        matrix( matrix_03 ), _
        vertex( vertex_x ) * matrix( matrix_10 ) + _
        vertex( vertex_y ) * matrix( matrix_11 ) + _
        vertex( vertex_z ) * matrix( matrix_12 ) + _
        matrix( matrix_13 ), _
        vertex( vertex_x ) * matrix( matrix_20 ) + _
        vertex( vertex_y ) * matrix( matrix_21 ) + _
        vertex( vertex_z ) * matrix( matrix_22 ) + _
        matrix( matrix_23 ) )
end function

function vertex_middle( va, vb )
    vertex_middle = vertex_new( _
        ( va( vertex_x ) + vb( vertex_x ) ) / 2.0, _
        ( va( vertex_y ) + vb( vertex_y ) ) / 2.0, _
        ( va( vertex_z ) + vb( vertex_z ) ) / 2.0 _
        )
end function

function vertex_close( va, vb, max )
    vertex_close = ( vertex_length( va, vb ) < max )
end function

function vertex_match( va, vb, tollerance )
    vertex_match = ( ( abs( va( vertex_x ) - vb( vertex_x ) ) < tollerance  ) and _
        ( abs( va( vertex_y ) - vb( vertex_y ) ) < tollerance  ) and _
        ( abs( va( vertex_z ) - vb( vertex_z ) ) < tollerance ) )
end function

function vertex_centroid( va, vb, vc )
    vertex_centroid = vertex_new( _
        ( va( vertex_x ) + vb( vertex_x ) + vc( vertex_x ) ) / 3.0, _
        ( va( vertex_y ) + vb( vertex_y ) + vc( vertex_y ) ) / 3.0, _
        ( va( vertex_z ) + vb( vertex_z ) + vc( vertex_z ) ) / 3.0 _
        )
end function
```

```
function vertex_average( vertices )
    dim result: result = vertex_new( 0.0, 0.0, 0.0 )
    dim index
    for index = lbound( vertices ) to ubound( vertices )
        result( vertex_x ) = result( vertex_x ) + vertices( index )( vertex_x )
        result( vertex_y ) = result( vertex_y ) + vertices( index )( vertex_y )
        result( vertex_z ) = result( vertex_z ) + vertices( index )( vertex_z )
    next
    dim total: total = array_length( vertices )
    result( vertex_x ) = result( vertex_x ) / total
    result( vertex_y ) = result( vertex_y ) / total
    result( vertex_z ) = result( vertex_z ) / total
    vertex_average = result
end function

function vertex_project( va, vb, vc )
    dim ua: ua = vector_create( va, vc )
    dim ub: ub = vector_normalize( vector_create( va, vb ) )
    dim ta: ta = vector_dot( ua, ub )
    vertex_project = vertex_translate( va, vector_scale( ub, ta ) )
end function

function vertex_flatten( pa, pb, pc, pd )
    dim u: u = vector_create( pa, pb )
    dim v: v = vector_create( pa, pc )
    dim n: n = vector_normalize( vector_cross( u, v ) )
    dim s: s = vector_create( pa, pd )
    dim t: t = vector_cross( n, s )
    dim l: l = vector_cross( t, n )
    vertex_flatten = vertex_translate( pa, l )
end function

function vertex_mirror( va, vb, vc, vd )
    dim projected: projected = vertex_flatten( va, vb, vc, vd )
    vertex_mirror = vertex_translate( projected, vector_create( vd, projected ) )
end function

function vertex_reflect( va, vb, vc )
    dim projected: projected = vertex_project( va, vb, vc )
    vertex_reflect = vertex_translate( projected, vector_create( vc, projected ) )
end function

function vertex_mutate( vertex )
    vertex_mutate = vertex_new( _
        vertex( vertex_x ) * number_random( -0.5, 0.5 ), _
        vertex( vertex_y ) * number_random( -0.5, 0.5 ), _
        vertex( vertex_z ) * number_random( -0.5, 0.5 )  _
        )
end function

function vertex_closest( vertex, vertices )
    dim closest:  closest  = 0
    dim distance: distance = vertex_length( vertex, vertices( closest ) )
    dim index
    for index = lbound( vertices ) + 1 to ubound( vertices )
        dim length: length = vertex_length( vertex, vertices( index ) )
        if( length < distance ) then
            distance = length
            closest  = index
        end if
    next
    vertex_closest = closest
end function

function vertex_inside( va, vb, vc, vd )
    dim na: na = vector_cross( vector_create( va, vb ), vector_create( va, vd ) )
    dim nb: nb = vector_cross( vector_create( vb, vc ), vector_create( vb, vd ) )
    dim nc: nc = vector_cross( vector_create( vc, va ), vector_create( vc, vd ) )
    vertex_inside = vector_align( na, nb ) and _
        vector_align( nb, nc ) and _
        vector_align( nc, na )
end function

function vertex_between( va, vb, vc )
    vertex_between = not ( ( vertex_length( va, vc ) + vertex_length( vb, vc ) ) >
vertex_length( va, vb ) )
end function
```

5.2 Geodesic spheres' properties

We have obtained the following geodesic spheres properties by using the described script and the deduced mathematical formulas related to the geometry.

Geodesic sphere level	Number of sides	Number of different sides	Number of faces	Maximal angle [°]	Accuracy [%]
1	30	1	20	40,81	76,192
2	60	2	80	18,029	92,835
3	180	4	180	11,359	96,692
4	360	6	320	7,802	98,112
5	600	9	500	5,813	98,783
6	900	12	720	4,588	99,152
7	1260	16	980	3,771	99,375
8	1680	20	1280	3,192	99,521
9	2160	25	1620	2,762	99,621
10	2700	30	2000	2,432	99,693
11	3300	36	2420	2,171	99,746
12	3960	42	2880	1,960	99,787
13	4680	49	3380	1,785	99,818
14	5460	56	3920	1,639	99,843
15	6300	64	4500	1,514	99,863
16	7200	72	5120	1,407	99,880
17	8160	81	5780	1,314	99,893
18	9180	90	6480	1,232	99,905
19	10260	100	7220	1,160	99,915
20	11400	110	8000	1,096	99,923
21	12600	121	8820	1,038	99,930
22	13860	132	9680	0,986	99,936
23	15180	144	10580	0,939	99,942
24	16560	156	11520	0,897	99,947
25	18000	169	12500	0,858	99,951
26	19500	182	13520	0,822	99,954
27	21060	196	14580	0,789	99,958
28	22680	210	15680	0,758	99,961
29	24360	225	16820	0,730	99,963
30	26100	240	18000	0,704	99,966
31	27900	256	19220	0,680	99,968
32	29760	272	20480	0,657	99,970
33	31680	289	21780	0,636	99,972
34	33660	306	23120	0,616	99,973
35	35700	324	24500	0,597	99,975
36	37800	342	25920	0,580	99,976
37	39960	361	27380	0,563	99,977
38	42180	380	28880	0,547	99,979
39	44460	400	30420	0,532	99,980
40	46800	420	32000	0,518	99,981
41	49200	441	33620	0,505	99,982
42	51660	462	35280	0,492	99,982
43	54180	484	36980	0,480	99,983
44	56760	506	38720	0,469	99,984
45	59400	529	40500	0,458	99,985
46	62100	552	42320	0,447	99,985
47	64860	576	44180	0,437	99,986
48	67680	600	46080	0,428	99,987
49	70560	625	48020	0,419	99,987
50	73500	650	50000	0,410	99,988

5.3 Comparison worksheet

These values have been produced with the finite-element calculation and with an *Excel* worksheet in which we have used the deduced theoretical formulas related to the shell theory. Thus, we only show the dead load case and the snow load case results.

5.3.1 DEAD LOAD CASE

5.3.1.1 Displacement

phi [°]	A : d (FE model,concrete+steel) [mm]	B : d (FE model,concrete) [mm]	C : d (theoretical,concrete) [mm]	D : d (theoretical,steel) [mm]
0,0	0,162	0,175	0,144	0,509
3,0	0,162	0,176	0,144	0,508
3,1	0,162	0,176	0,144	0,508
6,6	0,161	0,175	0,143	0,505
6,6	0,161	0,175	0,143	0,505
10,3	0,159	0,173	0,142	0,499
10,4	0,159	0,173	0,141	0,499
14,3	0,156	0,170	0,139	0,491
14,3	0,156	0,170	0,139	0,490
17,5	0,153	0,167	0,136	0,481
18,4	0,152	0,166	0,135	0,479
18,4	0,152	0,166	0,135	0,478
22,7	0,147	0,161	0,131	0,463
22,7	0,147	0,161	0,131	0,463
27,0	0,142	0,155	0,126	0,445
27,1	0,142	0,155	0,126	0,445
31,4	0,135	0,148	0,119	0,424
31,5	0,135	0,148	0,119	0,424
35,8	0,128	0,140	0,112	0,401
35,9	0,128	0,140	0,112	0,400
40,2	0,121	0,132	0,105	0,377
40,3	0,121	0,132	0,105	0,376
44,5	0,113	0,123	0,098	0,352
44,6	0,113	0,123	0,098	0,351
48,6	0,105	0,115	0,091	0,329
48,7	0,105	0,115	0,090	0,328
52,5	0,098	0,107	0,084	0,307
52,7	0,098	0,107	0,084	0,307
56,3	0,092	0,100	0,078	0,289
56,4	0,091	0,099	0,078	0,289
59,8	0,086	0,093	0,073	0,276
60,0	0,085	0,092	0,073	0,275
63,1	0,081	0,087	0,070	0,266
63,4	0,081	0,087	0,070	0,266
65,9	0,077	0,084	0,068	0,262
68,5	0,075	0,081	0,067	0,261
68,7	0,075	0,081	0,067	0,261
68,9	0,075	0,080	0,067	0,261
71,8	0,073	0,079	0,068	0,265
74,8	0,073	0,078	0,070	0,274
75,0	0,073	0,078	0,070	0,274
75,3	0,073	0,078	0,070	0,275
78,5	0,074	0,079	0,074	0,290

81,8	0,076	0,082	0,080	0,310
82,1	0,076	0,082	0,080	0,312
82,3	0,076	0,083	0,081	0,314
85,8	0,080	0,087	0,088	0,340
89,4	0,088	0,095	0,097	0,372
89,7	0,089	0,096	0,098	0,374
90,0	0,090	0,097	0,098	0,377
93,7	0,101	0,109	0,109	0,413
97,5	0,084	0,090	0,120	0,453
97,8	0,083	0,089	0,121	0,456
98,1	0,077	0,083	0,121	0,459
101,9	0,000	0,000	0,133	0,502

5.3.1.2 Circular normal force

phi [°]	A : n-θ (FE model,concrete+steel) [kN/m]	B : n-θ (FE model,concrete) [kN/m]	C , D : n-θ (theoretical,concrete or steel) [kN/m]
0,0	-2,82	-3,26	-3,26
3,0	-2,84	-3,24	-3,25
3,1	-2,85	-3,23	-3,25
6,6	-2,82	-3,16	-3,21
10,4	-2,75	-3,05	-3,13
14,3	-2,64	-3,01	-3,01
17,5	-2,54	-2,91	-2,88
18,4	-2,48	-2,84	-2,84
22,7	-2,28	-2,61	-2,62
27,0	-2,06	-2,38	-2,36
27,1	-2,03	-2,33	-2,36
31,4	-1,77	-2,06	-2,04
31,5	-1,73	-2,00	-2,04
35,8	-1,44	-1,69	-1,68
35,9	-1,39	-1,63	-1,68
40,2	-1,08	-1,28	-1,28
40,3	-1,01	-1,21	-1,27
44,5	-0,68	-0,84	-0,85
44,6	-0,61	-0,76	-0,84
48,6	-0,27	-0,38	-0,39
48,7	-0,19	-0,28	-0,37
52,5	0,15	0,10	0,09
52,7	0,24	0,21	0,10
56,3	0,58	0,59	0,57
56,4	0,67	0,71	0,59
59,8	1,03	1,11	1,06
60,0	1,15	1,23	1,08
63,1	1,49	1,60	1,54
63,4	1,66	1,76	1,58
65,9	1,84	2,00	1,96
68,5	2,26	2,43	2,38
68,7	2,26	2,44	2,42
68,9	2,47	2,66	2,45
71,8	2,72	2,95	2,93
74,8	3,25	3,51	3,45
75,0	3,25	3,51	3,50
75,3	3,51	3,79	3,54

78,5	3,83	4,13	4,13
81,8	4,47	4,82	4,78
82,1	4,47	4,81	4,83
82,3	4,78	5,15	4,88
85,8	5,14	5,54	5,60
89,4	6,01	6,50	6,39
89,7	6,00	6,48	6,46
90,0	6,55	7,10	6,52
93,7	7,20	7,75	7,40
97,5	6,00	6,38	8,35
97,8	5,84	6,19	8,43
98,1	2,22	2,28	8,50

5.3.1.3 Tangential normal force

phi [°]	A : n-φ (FE model,concrete+steel) [kN/m]	B : n-φ (FE model,concrete) [kN/m]	C , D : n-φ (theoretical,concrete or steel) [kN/m]
0,0	-2,82	-3,24	-3,26
3,0	-2,94	-3,27	-3,26
3,1	-2,92	-3,27	-3,26
6,6	-2,94	-3,27	-3,27
10,3	-2,95	-3,28	-3,27
10,4	-2,93	-3,28	-3,29
14,3	-2,96	-3,30	-3,29
17,5	-2,95	-3,30	-3,31
18,4	-2,98	-3,34	-3,35
22,7	-2,98	-3,34	-3,35
27,0	-3,03	-3,39	-3,39
27,1	-3,06	-3,41	-3,45
31,4	-3,09	-3,45	-3,45
31,5	-3,13	-3,48	-3,52
35,8	-3,23	-3,59	-3,52
35,9	-3,25	-3,62	-3,60
40,2	-3,32	-3,69	-3,60
40,3	-3,35	-3,73	-3,70
44,5	-3,42	-3,80	-3,70
44,6	-3,46	-3,85	-3,80
48,6	-3,53	-3,92	-3,81
48,7	-3,58	-3,98	-3,92
52,5	-3,65	-4,05	-3,93
52,7	-3,71	-4,12	-4,05
56,3	-3,78	-4,20	-4,06
56,4	-3,84	-4,27	-4,19
59,8	-3,90	-4,34	-4,20
60,0	-3,99	-4,42	-4,34
63,1	-3,95	-4,49	-4,49
63,4	-4,11	-4,58	-4,50
65,9	-4,12	-4,62	-4,63
68,5	-4,31	-4,70	-4,77
68,7	-4,38	-4,75	-4,78
68,9	-4,53	-4,87	-4,80
71,8	-4,56	-4,94	-4,97
74,8	-4,69	-5,07	-5,16
75,0	-4,75	-5,09	-5,18

75,3	-4,93	-5,30	-5,20
78,5	-4,95	-5,35	-5,43
81,8	-5,15	-5,57	-5,71
82,1	-5,17	-5,55	-5,73
82,3	-5,48	-5,88	-5,75
85,8	-5,44	-5,83	-6,08
89,4	-5,78	-6,21	-6,46
89,7	-5,72	-6,14	-6,49
90,0	-6,22	-6,67	-6,52
93,7	-6,07	-6,51	-6,97
97,5	-6,47	-6,92	-7,50
97,8	-6,73	-7,20	-7,54
98,1	-6,77	-7,37	-7,59

5.3.2 SNOW LOAD CASE

5.3.2.1 Displacement

phi [°]	A : d (FE model,concrete+steel) [mm]	B : d (FE model,concrete) [mm]	C : d (theoretical,concrete) [mm]	D : d (theoretical,steel) [mm]
0,0	0,105	0,114	-	-
3,0	0,105	0,114	0,123	0,435
3,1	0,105	0,114	0,123	0,435
6,6	0,103	0,113	0,122	0,431
6,6	0,103	0,113	0,122	0,431
10,3	0,101	0,111	0,120	0,423
10,4	0,101	0,111	0,120	0,423
14,3	0,098	0,108	0,116	0,412
14,3	0,098	0,108	0,116	0,412
17,5	0,095	0,104	0,113	0,400
18,4	0,094	0,103	0,112	0,396
18,4	0,094	0,103	0,112	0,396
22,7	0,089	0,098	0,106	0,377
22,7	0,089	0,098	0,106	0,377
27,0	0,084	0,092	0,099	0,354
27,1	0,084	0,092	0,099	0,354
31,4	0,077	0,085	0,092	0,329
31,5	0,077	0,085	0,092	0,329
35,8	0,071	0,077	0,084	0,302
35,9	0,071	0,077	0,084	0,302
40,2	0,064	0,070	0,076	0,276
40,3	0,064	0,070	0,076	0,275
44,5	0,057	0,063	0,069	0,251
44,6	0,057	0,063	0,069	0,250
48,6	0,051	0,056	0,062	0,228
48,7	0,051	0,056	0,062	0,228
52,5	0,047	0,051	0,056	0,209
52,7	0,047	0,051	0,056	0,208
56,3	0,043	0,046	0,051	0,194
56,4	0,043	0,046	0,051	0,193
59,8	0,040	0,043	0,048	0,183
60,0	0,040	0,043	0,048	0,182
63,1	0,039	0,041	0,046	0,175
63,4	0,038	0,041	0,045	0,174
65,9	0,037	0,040	0,044	0,170

68,5	0,036	0,039	0,043	0,168
68,7	0,036	0,039	0,043	0,167
68,9	0,036	0,039	0,043	0,167
71,8	0,036	0,039	0,043	0,166
74,8	0,036	0,039	0,043	0,165
75,0	0,036	0,039	0,043	0,165
75,3	0,036	0,039	0,043	0,165
78,5	0,036	0,039	0,043	0,165
81,8	0,036	0,039	0,043	0,164
82,1	0,036	0,039	0,043	0,164
82,3	0,036	0,039	0,043	0,164
85,8	0,036	0,039	0,043	0,163
89,4	0,036	0,039	0,042	0,161
89,7	0,036	0,039	0,042	0,160
90,0	0,036	0,039	0,042	0,160
93,7	0,036	0,040	0,041	0,155
97,5	0,028	0,030	0,039	0,148
97,8	0,027	0,029	0,038	0,148
98,1	0,025	0,027	0,038	0,147
101,9	0,000	0,000	0,036	0,138

5.3.2.2 Circular normal force

phi [°]	A : n-θ (FE model,concrete+steel) [kN/m]	B : n-θ (FE model,concrete) [kN/m]	C , D : n-θ (theoretical,concrete or steel) [kN/m]
0,0	-2,29	-2,68	-2,72
3,0	-2,30	-2,64	-2,70
3,1	-2,27	-2,63	-2,65
6,6	-2,21	-2,54	-2,54
10,3	-2,20	-2,52	-2,54
10,4	-2,10	-2,40	-2,39
14,3	-2,07	-2,36	-2,39
17,5	-1,96	-2,23	-2,23
18,4	-1,88	-2,13	-2,18
22,7	-1,63	-1,86	-1,91
27,0	-1,39	-1,59	-1,60
27,1	-1,34	-1,53	-1,59
31,4	-1,06	-1,23	-1,24
31,5	-1,01	-1,17	-1,23
35,8	-0,71	-0,84	-0,85
35,9	-0,65	-0,77	-0,85
40,2	-0,34	-0,44	-0,45
40,3	-0,28	-0,37	-0,44
44,5	0,02	-0,04	-0,05
44,6	0,09	0,04	-0,04
48,6	0,37	0,35	0,34
48,7	0,44	0,43	0,35
52,5	0,69	0,72	0,71
52,7	0,76	0,79	0,72
56,3	0,99	1,06	1,04
56,4	1,04	1,13	1,06
59,8	1,26	1,37	1,34
60,0	1,32	1,44	1,36
63,1	1,52	1,64	1,63

63,4	1,67	1,69	1,81
65,9	1,78	1,97	1,99
68,5	1,84	2,00	2,00
68,7	1,89	2,02	2,02
68,9	2,12	2,18	2,34
71,8	2,15	2,32	2,36
74,8	2,19	2,35	2,37
75,0	2,29	2,39	2,50
75,3	2,39	2,49	2,62
78,5	2,40	2,58	2,62
81,8	2,49	2,59	2,72
82,1	2,50	2,64	2,72
82,3	2,61	2,69	2,70
85,8	1,94	2,70	2,63
89,4	1,90	2,80	2,62
89,7	0,59	0,60	2,61
90,0	-2,30	-2,65	-2,70
93,7	-2,31	-2,64	-2,70
97,5	-2,27	-2,56	-2,65
97,8	-2,21	-2,54	-2,54
98,1	-2,10	-2,40	-2,39

5.3.2.3 Tangential normal force

phi	A : n-φ (FE model,concrete+steel)	B : n-φ (FE model,concrete)	C , D : n-φ (theoretical,concrete or steel)
[°]	[kN/m]	[kN/m]	[kN/m]
0,0	-2,29	-2,68	-2,72
3,0	-2,39	-2,70	-2,72
3,1	-2,37	-2,69	-2,72
6,6	-2,38	-2,70	-2,72
10,4	-2,37	-2,69	-2,72
14,3	-2,37	-2,69	-2,72
17,5	-2,37	-2,70	-2,72
18,4	-2,37	-2,69	-2,72
22,7	-2,38	-2,69	-2,72
27,0	-2,39	-2,69	-2,72
27,1	-2,40	-2,69	-2,72
31,4	-2,40	-2,69	-2,72
31,5	-2,41	-2,70	-2,72
35,8	-2,41	-2,69	-2,72
35,9	-2,42	-2,71	-2,72
40,2	-2,42	-2,69	-2,72
40,3	-2,43	-2,71	-2,72
44,5	-2,43	-2,70	-2,72
44,6	-2,44	-2,72	-2,72
48,6	-2,44	-2,70	-2,72
48,7	-2,45	-2,73	-2,72
52,5	-2,44	-2,71	-2,72
52,7	-2,46	-2,73	-2,72
56,3	-2,44	-2,71	-2,72
56,4	-2,46	-2,74	-2,72
59,8	-2,44	-2,74	-2,72
60,0	-2,47	-2,74	-2,72
63,1	-2,42	-2,71	-2,72
63,4	-2,44	-2,72	-2,72
65,9	-2,45	-2,67	-2,72

68,5	-2,48	-2,73	-2,72
68,7	-2,51	-2,69	-2,72
68,9	-2,54	-2,72	-2,72
71,8	-2,51	-2,67	-2,72
74,8	-2,53	-2,71	-2,72
75,0	-2,51	-2,68	-2,72
75,3	-2,54	-2,70	-2,72
78,5	-2,50	-2,67	-2,72
81,8	-2,51	-2,69	-2,72
82,1	-2,49	-2,67	-2,72
82,3	-2,51	-2,68	-2,72
85,8	-2,48	-2,66	-2,72
89,4	-2,48	-2,66	-2,72
89,7	-2,47	-2,64	-2,72
90,0	-2,44	-2,61	-2,72
93,7	-2,53	-2,72	-2,72
97,5	-2,38	-2,60	-2,72
97,8	-2,40	-2,62	-2,72
98,1	-2,31	-2,68	-2,72